EXPERIMENTAL AND FINITE ELEMENT ANALYSIS OF A DAMAGED REINFORCED CONCRETE BRIDGE STRENGTHENED WITH SPRAYED GLASS FIBER REINFORCED POLYMERS

by

Seyedali Reza Mortazavi

M.Sc. (Mechanical Engineering), University of Utah, Salt Lake City, Utah, 1985
Ph. D. (Mechanical Engineering), University of Utah, Salt Lake City, Utah, 1990

A THESIS SUBMITTED IN PARTIAL FULFILLMENT OF
THE REQUIREMENTS FOR THE DEGREE OF
MASTER OF APPLIED SCIENCE

in

THE FACULTY OF GRADUATE STUDIES
DEPARTMENT OF CIVIL ENGINEERING

We accept this thesis as conforming
to the required standard:

THE UNIVERSITY OF BRITISH COLUMBIA

© Ali R Mortazavi, 2004

Library Authorization

In presenting this thesis in partial fulfillment of the requirements for an advanced degree at the University of British Columbia, I agree that the Library shall make it freely available for reference and study. I further agree that permission for extensive copying of this thesis for scholarly purposes may be granted by the head of my department or by his or her representatives. It is understood that copying or publication of this thesis for financial gain shall not be allowed without my written permission.

Name of Author *(please print)* ***Seyedali Reza Mortazavi*** Date (dd/mm/yyyy) **12/08/2004**

Title of Thesis: **Experimental and Finite Element Analysis of a Damaged Reinforced Concrete Bridge Strengthened with Sprayed Glass Fiber Reinforced Polymers**

Degree: **Master of Applied Science** Year: **2004**

Department of **Civil Engineering**
The University of British Columbia
Vancouver, BC Canada

EXPERIMENTAL AND FINITE ELEMENT ANALYSIS OF A DAMAGED REINFORCED CONCRETE BRIDGE STRENGTHENED WITH SPRAYED GLASS FIBER REINFORCED POLYMERS

by

Seyedali Reza Mortazavi

M.Sc. (Mechanical Engineering), University of Utah, Salt Lake City, Utah, 1985
Ph. D. (Mechanical Engineering), University of Utah, Salt Lake City, Utah, 1990

A THESIS SUBMITTED IN PARTIAL FULFILLMENT OF
THE REQUIREMENTS FOR THE DEGREE OF
MASTER OF APPLIED SCIENCE

in

THE FACULTY OF GRADUATE STUDIES
DEPARTMENT OF CIVIL ENGINEERING

We accept this thesis as conforming
to the required standard:

.....

.....

.....

THE UNIVERSITY OF BRITISH COLUMBIA

© Ali R Mortazavi, 2004

ABSTRACT

A vast number of bridges throughout North America are deteriorated or distressed to such a degree that structural strengthening and rehabilitation of the bridge or lowering the allowable truck loading on the bridge by load posting has become necessary to extend the service life of the bridge. One of the most recent techniques of strengthening these type of bridges is placement of Sprayed Glass Fiber Reinforced Polymers. Safe Bridge is the first bridge in the world that was retrofitted by Sprayed Fiber Reinforced Polymers. This paper presents the experimental and finite element analysis of the Safe Bridge prior to and after the application of Sprayed GFRP. The truck loading was applied to the bridge model at different locations, as in an actual bridge test. The non-linear analyses were carried out by ANSYS. A good agreement between model and tests was obtained. Thus, FEM models can be effectively utilized for analyzing and designing strengthening strategies.

TABLE OF CONTENTS

Abstract ii

Table of Contents iii

List of Tables viii

List of Figures x

Acknowledgements xvii

Chapter 1 – Introduction 1

Chapter 2 - Literature Survey

2.1 - Introduction 5

2.2 – Steel Plates 7

2.3 – FRP Wraps 8

2.4 – FRP as a Shear or Flexural Strengthening Reinforcement. 10

2.5 – Field Application of FRPs 16

2.6 – FRP Sprays 23

2.7 – Finite Element Modeling of Bridge Elements 23

Chapter 3 – Equipment and Materials

3.1 - Equipment 28

3.2 – Reinforced Concrete Properties. 29

3.3 – Fiber Reinforced Polymers 29

3.3.1 - Resin 30

3.3.2 - Catalyst 30

3.3.3 – Coupling Agent 30

3.3.4 – Glass Fiber 31

3.3.5 - Solvent 31

Chapter 4 – Bridge Description and Repair plan

4.1 – Safe Bridge 35

4.2 – Repair Procedure 36

4.2.1 - Laboratory Testing of GFRP Materials 36

4.2.2 - Surface Preparation, Instrumentation and Patching Repair 36

4.2.3 - Application of GFRP on Bridge Girders 37

4.3 – Loading Conditions 38

4.3.1 – Static Load Test. 39

4.3.2 – Rolling Load Test. 39

Chapter 5 – Comparison of Experimental Results Before and After the Retrofit

5.1 – Static Load Test Results 53

5.2 – Rolling Load Test Results 54

5.3 – Load Test Comparison 55

Chapter 6 – Finite Element Analysis of Safe Bridge

6.1 – Element Description 72

6.1.1 – Reinforced Concrete 72

6.1.1.1 – Assumptions and Restrictions 72

6.1.1.2 – Descriptions 73

6.1.1.2.1 - Linear Behaviour – General 73

6.1.1.2.2 - Nonlinear Behaviour – Concrete 74

6.1.1.2.2.1 - Modeling of a Crack 74

6.1.1.2.2.2 - Modeling of a Crushing 77

6.1.2 – Glass Fiber Reinforced Polymers 77

6.1.3 - Contact Surface between GFRP and Concrete 78

6.2 – Material Properties 78

6.2.1 - Concrete. 78

6.2.1.1 – Concrete Input Data 79

6.2.1.2 – Failure Criteria for Concrete 80

6.2.2 – Steel Reinforcement. 81

6.2.3 – Sprayed FRP Composites 81

6.3 – Finite Element Modeling 82

6.3.1 – Bridge Modeling and Analysis Assumptions 83

6.3.2 – Finite Element Discretization 83

6.4 – Frequency Analysis 84

6.5 – Static Analysis 85

6.6 – Parametric Study 86

6.7 – Ultimate Bridge Capacity 87

Chapter 7 – Finite Element Analysis of Full-Scale Specimens

7.1 – Experimental Testing of MOTH Beam. 116

7.1.1 – Beam Description 116

7.1.2 – Specimen Preparation 116

7.1.3 - Experimental Setup and Results 116

7.2 – Finite Element Modeling of MOTH Beam 117

7.2.1 - Element Description 117

7.2.1.1 – Reinforced Concrete 117

7.2.1.2 – Sprayed Glass Fiber Reinforced Polymers. 117

7.2.1.3 - Wrapped Glass Fiber Reinforced Polymers 117

7.2.2 – Material Properties 118

7.2.2.1 – Concrete and Steel Reinforcement. 118

7.2.2.2 – Sprayed GFRP Composites 118

7.2.2.3 - Wrapped GFRP Composites 118

7.2.3 – FEM Modeling 120

7.2.3.1 – Geometry 120

7.2.3.2 – Finite Element Discretization 121

7.3 – Load-Deflection Results 122

7.4 – Comparison of Experimental and Numerical Results. 122

Chapter 8 – Conclusion and Recommendations

8.1 – Experimental Results 133

8.2 – Finite Element Results 134

8.3 – Parametric Study 135

8.4 – Recommendations on FEM Modeling 136

References 137

LIST OF TABLES

Table 2.1: Field survey on use of externally bonded FRP in RC flexural members [14,45]. 19

Table 3.1: Mechanical and material properties of K-1907 Polyester Resin [58] 33

Table 3.2: Mechanical and Material properties of Derakane 8084 Vinyl Ester Resin [60] 33

Table 3.3: Mechanical and material properties of Advantex® Glass Fiber [61] 34

Table 4.1: Properties of FRP Sprayed Beam (60 x 60 x 300 mm) Specimens [62] . . . 42

Table 5.1: Mid-span strains at various load positions before application of GFRP . . . 57

Table 5.2: Mid-span strains at various load positions after application of GFRP. 57

Table 5.3: Mid-span deflections at various load positions before application of GFRP 58

Table 5.4: Mid-span deflections at various load positions after application of GFRP. . 58

Table 5.5: Mid-span strains at various ROLL positions before application of GFRP. . 68

Table 5.6: Mid-span strains at various ROLL positions after application of GFRP . . . 68

Table 5.7: Mid-span deflections at various load positions before application of GFRP 69

Table 5.8: Mid-span deflections at various load positions after application of GFRP 69

Table 5.9: Comparison of results before and after application of GFRP for static test 70

Table 5.10: Comparison of results before and after application of GFRP for ROLL test 70

Table 6.1: Summary of the number of elements used in the bridge model 94

Table 6.2: Natural circular frequency, natural frequency and natural period for the first twenty modes extracted from the FEM frequency analysis before application of GFRP 95

Table 6.3: Natural circular frequency, natural frequency and natural period for the First twenty modes extracted from the FEM frequency analysis after application of GFRP 95

Table 7.1: Number of elements used in the control beam 129

Table 7.2: Number of elements used in the sprayed GFRP beam 129

Table 7.3: Number of elements used in the wrapped GFRP beam 129

Table 7.4: Comparison between experimental ultimate loads and FEM final loads . . 130

LIST OF FIGURES

Figure 1.1: Diagram of the full-height circular steel jacket used to retrofit the reinforced concrete bridge columns on the Hanshin Expressway in Kobe [14] 2

Figure 1.2: Carbon fiber sheet jacketing of Hollow reinforced concrete piers, Sakawagawa Bridge, Tomei expressway, Japan Highway Public Corporation [15] 3

Figure 1.3: Sprayed GFRP on scaled column [16]. 3

Figure 2.1: Plate positions [7] 6

Figure 2.2: Horsetail Creek Bridge [43] (1998, prior to retrofit) 17

Figure 2.3: Elevation of Horsetail Creek Bridge [43] 17

Figure 3.1: GFRP spraying equipment 32

Figure 3.2: GFRP spraying gun assembly 32

Figure 4.1: View of Safe Bridge in Duncan, British Columbia 40

Figure 4.2(a): Longitudinal steel rebar exposed at mid-span 40

Figure 4.2(b): Longitudinal and stirrup reinforcement exposed near support section . 41

Figure 4.2(c): Longitudinal and stirrup reinforcement exposed at support section . . . 41

Figure 4.3(a): Strain gauge was mounted on well-prepared steel surface 42

Figure 4.3(b): Strain gauge was protected using waterproof material 43

Figure 4.4(a): Applying hybrid fiber reinforced mortar on the damaged surfaces 43

Figure 4.4(b): Applying hybrid fiber reinforced mortar on the damaged surfaces 44

Figure 4.5: Location of six transducers along the mid-span 44

Figure 4.6: Location of six transducers and strain gauges along the mid-span 45

Figure 4.7: Data recorded using a data acquisition system 45

Figure 4.8: Spraying GFRP on the girder legs 46

Figure 4.9: Finished surface of sprayed GFRP 46

Figure 4.10: Final configuration of sprayed and wrapped girders 47

Figure 4.11(a): Cutting the glass fiber fabric to desired dimension 47

Figure 4.11(b): Placing the GFRP mat on the girder legs 48

Figure 4.11(c): The finished surface of the wrapped GFRP mat 48

Figure 4.12: Dimensions and weight distribution of the truck 49

Figure 4.13(a): Position 1, truck placed close to curb with second rear axle at mid-span 49

Figure 4.13(b): Position 2, truck placed close to curb with first rear axle at mid-span 50

Figure 4.13(c): Position 3, truck placed close to curb with second rear axle at mid-span 50

Figure 4.13(d): Position 4, truck placed close to curb with first rear axle at mid-span 51

Figure 4.13(e): Position 5, truck placed centrally with second rear axle at mid-span . 51

Figure 4.13(f): Position 6, truck placed centrally with first rear axle at mid-span 52

Figure 5.1: Mid-span strains at various load positions before application of GFRP . . 59

Figure 5.2: Mid-span strains at various load positions after application of GFRP 59

Figure 5.3: Mid-span deflections at various load positions before application of GFRP 60

Figure 5.4: Mid-span deflections at various load positions after application of GFRP 60

Figure 5.5: Performance of Bridge before and after application of GFRP 61

Figure 5.6: Performance of Bridge before and after application of GFRP 61

Figure 5.7: Micro strain versus time before the application of GFRP (ROLL I). 62

Figure 5.8: Micro strain versus time after the application of GFRP (ROLL I). 62

Figure 5.9: Mid-span deflection versus time before the application of GFRP (ROLL I) 63

Figure 5.10: Mid-span deflection versus time after the application of GFRP (ROLL I) 63

Figure 5.11: Micro strain versus time before the application of GFRP (ROLL II). . . . 64

Figure 5.12: Micro strain versus time after the application of GFRP (ROLL II). 64

Figure 5.13: Mid-span deflection versus time before the application of GFRP (ROLL II) 65

Figure 5.14: Mid-span deflection versus time after the application of GFRP (ROLL II) 65

Figure 5.15: Micro strain versus time before the application of GFRP (ROLL III). . . 66

Figure 5.16: Micro strain versus time after the application of GFRP (ROLL III). 66

Figure 5.17: Mid-span deflection versus time before application of GFRP (ROLL III) 67

Figure 5.18: Mid-span deflection versus time after application of GFRP (ROLL III). .67

Figure 6.1: SOLID65 3-D Reinforced Concrete Solid [63] 89

Figure 6.2: LINK8 3-D Spar [63] 89

Figure 6.3: SHELL43 Plastic Large Strain Shell [63] 90

Figure 6.4: CONTA174 3-D Surface-to-Surface Contact Element (8 nodes) [63] . . . 90

Figure 6.5: TARGE170 Target Surface Element [63] 91

Figure 6.6: Typical uniaxial compressive and tensile stress-strain curve for concrete [65] 91

Figure 6.7: Failure Surface in Principal Stress Space σ_{zp} close to zero [63] 92

Figure 6.8: Stress-strain curve for steel reinforcement [63] 92

Figure 6.9: Truckload simplification: (a) and (b) show configurations of the dump truck and the simplified truck, respectively 93

Figure 6.10: An isometric view of the finite element model of the bridge 94

Figure 6.11: Mode shape corresponding to fundamental vibration frequency before the application of GFRP 96

Figure 6.12: Mode shape corresponding to fundamental vibration frequency after the application of GFRP 96

Figure 6.13: Deflection under static load position 1, before the application of GFRP. .97

Figure 6.14: Stress distribution under static load position 1, before application of GFRP 97

Figure 6.15: Deflection under static load position 2, before the application of GFRP. .98

Figure 6.16: Stress distribution under static load position 2, before application of GFRP 98

Figure 6.17: Deflection under static load position 3, before the application of GFRP. .99

Figure 6.18: Stress distribution under static load position 3, before application of GFRP 99

Figure 6.19: Deflection under static load position 4, before the application of

GFRP 100

Figure 6.20: Stress distribution under static load position 4, before application of GFRP 100

Figure 6.21: Deflection under static load position 5, before the application of GFRP. 101

Figure 6.22: Stress distribution under static load position 5, before application of GFRP 101

Figure 6.23: Deflection under static load position 6, before the application of GFRP. 102

Figure 6.24: Stress distribution under static load position 6, before application of GFRP 102

Figure 6.25: Comparison between the experimental and ANSYS results before the application of GFRP 103

Figure 6.26: Comparison between the experimental and ANSYS results before the application of GFRP 103

Figure 6.27: Deflection under static load position 1, after the application of GFRP. 104

Figure 6.28: Stress distribution under static load position 1, after application of GFRP 104

Figure 6.29: Deflection under static load position 2, after the application of GFRP. . 105

Figure 6.30: Stress distribution under static load position 2, after application of GFRP 105

Figure 6.31: Deflection under static load position 3, after the application of GFRP. . 106

Figure 6.32: Stress distribution under static load position 3, after application of GFRP 106

Figure 6.33: Deflection under static load position 4, after the application of GFRP. . 107

Figure 6.34: Stress distribution under static load position 4, after application of GFRP 107

Figure 6.35: Deflection under static load position 5, after the application of GFRP. .108

Figure 6.36: Stress distribution under static load position 5, after application of GFRP 108

Figure 6.37: Deflection under static load position 6, after the application of GFRP. .109

Figure 6.38: Stress distribution under static load position 6, after application of GFRP 109

Figure 6.39: Comparison between the experimental and ANSYS results after the application of GFRP 110

Figure 6.40: Comparison between the experimental and ANSYS results after the application of GFRP 110

Figure 6.41: Effect of GFRP modulus of elasticity on reduction of maximum girder deflection (girder 6) 111

Figure 6.42: Effect of GFRP modulus of elasticity on reduction of maximum stress in reinforcing steel (girder 6) 111

Figure 6.43: Effect of GFRP thickness on reduction of maximum girder deflection (girder 6) 112

Figure 6.44: Effect of GFRP thickness on reduction of

maximum stress in reinforcing steel (girder 6) 112

Figure 6.45: An isometric view of the finite element model using the transverse symmetry 113

Figure 6.46: Load deflection response for the Safe bridge 113

Figure 6.47: Crack patterns for the Safe bridge 114

Figure 7.1: MOTH channel beam dimensions [12] 124

Figure 7.2: MOTH channel beam reinforcement details [12] 124

Figure 7.3: MOTH channel beam sprayed GFRP locations [12] 125

Figure 7.4: MOTH channel beam wrapped specimen fabric orientation [12] 125

Figure 7.5: Schematic of MOTH channel beam test setup [12] 126

Figure 7.6: MOTH channel beam – load deflection curves [12] 126

Figure 7.7: SOLID45 3-D Structural Solid [63] 127

Figure 7.8: SOLID46 3-D Layered Structural Solid [63] 127

Figure 7.9: Use of a quarter beam model 128

Figure 7.10: Cross-section of quarter beam model 128

Figure 7.11: FEM Load – Deflection plot 130

Figure 7.12: Crack pattern for the sprayed GFRP beam at maximum load 131

Figure 7.13: Deflection distribution for the sprayed GFRP beam at maximum load 131

Figure 7.14: Stress distribution for the sprayed GFRP beam at maximum load 132

ACKNOWLEDGEMENT

I wish to express my sincere gratitude to my advisor professor Nemy Banthia for many valuable suggestions and encouragement offered during the course of this project. His devotion and many hours of consultation are greatly appreciated. I would also like to thank Professor Aftab Mufti for his valuable suggestions.

I am also greatly in debt to my family especially my wife and daughter, Poupak and Mana, for their special help, encouragement and love throughout.

1

INTRODUCTION

Due to growing concerns with structural inadequecy of our infrastructures, many researchers developed new strategies for upgrading and retrofitting these structures. In case of bridges, most bridges were designed in 1950s and 1960s so they no longer fulfill the requirements that have been set by the new codes. For example, more than 40% of all bridges in North America are currently considered structurally deficient in shear [1,2]. Most of them were built when the code shear design requirements were much lower and the allowable truckloads were much smaller. Since then, the minimum internal steel stirrup requirement has been more than doubled, and allowable truckloads have gone up from a maximum single wheel load of 71.2 kN to 175 kN [3]. As a result of these changes, they no longer satisfy the shear resistance requirements. Furthermore, shear failure in reinforced concrete beams is very brittle and catastrophic. Thus it is simply not acceptable to continue using them in such a substandard condition. Therefore, considerable efforts have been made at developing new techniques to strengthen the shear capacities up and beyond the required levels [4-5]. Some of the

various retrofitting techniques proposed by researchers include steel jacketing, advanced composite wrapping, and more recently Sprayed Fiber Reinforced Plastics [4-10]. Figures 1.1 through 1.3 show three different retrofitting techniques, and although all have been proven to be effective in increasing the strength and ductility of substandard bridge girders, Sprayed Fiber Reinforced Plastics have demonstrated a particular promise [10-13]. The above retrofitting techniques can also be extended to strengthening of damaged bridge girders after earthquake.

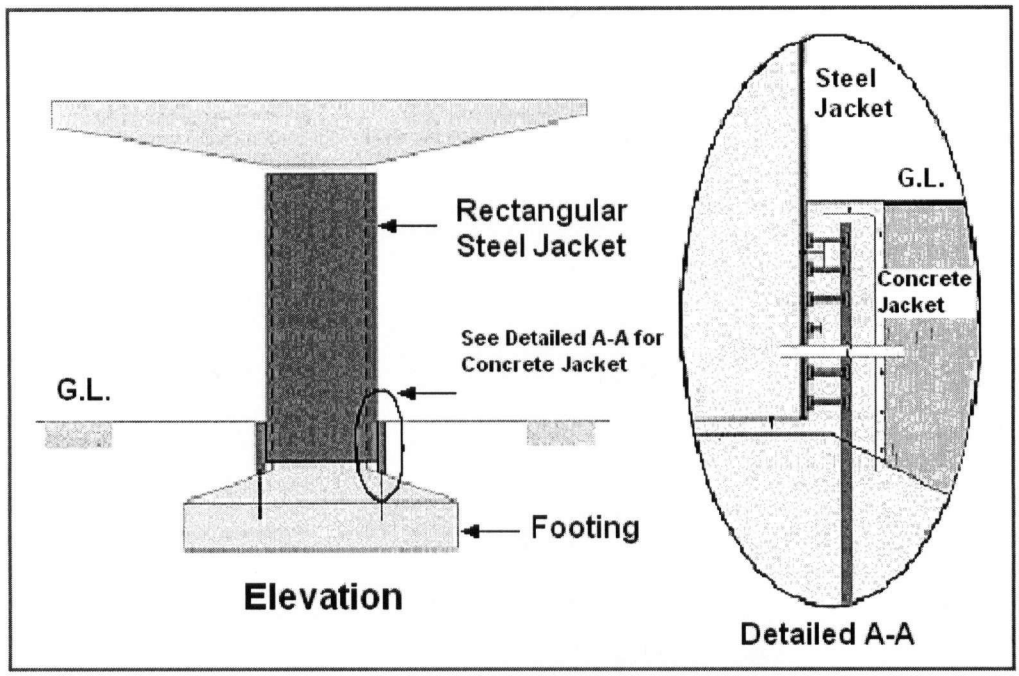

Figure 1.1: Diagram of the full-height circular steel jacket used to retrofit the reinforced concrete bridge columns on the Hanshin Expressway in Kobe [14].

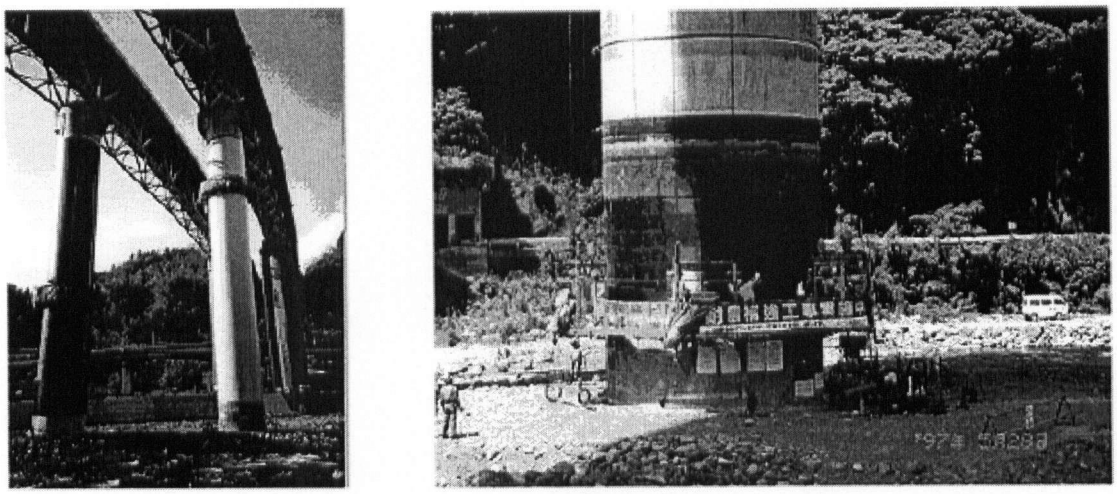

(a) Retrofitted East and west Bound Bridge (b) Wrapping of Carbon Fiber Sheets

Figure 1.2: Carbon fiber sheet jacketing of Hollow reinforced concrete piers, Sakawa-gawa Bridge, Tomei expressway, Japan Highway Public Corporation [15].

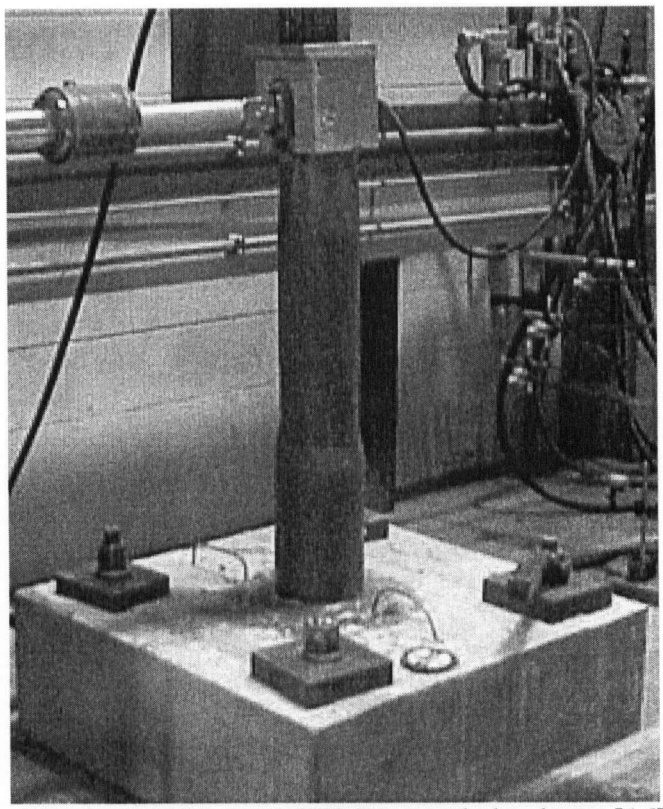

Figure 1.3: Sprayed GFRP on scaled column [16].

The project described in this thesis involved full-scale experimental and numerical study designed to validate the effectiveness of the Sprayed Fiber Reinforced Plastic strengthening technique. A direct comparison between retrofitted and unretrofitted girders was carried out.

2

LITERATURE SURVEY

2.1 - Introduction

Inadequate infrastructure throughout the world has created an urgent need for cost effective and innovative rehabilitation techniques. More than 40 percent of the bridges in both Canada and United States are structurally deficient. Inadequacy also emerges from new load requirements imposed on the bridges [1]. In Canadian province of Alberta, more than 5,000 bridges are expected to be rehabilitated within the next 10-20 years. Among those, 3,000 are estimated to be deficient in shear that is due to recent increase of more than 30% in allowable truckloads combined with less stringent shear design requirement at the time these bridges were designed [14]. The research described here involved the use of sprayed glass fibre reinforced polymers for the rehabilitation of reinforced concrete members. Since it is a novel technique in the area of rehabilitation, there are not many studies performed using this technique and hence there are only few publication that could be referred [10-13]. Nevertheless, it can be considered an

extension of previous studies performed on the rehabilitation techniques. Fundamentally, in all various techniques, there involves an attachment of an external reinforcement to confine the outer surface of the existing reinforced concrete members.

Plates can be bonded to every side of a beam. They can be bonded to tension, shear, or compression faces of the beams. Tension faceplates (Figure 2.1a) are mechanically efficient as they act at the maximum tension zone and therefore, acquire the highest increase in flexural strength and stiffness. However, the use of tension faceplates decreases the ductility of the beam, which then results in limiting the increase in strength.

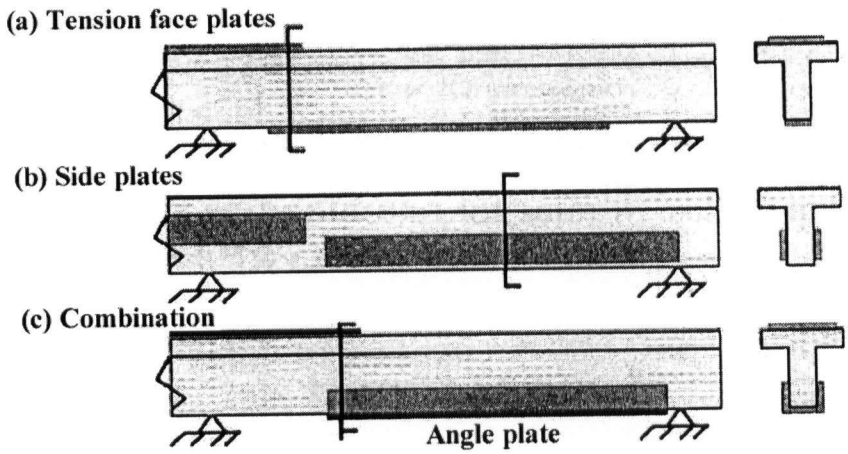

Figure 2.1: Plate positions [7].

Side plates (Figure 2.1b) enhance both shear and flexural capacities. In fact, in theory the beams with side plates can increase the flexural capacity significantly without a loss of ductility. Plates can also be bonded to the compression face in a continuous beam by extending a tension faceplate beyond the point of contraflexure. This is useful in inhibiting but not preventing debonding. Angle sections and channel sections can also be bonded to beams (Figure 2.1c). They provide the characteristics of both tension face and

side plates. Furthermore, any combination of these plating techniques can be used to provide more strengthening [7].

2.2- Steel Plates

Steel plates are the first type of reinforcement of this kind [7-9]. External Bonding of steel plates for repairing or retrofitting of reinforced concrete structures has proven to be quite efficient. Steel plates have been used for many years due to their low cost, simplicity in handling and applying and to their effectiveness for strengthening. The properties and behavior of steel-concrete structures are also well known providing reliable design techniques. Steel plates are particularly effective when used as bending reinforcement due to their high tensile strength and stiffness. Research on how to improve the ductility of these types of retrofitted structures continues to be performed [15]. Steel plates can also be used as external shear reinforcement; however, labor costs might rise quicker than anticipated. Steel stirrups have to be bent or welded and very often anchored with bolts in the concrete compression zone. When several stirrups per meter are needed, the costs can make this technique economically less attractive. Although steel is inexpensive and unobtrusive, and has a negligible effect on the overall dimensions of the structure, steel is also highly corrosive and heavy to handle on construction sites. Some of the advantages of using advanced composites over steel plates, especially with carbon fiber reinforced plastics, in bridge construction are [17]:

1- In the case of steel, corrosion at the interface between steel and concrete will occur and cause interfacial debonding.

2- Steel plates are heavy to handle on construction sites, especially inside a box girder, and often expensive scaffolding are required to bond the steel plates to the structure.

3- As a result of heavy weight, the length of the steel plates in general is restricted to 6 to 10 meters. In cases where greater lengths are required, joints are necessary. But they cannot be welded since it can destroy the adhesive bonding.

2.3- FRP Wraps

Advanced fibrous composites have opened more alternatives in retrofit and design in construction industry. There are different fibres such as glass, aramid, and carbon, with carbon being the most popular due to its superior stiffness and durability characteristics [17]. They are combined with unsaturated polyesters, epoxies, and vinyl esters matrices, to produce composites with superb bonding capabilities with concrete [17]. Fiber reinforced plastics have been used by the aerospace industry for several decades, and are becoming increasingly popular in the construction industry for strengthening purposes. They have many attractive properties such as corrosion resistance, formability, lightweight, and ease of fabrication. Depending on the required physical and mechanical properties different combination of these two variables can make significant number of FRP materials [18]. They have also been used by the military for both repair of concrete structures and for floating structures or military causeways [19-20].

FRP plates and sheets are produced using the pultrusion process and carry unidirectional fibers in the longitudinal direction. FRPs are, therefore, anisotropic, with very high strength in the fiber direction and very low strength perpendicular to the fiber direction.

They tend to behave linearly elastic up to failure without showing a definite yield point [21]. These materials, unlike steel plates, can be made to any desired length. They are light, corrosion resistant, possess outstanding fatigue performance, and they offer greater efficiency in construction. Therefore, advanced composite materials can replace steel plates in strengthening projects with the following benefits :

1- FRPs are corrosion resistant.

2- FRPs are easier to handle on construction site and can be bonded to the structure with a scissors-lift or similar lift without expensive scaffolding.

3- FRPs are available endless on bobbins, therefore no joints are necessary.

4- Most FRPs, especially CFRPs, show outstanding fatigue behaviour [17].

Application of FRPs in the fabric form usually consist of:

1- Surface preparation: repair and sealing of cracks, rust proofing of rebars, smoothening of surface by sandblasting down the aggregates to assure a good bond between the FRP and the concrete, etc.

2- Application of a coupling agent on the surface.

3- Application of resin undercoat.

4- Placement of fabric sheets.

5- Application of resin top coat.

6- Application of a protective layer and a fire proofing coat, if needed.

On the other hand, the laminated FRP plates or pre-impregnated sheets require only concrete surface preparation (as indicated above) and a layer of epoxy adhesive or coupling agent spread over the surface where the FRP is placed. However, in order to

optimize the workability between the FRP and concrete, the FRP surface must first be worked to remove the outermost matrix-rich layer and expose the fibers [12].

2.4 – FRP as a Shear or Flexural Strengthening Reinforcement

Investigating the behaviour of RC beams strengthened with FRP plates show different types of failure modes. Ultimate strength of the beam is generally controlled by rupture of the plate or compression crushing of concrete [22]. However, local failure can occur in concrete beam at the plate end due to stress concentration or debonding of the plate that results in premature failure of the strengthened beam. Some of the reasons for local failure are shear and normal (peeling) stress concentrations at the cut-off point or around flexural cracks.

Saadatmanesh and Malek [6,23] investigated the failure modes of FRP plate for flexural strengthening of RC retrofitted beams. They divided the failure modes into two general categories of flexural and local failures. Flexural failure is defined as concrete crushing in compression or plate rupture in tension. Local failure is defined as the peeling of the FRP plate at concrete layer between the plate and the longitudinal reinforcement. This layer is considered to be the location of high interfacial stresses and potential shear failure. Flexural failure has been investigated analytically [22] indicating that this mode of failure results from a local stress concentration at the plate end as well as at the flexural cracks. Local failure of concrete beams occur at the plate cut-off point due to shear concentration at the flexural cracks.

Bonacci and Maalej [24] generated a database on behavioural trends of RC beams strengthened with externally bonded FRP. This analysis included failure mode, strength

gain, and deformability. They noted that failure by debonding of FRP plates were prevalent among the specimens in the database. Moreover, they noted 50% or more increase in strength and deflection capacity [24]. They concluded that debonding failure were more difficult to characterize and analyze than the other potential modes, because they depend on factors that are not common to analyses of conventional members such as epoxy thickness, mechanical response, surface preparation before the application of FRP, and sensitivity to faulting motions along the member cracks spreading to the tension face.

Experimental studies carried on by Saadatmanesh and Ehsani [25], Sharif et al. [26], Arduini and Nanni [27], Sheikh [28], and Ross et al. [29] have concluded that epoxy bonding FRP plates to the tension face of reinforced concrete beams will considerably increased the ultimate flexural capacity. The amplified capacity can be as high as three times of the original capacity of the beams. It depended on such factors as reinforcing steel ratio, concrete compressive strength, FRP mechanical properties, and the severity of the predamage to the beam. Sharif et al. [26] also studied the effect of plate thickness on failure mechanism of the beams and found out that for relatively thin plates, the shear and normal stresses at the end of FRP plate are low, and for a sufficiently under-reinforced beam, the repaired beam will fail by rupturing of the plate. As the plate thickness is increased, the shear and normal stresses developed at the end of the plate will increase and result in premature failure by virtue of plate separation accompanied by local shear failure in the concrete along the internal longitudinal steel.

An et al. [22] performed a parametric study to predict the behaviour of composite beams plated for flexural reinforcing, and detected an increase in the stiffness, yield moment,

and flexural strength especially for the beams with a relatively low steel reinforcement ratio.

Results for reinforced concrete beams strengthened with externally bonded FRP reinforcement show different modes of failures and can be summarized as:

1- Crushing of concrete in compression before yielding of the reinforcing steel.
2- Yielding of the reinforcing steel bars in tension followed by rupture of FRP laminate.
3- Yielding of the reinforcing steel bars in tension followed by concrete crushing.
4- Shear or tension failure of the concrete substrate.
5- Diagonal tension failure resulting from shear in the section.
6- Debonding of FRP plates due to vertical section translations resulting from cracking.

Norris et al. [30] investigated the flexural strengthening of RC beams with CFRP sheets, and tested beams that were precracked prior to retrofitting to more closely simulate the field condition. They noted 20 to 100% of increase in strength over the control, unretrofitted beams. They also noted that the orientation of fibers has a major effects on the results, and placing the fibers perpendicular to the cracks in the beam results in the largest increase in both stiffness and strength. A brittle failure was seen to occur due to concrete rupture as a result of stress concentration near the ends of the CFRP.

Chajes et al. [31] studied flexural and shear strengthening of reinforced concrete beams using externally applied FRP sheets. The beam specimens in their experiments were intentionally left under-reinforced to allow failure in flexure. CFRP sheets were applied on the bottom for flexural and on the sides for shear reinforcement. Flexural

reinforcement resulted in 160% increase in the ultimate load, but the failure mode changed from concrete crushing in compression zone to shear failure.

Further studies by Chajes et al. [32] inspected the effect of different fibers on shear strengthening of reinforced concrete beams. Three fibers were studied, including glass, carbon and aramid. Bi-directional fiber fabrics were applied to the bottom and sides of the beams and oriented with the fiber directions at 0/90°. Results showed an increase of 80, 85, and 88% in ultimate strength, respectively, for aramid, glass and carbon fiber fabrics. Moreover, a pair of beams was retrofitted with carbon fiber fabric, but this time oriented at ±45°. This produced a 122% increase in peak load. This study also indicated that an applied FRP material could act as shear, as well as flexural, reinforcement. Furthermore, it showed that a 45° fiber orientation is more effective for such strengthening. The authors acknowledged a number of problems related to FRP plate bonding, like, the requirement of surface preparation to generate a flat surface for bonding, increased costs related to the production of large FRP plates and difficulties in accomplishing a satisfactory bond between the concrete and FRP. On the other hand continuous fiber fabrics can conform to minor irregularities in the surface and are available in rolls of virtually any length. They also produce much stronger bonds with the concrete. This enhanced bonding ability is believed to be linked to the fact that the adhesive actually penetrates into the reinforcement fabric, which it is not true with pre-made FRP plates.

Khalifa and Nanni [33] investigated the wrapping scheme, CFRP amount, 90/0 degree ply combination, and CFRP end anchorage for shear strengthening of full-scale RC beams with T-section. The test results indicated that the externally bonded CFRP

reinforcement could be used to increase the shear capacity of the beams from 35 to 145%. The followings are their conclusions:

- The performance of externally bonded CFRP can be improved significantly if there is adequate anchoring provided.
- A U-anchor system is suggested for situations where the bond and/or development length of FRP are critical.
- Application of CFRP on the beam sides merely gives less shear contribution compared to a U-wrap.
- Although the CFRP amount in one of the beams was 40% of that used in the other, the same strengthening effect was achieved. This indicates that there is an optimum FRP quantity, beyond which strengthening effectiveness is doubtful.
- CFRP strips may be as effective as continuous CFRP sheets in the laboratory, but they are not recommended for field application. Continuous sheets may be safer than strips because the damage to an individual strip would adversely affect the overall shear capacity.
- No contribution was noticed in shear strength for a 0 degree ply.
- A comparison with the test results indicates that the shear design algorithm provides acceptable but conservative estimates.

Boyd [12] investigated the mechanical enhancement of concrete structures retrofitted by sprayed fiber-reinforced polymers and FRP wraps, and noted that although FRP wraps and spray considerably enhanced the strength of structure, the real advantage lies in

enhancement of ductility and capacity to absorb energy. He also noticed that among the continuous fiber wraps, those with fibers oriented at ±45° with respect to the principal direction were not as effective as those with fibers oriented at 0-90°.

Saadatmanesh et al. [30] extensively studied the strengthening of reinforced concrete beams with FRPs. Their studies included shear strengthening, flexural strengthening, analytical predictions approaches [6,23,34-35], and the physical and mechanical properties of various FRP materials [18,36].

One of the major issues related to the use of FRPs for strengthening is the performance of the adhesive bond between the FRPs and the concrete. A number of researchers have studied the characteristics of this bond. Boyd [12] investigated the bond created by the sprayed FRP technique. There are a number of fundamental differences between the bonds created between fabric or FRP plate and concrete and those created by the sprayed FRP technique. For the FRP plate an adhesive layer is used to bond the fabric or plate to the concrete surface, and due to separate application of this adhesive, it essentially creates two bonds; one between the adhesive layer and the concrete surface and the second between the adhesive and the FRP plates or fabrics. Due to the compatibility between the adhesive and the FRP matrix resin, achieving a good bond is relatively easy. However, a strong bond between the adhesive and the concrete is more difficult to achieve. With the sprayed FRP, the adhesive and the matrix resin are the same entity, and results in a single unified bond. For the case of bonding the FRP plates to concrete, many researchers have investigated bond failure either due to applied forces or a severe environment [32,37-40]. The debonding occurs either as peeling failure or shear failure.

Karbhari et al. [38] suggests that the peel test is a more representative measure of the actual bond strength since it is the most common mode of debonding failure in the field.

2.5 – Field Application of FRPs

Many bridges in North America have already been strengthened by FRP wraps [41-44]. McCurry et al. [43] reported on the use of CFRP and GFRP wraps on the Horsetail Creek Bridge, and found that the use of FRP composites for structural strengthening provided a static capacity increases of approximately 150% over the unstrengthened sections. Some of the other observations were as follows:

- Horsetail Creek Bridge beams retrofitted only with flexural CFRP would still results in diagonal tension failure although at a 31% greater load. Since the CFRP was intended to provide flexural reinforcing, it was horizontally unidirectional. The CFRP was wrapped up the sides a sufficient amount to provide resistance across the diagonal tension crack. In addition, the increased stiffness provided by CFRP decreased the deformation and offset cracking by reducing strain in the beam.
- The addition of GFRP for shear was adequate to offset the lack of stirrups and cause conventional RC beams failure by steel yielding at the midspan. This allowed ultimate deflections to be 200% higher than shear deficient control beam, which prematurely failed due to a significant diagonal tension crack.

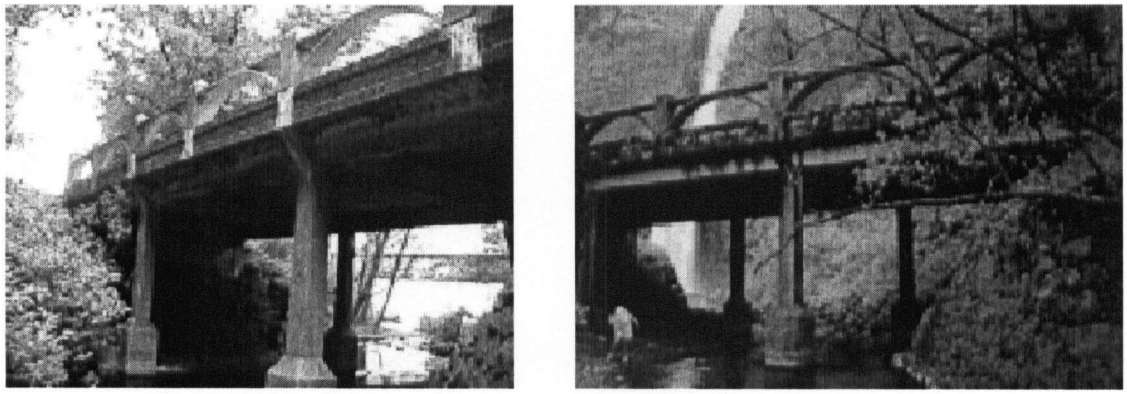

Figure 2.2: Horsetail Creek Bridge [44] (1998, prior to retrofit).

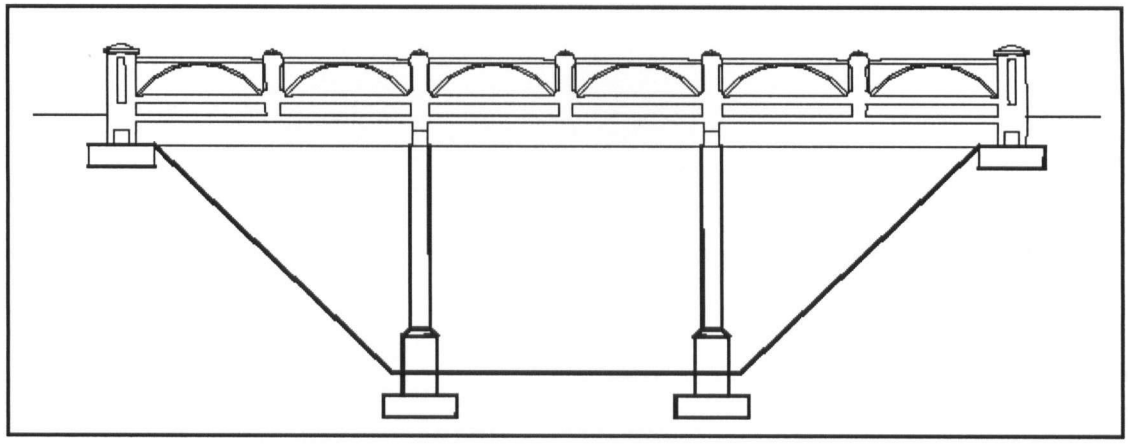

Figure 2.3: Elevation of Horsetail Creek Bridge [44].

- Horsetail Creek Bridge beams retrofitted with both the GFRP for shear and CFRP for flexure well exceed the static demand required by the new traffic loads.
- Load at first crack was increased, primarily due to added flexural CFRP, by approximately 23%. The flexural CFRP reduced the post-cracking deflections, which in turn lowered the strains and stresses in the cross section.

- Addition of flexural CFRP offset the yielding load of steel beyond 33%.
- An imperfect bond was observed from the strain lag of CFRP from the expected plane-section-remain-plane assumption. Due to the extremely small sample size of the experiment (i.e. only four specimens each with different reinforcing), further study is necessary to determine if this effect is of significance in structural analysis and safety.

Application of FRPs does not restrict only on bridges and there are many other structures in the world that have been retrofitted by FRP. Table 2.1 summarizes some of the field applications of FRP external reinforcement that have been reported in the literature [14,45]. As it was shown in the table, most of the documented repairs were made to highway structures and buildings. In these cases, FRP external reinforcement

Table 2.1: Field survey on use of externally bonded FRP in RC flexural members [14,45].

Structure type	Repaired (built)	Country	Problem/need/comments
Hollow box girders (Kattenbusch Bridge)	1987	Germany	Bottom slabs of box girders exhibited wide transverse cracks at working joints; low reinforcement ratio led to yielding of steel in bottom slabs; one joint strengthened with GFRP; four joints strengthened with steel plates; span = 478 m.
Multispan box-beam PC bridge (Ibach Bridge)	1991 (1969)	Switzerland	Bridge strengthened with CFRP after prestressing tendon accidentally damaged; span = 228 m.
RC tall chimneys	—a	Japan	Chimneys strengthened with CFRP for enhanced earthquake resistance; CFRP provided flexural strengthening and confinement for the chimneys.
RC T-beam bridge (Jiezi Bridge)	1992	China	Insufficient bending resistance, wide crack openings, severe deflection; bridge strengthened with GFRP laminates; span = 69.7 m.
RC T-beam bridge (Meixi Bridge)	1992	China	Bridge strengthened to carry higher volume of traffic; bridge strengthened with GFRP laminates; span = 110.33 m .
RC box-culvert (Fujimi Bridge)	1993	Japan	Culvert repaired by applying CFRP sheets onto its sides and soffit.
PC highway bridge	—a	Japan	Bridge repaired with bonded CFRP material.
RC apartment floor	—a	Japan	Floor developed wide cracks (up to 4 cm); CFRP bonded over cracks to prevent crack growth and corrosion of existing steel reinforcement.
RC bridge slab	1993 (1962)	Japan	Insufficient transverse reinforcement; cracking developed in longitudinal and transverse directions on lower faces; CFRP sheets were bonded to bottom of slab in both directions.
RC building slab	—a	Switzerland	Slab strengthened with CFRP prior to cutting rectangular hole in slab.
RC bridge (Shirota Bridge)	1994	Kyushu, Japan	Bridge strengthened with four CFRP layers to increase its load rating from 20 to 25 tons; span = 23.8 m.
Cantilevered RC wing slab (Hata Bridge)	1994	Japan	Soffit of slab was strengthened with two piles of carbon fiber sheets to accommodate larger windbreak walls; total concrete area of 110 m2 was covered with CFRP material.
RC bridge deck	1994	Japan	Deck strengthened with two plies of carbon fiber sheets to increase load rating of structure; soffit of deck also had significant map cracks; total concrete area of 164 m2 was covered with CFRP material.
RC beams and deck of waterfront pier (Wakayama Oil Refinery)	1994	Japan	Beams and deck repaired with single ply of CFRP sheets to arrest steel reinforcement corrosion; concrete area of 390 m2 (beams: 300 m2; deck soffit: 90m2) was covered with CFRP material.
Concrete lining of twin tunnels (Yoshino Route)	1994	Kyushu Island, Japan	FRP reinforcement was used to strengthen and stiffen lining as well as repair cracking resulting from fluctuations in underground water pressure; total concrete area of 1,090 m2 was covered with FRP material.

Table 2.1: (Continued)

Structure type	Repaired (built)	Country	Problem/need/comments
Floor slabs in shopping center	—a (1968)	Switzerland	RC slabs, 350 mm thick, strengthened with 1.2-mm-thick CFRP strips prior to cutting openings in slabs to accommodate installation of freight elevator and escalator; part of multistory building was transformed into new shopping center.
RC beams	—a	Phoenix	Corrosion-damaged RC beams in nuclear power plant were strengthened in flexural and shear with epoxy-bonded E-glass fabric.
RC beams (Fear Not Mills Road Bridge)	—a (1994)	Butler County, Ohio	Bridge has conventionally reinforced precast concrete box-beam superstructure; deck comprised 10 box beams; two exterior beams strengthened in flexure using graphite/epoxy system; span = 8.05 m.
RC double-T beams	—a	South Florida	Beams support condominium; beams severely corroded, with concrete spalling and loss of cross section; concrete section restored, and single layer of CFRP was bonded to cap surface.
PC bridge (I-95 Bridge over Blue Heron Boulevard)	—a	West Palm Beach, Fla.	Exterior and first interior girders severely damaged due to collision of oversized vehicles (about 20% strength loss); strength of bridge restored to original capacity using two layers of CFRP; repair was completed within 6 working days.
RC T-beams (concrete bridge)	—a	Alabama	Thirty-year-old bridge with 13 simple spans, each 10.34 m in length; each span is composed of four RC T-beams; T-beams showed significant flexural cracking; one span was retrofitted with CFRP and GFRP applied to bottoms and sides of T-beams, respectively.
PC box-beams (Foulk Road Bridge)	—a	Wilmington, Del.	Bridge superstructure composed of 24 PC box-beams; beams showed cracking due to lack of transverse reinforcement; five beams retrofitted with one layer of CFRP, and one beam retrofitted with two layers; CFRP sheets were installed with fibers running transverse to beam; span = 16.5 m.
PC beams (Southshore Mall Parking Garage)	1996	Massachusetts	Three RC concrete beams (0.46 3 0.91 3 18.29 m3) could not be posttensioned to design specification; several tensioning strands had failed; three beams were strengthened with two to four 76-mm-wide CFRP strips.
Precast-concrete-girder bridge	—a	Alberta, Canada	Ten precast concrete girders were strengthened in shear using CFRP sheets; some repaired girders showed notable shear cracks; total cost of bridge repair was estimated to be $70,500; alternative rehabilitation method using external steel stirrups would have cost $100,000.
RC beams (Gazzette del Mezzogiorno Exhibition Pavilion)	1996 (1960)	Bari, Italy	RC beams supporting 35.45 3 35.00 m2 two-way waffle slab; beams suffered from reinforcement corrosion, concrete spalling, and deficient shear reinforcement; conventional steel rebars were used to replace corroded steel, and externally bonded CFRP was used to strengthen beams in shear.

Table 2.1: (Continued)

Structure type	Repaired (built)	Country	Problem/need/comments
PC bridge girders	1996	Rome, Italy	Bridge has four PC girders (1.0 3 1.5 3 10.5 m3) that were damaged by vehicularimpact; for each beam, three (0.33 3 3.00 m2) CFRP sheets were bonded longitudinally to soffit to make up for lost prestress, and four (0.16 3 3 m2) strips were bonded transversely around three beam sides.
PC balcony slabs	—a	Germany	RC slabs, 140-mm-thick, strengthened with 1.2-mm-thick CFRP strips; insufficient reinforcement led to excessive deflection (15–30 mm).
Highway deck slabs (Hiyoshigura Viaduct)	—a	Tokyo	CFRP sheets were used to strengthen deck slabs along tall Hiyoshigura Highway Viaduct.
Concrete precast roof structure	1996 (1930)	Winnipeg, Manitoba, Canada	Roof structure strengthened with CFRP to accommodate installation of large equipment on existing roof, which created significant snow drift load.
PC bridge girder (Overpass No. 38/18 on Highway #10)	1996 (1972)	France	Bridge consists of eight PC girders that are 16.25 and 9.2 m long; CFRP external reinforcing system was used to strengthen girders and repair longitudinal cracks in soffits of certain beams as well as vertical cracks in webs near supports.
RC deck (Oberriet Bridge)	1997 (1963)	Oberriet, Switzerland	Bridge deck, supported by steel girders, is subject to increasing loads; deck was strengthened by adding 80-mm top concrete and bonding CFRP strips transversely on bottom surface between steel girders.
RC box girder (Furstenland Bridge)	—a (60 year old)	Bauhalle, Switzerland	Parts of bridge suffered significant reinforcing steel corrosion caused by trapped chloride contaminated moisture; two CFRP strips were bonded to lower portion of inside walls of box girder to provide torsional stiffness during replacement of bottom flange of girder , without closing bridge.
RC bridge deck	1997	South Carolina	Bridge barely carrying legal loads in the state; bridge deck strengthened using two layers of CFRP to carry one 36-ton, three axle truck.
RC beams of Webster Parkade (parking garage)	—a (1959)	Sherbrooke, Quebec, Canada	FRP composites were used to strengthen beams that did not conform to present standards with respect to bending and/or shear capacities.
RC slab of parking garage	—a	Missouri	RC slab strengthened with two double-ply CFRP strips to correct deficiency in number of steel tendons in structure.
Parking structure	—a	Oklahoma City	Parking structure will be upgraded using FRP composites; 18,500 m2 (approximately 200,000 ft2) of FRP material will be required for this project.
RC slab (strip mall)	—a	South Florida	CFRP sheets were added to top and bottom surfaces of RC slab where opening was cut to accommodate installation of restaurant ventilation system; CFRP was used to strengthen edges of openings and control cracking of corners.
RC pier caps (Manette Washington State Bridge)	—a	Washington, D.C.	FRP was used to strengthen severely corroded pier caps; strengthening was required to upgrade shear, flexural capacity and ductility as per DOT specifications.

Table 2.1: (Continued)

Structure type	Repaired (built)	Country	Problem/need/comments
PC two-way flat slab (office building)	—a	North Carolina	FRP sheets were installed between all columns in positive moment area and in negative moment area (where required) to increase specified load of slab from 50 psf to 120 psf.
RC pier (Highland Drive Bridge)	—a	Salt Lake City	CFRP was used to rehabilitate bridge pier damaged by freeze-thaw and severe corrosion; rehabilitation included wrapping of columns, cap beam-column joints, and cap beam haunches with CFRP material.
RC slab of precast concrete box culvert (Greenbridge Subway)	—a (1960s)	United Kingdom	CFRP was used to strengthen RC slab in flexure to meet current highway loading standards.
RC smoke stacks of cement plant	—a	San Antonio	Cement plant was to be renovated into retail and entertainment complex; three severely cracked RC stacks were repaired and strengthened in flexure as well as shear using GFRP.
RC box girder (Maryland Bridge)	—a	Winnipeg, Manitoba, Canada	The 27-year-old girders of this bridge were analyzed and found to be deficient in shear capacity using the AASHTO code.
RC deck slab (Country Hills Boulevard Bridge)	—a	Calgary, Alberta, Canada	One of the main problems with this aging bridge was that its thin deck would be over-stressed in lateral bending under full loads. Conventional strengthening methods presented logistical problems and so, an uniintrusive strengthening method of applying carbon FRP strips was chosen.
RC T-beams (Sainte Emelie de lEnergie bridge)	1998	Quebec, Canada	The four T-beams were reinforced in order to demonstrate the potential increase in bending and shear strength as was requested.
Roof beam (Centennial Park School & Gabrielle Roy School)	1998	Quebec, Canada	Glass FRP sheets were used to strengthen 1,800 beams in two similar schools in Chateauguay, Quebec that were damaged as a result of the 1998 ice storm. Following the storm, previously existing shear cracks in the roof beams widened and, in a few cases, partial failure occured.
Beams, columns (Pollution Control Plant)	—a	Ontario, Canada	The installation of a new centrifuge pump necessitated strengthening beams, columns, and a slab. Carbon FRP sheets were applied in three configurations and then covered in a cement based mortar match the concrete.

a: Not reported.

was used to stop crack growth, reduce cracking which is caused by insufficient transverse and/or flexural reinforcement, control excessive deflection, increase load-carrying capacity, compensate for accidental loss of prestress, adapt a structure for a different function, and repair corrosion damage [14].

2.6- FRP Sprays

Recently a novel technique has been developed at the University of British Columbia for retrofitting of old and deteriorating structures Sprayed Fiber Reinforced Polymers. This technique has shown enhancement of ductility and energy absorption capacity compared to the conventional techniques [46-48]. Some of the other advantages of this technique compared to traditional wrapping technique [10-13] are:

- The bond between concrete and FRP is much stronger due to elimination of extra layer between FRP and adhesive surface.
- 2-Dimensional isotropic random distribution of fibers giving an isotropic material in the plane of its application.
- Fiber volume fraction and fiber length can be easily varied depending on the application.
- Ease of application especially around the corners and difficult and rough areas.
- Minimal surface preparation needed and in some cases not at all.
- More economical.

2.7 – Finite Element Modeling of Bridge Elements

Availability of new software packages has created possibilities of use of Finite Element Modeling techniques in studying a wide variety of complicated structural analysis problems especially in retrofitting techniques for Bridges [49-56]. Although most softwares are well known and efficient to use, ANSYS has proven to be the most

effective among the others in modeling the complex interaction between Concrete and FRP plates or laminates.

Zhao et al. [49] studied the fatigue crack performance of the Arkansas River Steel Bridge and verified their proposed repair methods by a finite element analysis. Meng et al. [50] investigated the seismic response of a skew reinforced box girder bridge by finite element models. The effects of superstructure flexibility, substructure boundary conditions, structural skewness and stiffness eccentricity were evaluated using spectral analyses. The dynamic response of this under crossing was studied by response spectrum analysis using SAP2000 finite element program. Four-node quadrilateral shell elements, which combined separate membrane and plate-bending behaviors, were used to model the bridge deck and a frame element were used to model the cap beams and supporting columns. Based on their study, the following conclusions were drawn:

- The effect of superstructure flexibility is important and should not be ignored in a dynamic analysis.
- The displacement of the deck is underestimated by these simplified models.
- Boundary conditions of the supporting columns play a very important role in the seismic behavior of skew bridges.
- Skewness also plays an important role in the dynamic behavior of a bridge.

Qiao et al. [51] proposed a systematic analysis and design approach for single-span FRP deck/stringer bridges. They used 8-node isoparametric layered shell elements to model the deck using NISA finite element program. To validate the accuracy of the results an actual deck was also tested under centric and asymmetric loading. The results for

measured displacements and strains indicated a good correlation between experimental data and FE models. Halling et al. [52] studied the dynamic behavior of bridge bent using finite element, while Hibino et al. [53] investigated the flexural behaviors of concrete by the use of isoparametric crack element. In all these cases, the results compared well with the experimental findings.

Arduini et al. [54] numerically modeled and studied the failure mechanism of RC beams strengthened with FRP plates. The numerical model was based on finite element analysis using the smeared crack approach. They noted that for FRP flexible sheets, mechanical and geometrical properties refer to the fiber and not the composite, and since no experimental data was available for the determination of the shear capacity at the concrete-adhesive interface, the value of 4.5 MPa was chosen which showed good correlation, but the need to improve the knowledge on adhesive performance was stressed. Complimentary to the findings of Arduini et al. [54], the complexity in finite element analysis of reinforced concrete structures due to the difficulty in characterizing the material properties was also noted in Reference [55].

Much effort has been made in search of a realistic model to foresee the behavior of reinforced concrete structures. Due to the composite nature of concrete, proper modeling of such structures is a challenging task. ANSYS provides a three-dimensional eight nodded solid isaparametric element, SOLID65, to model the nonlinear response of brittle materials based on constitutive model for the tri-axial behavior of concrete after William and Warnke [56]. The element includes a smeared crack analogy for cracking in tension zones and a plasticity algorithm to account for concrete crushing in the compression zones. Each element has eight integration points at which cracking and crushing checks

are performed. The element behaves in a linear elastic manner until either of the specified tensile or compressive strengths limits is exceeded. Cracking or crushing of an element is initiated once one of the element principal stresses, at an element integration point, exceeds the tensile or compressive strength of the concrete. Cracked or crushed regions, as opposed to discrete cracks, are then formed perpendicular to the relevant principal stress direction with stresses being redistributed locally. The element is thus nonlinear and requires an iterative solver. The magnitude of shear transfer across a crack can be varied between complete shear transfer and no shear transfer at a cracked section. The crushing algorithm is analogous to a plasticity law. Therefore, once a section has crushed, any further application of load in that direction develops increasing strains at constant stress. Following to the formation of an initial crack, stresses tangential to the crack face may cause a second, or third, crack to happen at an integration point. The internal reinforcement can be modeled as an additional smeared stiffness distributed through an element in a specified orientation or alternatively by using discrete truss bars or beam elements connected to the solid elements. Fanning [55] and Barbosa et al. [57] investigated the nonlinear models of RC beams using SOLID65 concrete element in ANSYS program and compared it to experimental tests. Fanning [55] found that the optimum modeling, in terms of controlling mesh density and accurately locating the internal reinforcement, was to model the primary reinforcing in a discrete manner. Hence for ordinary reinforced concrete beams all internal reinforcement should be modeled discretely. In terms of using finite element models to predict the strength of existing beams the assignment of suitable material properties is critical. He found that for a known compressive strength of concrete that can be measured experimentally,

existing formulas for the Young's modulus and concrete tensile strength are sufficient for inclusion in the numerical models. He also found a good correlation between test and numerical results but noted sensitivity to the Young's modulus of concrete and the yield strength of the reinforcement.

Other than the researchers cited here, there are many others who have studied the use of FRP for repairing and retrofitting of reinforced concrete beams. But they all come to one conclusion that the use of FRP for strengthening of reinforced concrete beams is an effective, economical and very promising technique. Therefore, further discussion of these other investigations were not carried out due to either the repetitive nature of the results or due to the fact that many have analyzed very specific issues that do not directly apply to the sprayed FRP technique discussed here.

3

EQUIPMENT AND MATERIALS

3.1 – Equipment

Figure 3.1 shows the FRP spraying equipment that was mounted on a truck. There are three basic components: resin pump, the catalyst pump, and the chopper gun unit. All three major components are operated by compressed air. No electricity is needed for the machine unless an optional resin heater is needed for placement in cold weather conditions (recommended below 16°).

The resin line, the catalyst line and the air line are being fed into the spray gun separately. As it is shown in Figure 3.2, the spray gun has a chopper unit built on top that is also operated by compressed air. The resin and catalyst pass through the gun block separately and do not actually come into contact until they reach the tip of the nozzle, the mixture then exits the nozzle at high speed and lands on the surface of

concrete element. There is also a solvent line built in the nozzle to wash out the resin and catalyst mixture for cleaning. The equipment does not require disassembly or major cleaning unless it is going to remain idle for an extended period of time.

Glass fibers are fed in the form of one or two rovings (depending on the fiber percentage required for the operation) into the nozzle where they are chopped by rotating blades. The length of the fibers can be adjusted from 8 to 48 mm. The chopped fibers are forced out of the nozzle by compressed air. On the chopper unit there are adjustment knobs for adjusting the speed of rollers and the air pressure which controls the overall fiber volume fraction in the finished composite.

3.2 - Reinforced Concrete Properties

The properties used in this investigation were assumed to be a concrete with lightweight aggregate, a density of 1900 kg/m^3, and a compressive strength of 20 MPa. The channel beam had three different imperial sizes of steel reinforcement that ranged in tensile strength from 304-408 MPa. The reinforcement ratio based on crude old drawings was assumed to be 1%. The spacing of shear reinforcement ranged from 125 mm at the ends of the beam to maximum of 760 mm in the center portion of the beam.

3.3 – Fiber Reinforced Polymers

The GFRP sprayed on sides of the girders in this study consisted of 30% glass fiber, 68.8% resin and 1.2% catalyst by volume. The catalyst was needed to cure the resin, which in turn formed the matrix to encapsulate the fibers inside. In addition to this

composition, a coupling agent (Derakane 8084) was used to improve the bond between the concrete and the GFRP.

3.3.1 - Resin

The resin used was a K-1907 polyester resin manufactured by Ashland Chemical Canada Ltd. The mechanical properties of the resin are listed in Table 3.1 [58], although these properties refer to a clear casting not sprayed resin. The properties of a sprayed resin varied considerably when tested in a laboratory [12].

3.3.2 - Catalyst

The catalyst used to induce curing of the resin was Methyl Ethyl Ketone Peroxide (MEKP). The MEKP [59] used in this experiment was manufactured by Ashland Chemical Canada Ltd. The GFRP used to spray the girders contained 1.2% by weight MEKP.

3.3.3 - Coupling Agent

The coupling agent used was Derakane 8084, which is a common coupling agent used with GFRP for the purpose of reinforcing concrete structures. Derakane 8084 is a vinyl ester resin that is manufactured by The Dow Chemical Company. Unfortunately there is not sufficient information available on the bond strength between the concrete. The mechanical properties of this coupling agent are listed in Table 3.2 [60].

3.3.4 - Glass Fiber

The fiber used for the spraying of the girders was Advantex® 360RR chopper roving, which is manufactured by Owens Corning. The mechanical properties are listed in Table 3.3 [61]. The spray consists of a polyester resin and the catalyst with glass fibers randomly distributed. Overall the Sprayed GFRP was assumed to have isotropic material properties with an elastic modulus of 33700 MPa.

3.3.5 - Solvent

A solvent is mandatory for cleaning purposes when spraying with resins. The spraying equipment requires periodic flushing to prevent resin from hardening within the nozzle of the gun. The solvent for this project was acetone, supplied by Ashland Chemical Canada Ltd.

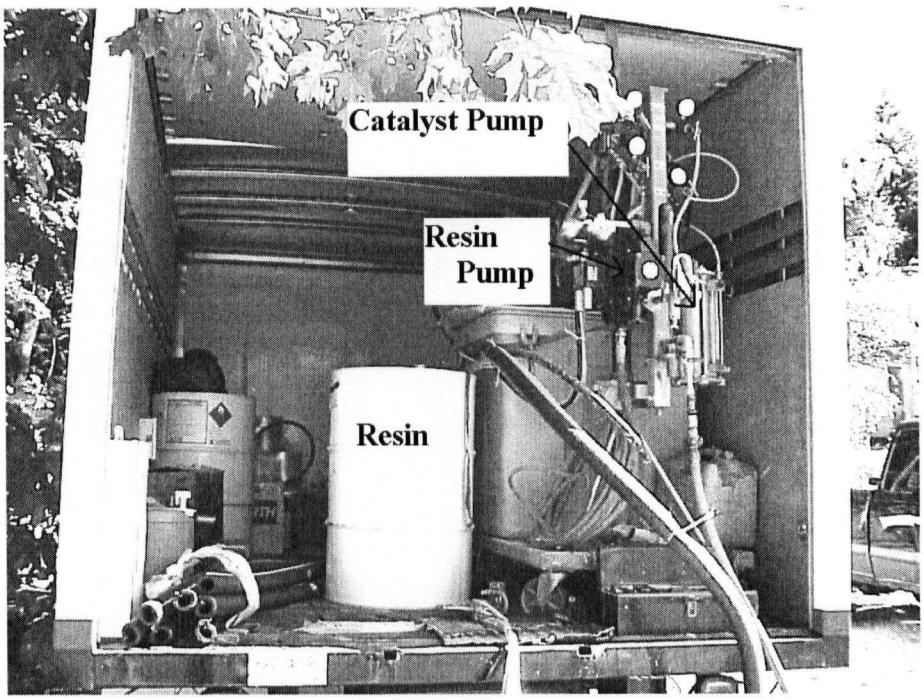

Figure 3.1 : GFRP spraying equipment.

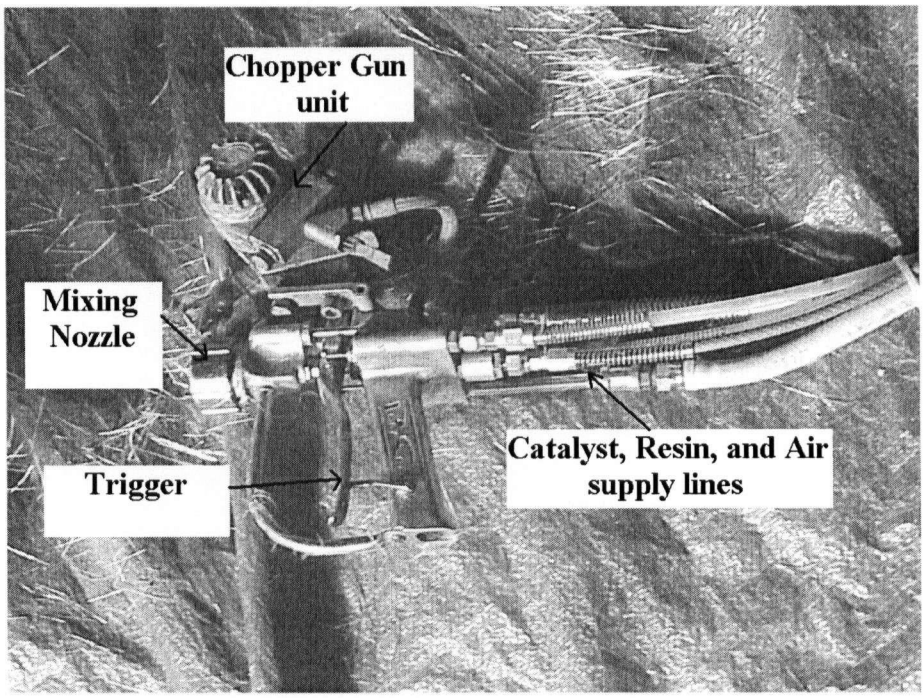

Figure 3.2: GFRP spraying gun assembly.

Table 3.1: Mechanical and material properties of K-1907 Polyester Resin.

Properties of K-1907 Polyester Resin.		
Property	**Value**	**Unit**
Density	1070	kg/m^3
Tensile Strength	75.8	MPa
Elastic Modulus	3.77	GPa
Shear Strength	48	MPa
Elongation at Failure	2.4	%

Table 3.2: Mechanical and material properties of Derakane 8084 Vinyl Ester Resin.

Properties of Derakane 8084® Vinyl Ester Resin.		
Property	**Value**	**Unit**
Density	1150	kg/m^3
Tensile Strength	72	MPa
Elastic Modulus	4.6	GPa
Elongation at Failure	10	%
Adhesive Strength		
Carbon Steel	1430	psi
304 Stainless Steel	1530	psi
2024T3 Aluminium	970	psi

Table 3.3: Mechanical and material properties of Advantex® Glass Fiber.

Properties of Advantex® Glass Fiber		
Property	**Value**	**Unit**
Density	2620	kg/m^3
Diameter	11	μm
Tensile Strength	3100-3800	MPa
Elastic Modulus	80-81	GPa
Elongation at Failure	4.6	%

4

BRIDGE REPAIR

4.1 – The Safe Bridge

The Safe Bridge consists of one span channel beam bridge built in 1955 (Figure 4.1). The span is 7200 mm and there are 10 channel beams, each 910 mm wide. There is a sidewalk separated from traffic by a concrete curb. The width of bridge including the sidewalk is 9100 mm. The clearance under the bridge is about 1200 mm at the upstream and 2100 mm at the downstream end. There were four girder legs with fairly severe spalling over a length of about two meter in each case. The rest of the girders had localized spalling. Stirrup spacing in girders is quite far apart. The concrete is light weight concrete. The longitudinal reinforcing is a bit unusual; it is square shaped instead of round (approx 25.4mm x 25.4mm). It has small bumps on the surface at approximately 50.8mm spacing. The deck has an asphalt overlay and there was some water leaking through to the underside of the girders. As seen in Figure 4.2, the concrete on the girders was severely spalled and the girder surfaces needed to be rehabilitated

before the application of spray GFRP. In addition to spalling, noticeable cracking in the girder sections close to the support was observed. It was decided to repair the girder sections by high performance hybrid fiber reinforced mortar before applying the sprayed GFRP [62].

4.2 - Repair Procedure

4.2.1 – Laboratory Testing of GFRP Materials

Tests have been performed at UBC Materials Lab [62] to characterize the sprayed GFRP. GFRP was sprayed vertically on concrete panels (square panel of size 610 mm x 610 mm and the thickness of 60 mm) to 10 mm thickness. Polyester resin was used as the matrix. Chopped glass fiber of 50 mm long was used to reinforce the matrix. Flexural toughness tests were carried out on beam specimens 60 mm x 60 mm x 300 mm sawed from concrete panels and flexural strength and flexural toughness factor were calculated (Table 4.1). It was noted that a 10 fold increase in the flexural strength can be achieved with a 10 mm thickness of GFRP. Moreover, a remarkable increase in fracture energy (42 times) was noted.

4.2.2 - Surface Preparation, Instrumentation and Patching Repair

Prior to patch repair with hybrid fiber-reinforced mortar, the loose cover concrete was removed using jackhammer and scales on steel surface were cleaned thoroughly by steel brush so that fiber reinforced mortar bonded well with substrate (Figure 4.2). For instrumentation, strain gauges were welded on six selected girders at the mid-span. After welding, the gauges were thoroughly covered by waterproof packing material as seen in

Figure 4.3. The SIKATOP 123 traffic patch product was used with carbon and polypropylene fibers to repair the patches on girders. It is a fast setting, non-sag mortar for structural repair of vertical and overhead concrete surfaces (Figure 4.4).

The bridge was tested for static and dynamic loading before and after applying the spray and for the purpose displacement transducers were installed on a wooden beam, as seen in Figure 4.5. For each static or dynamic load position, displacements and strains (Figure 4.6) were measured on six different girders (Girder # 2, 4, 6, 8, 10A, 10B). The mid-span was chosen for measurements where the displacements and strains would yield a maximum value. Six displacement transducers and six strain gauges were then connected to a computer and calibrated (Figure 4.7). The displacement transducers were removed after the bridge testing whereas the strain gauges are now a part of the bridge.

4.2.3 - Application of GFRP on Bridge Girders

The spraying equipment was operated from a truck standing nearby the bridge. Polyester resin, catalyst and air were conveyed to the target using considerably long hoses. Tow of Glass fibers were chopped to 50mm long fibers and sprayed simultaneously with the resin and catalyst. Volume fraction of fiber was kept at 30% by weighing of glass fibers while the spray process continued. Figure 4.8 shows the spray operation. The sprayed surfaces were finished using a hand held roller. The finished surfaces of first two girders (Girder # 1 and 2) can be seen in Figure 4.9. From the ten girders, girders #1 and 2 were fully sprayed with GFRP; whereas girders # 3 were sprayed onto one of the channel legs only. The other channel legs of girders # 3, and the remaining girders # 5, 6, 7, 8, 9, and 10 were retrofitted by GFRP mats with the same fiber volume fraction as the spray

(Figure 4.10). Figure 4.11 shows the various stages of mat placement on the girders. Unlike spraying technique, this technique was time consuming due to the fact that the desired thickness could be achieved through number of layers. Also, a large amount of air was entrapped between the layers, in this technique. The finished surface was poor and mats at the ends of girders couldn't be tapered.

4.3 - Loading Conditions

Two tests were conducted by UBC and Ministry of Transportation and Highways of BC (MOTH). They would be referred to as the "Static test", and the "Rolling test". For each test, strain data and mid-span deflection data were collected with a full truck at six static load positions, and for 3 roll tests on the Bridge. To measure the damage of bridge and the effectiveness of repair by sprayed fiber reinforced plastics, a fully loaded dump truck weighing 28.0 ton was used to apply standard truck loading on the bridge. As per Canadian Standards Association [3], the 3-axle truck, with two closely spaced rear axles was chosen. The distance between the front axle and the first rear axle is 4.67 m, and the distance between the rear axles is 1.35 m. Figure 4.12 shows the schematic of the truck and its load distribution. Along the length of the bridge, two truck positions were investigated, with the rear two axles placed successively at the mid-span. It was intended to record maximum deflection at the mid-span with the truck being placed as eccentric as possible (in the transverse direction). It was decided to include at least 3 transverse positions, including mirror image eccentric positions, and the truck placed centrally. The loading positions are shown on Figure 4.13.

4.3.1 - Static Load Test

For each static loading position, all gauges were read an average of 127 times per second for a total of 31 seconds by a computer. The static loading positions of the 28-ton, three-axle truck are as follows:

In the Westbound lane (tightly against upstream curb)

Truck directly over girders 8 and 10.

Load Position 1 Second rear axle at mid span

Load Position 2 First rear axle at mid span

In the Eastbound lane (tightly against downstream curb)

Truck directly over girders 4 and 6.

Load Position 3 Second rear axle at mid span

Load Position 4 First rear axle at mid span

Eastbound (truck centered symmetrically over bridge double lane width)

Truck directly over girders 6 and 8.

Load Position 5 Second rear axle at mid span

Load Position 6 First rear axle at mid span

4.3.2 - Rolling Load Test

In addition to the six static loading tests, three dynamic rolling tests were also performed at low speeds (5-10 km/h). The first test, "ROLL 1", involved the truck running along closely to the upstream curb of the bridge (i.e. closest to girder # 10). The second test, "ROLL 2", was performed along the down stream curb, and the third test, "ROLL 3", took place along the centreline of the bridge.

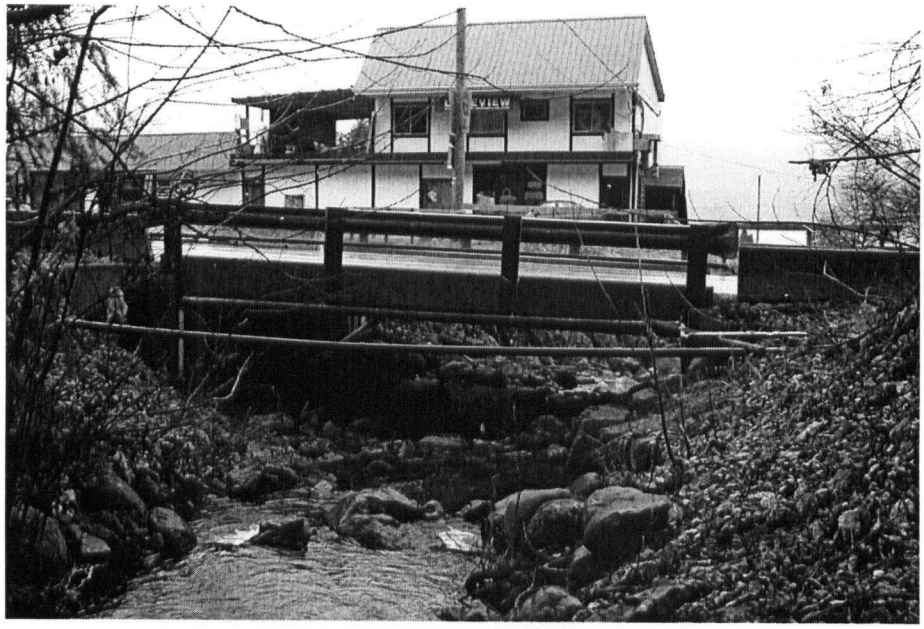

Figure 4.1: View of Safe Bridge in Duncan, British Columbia.

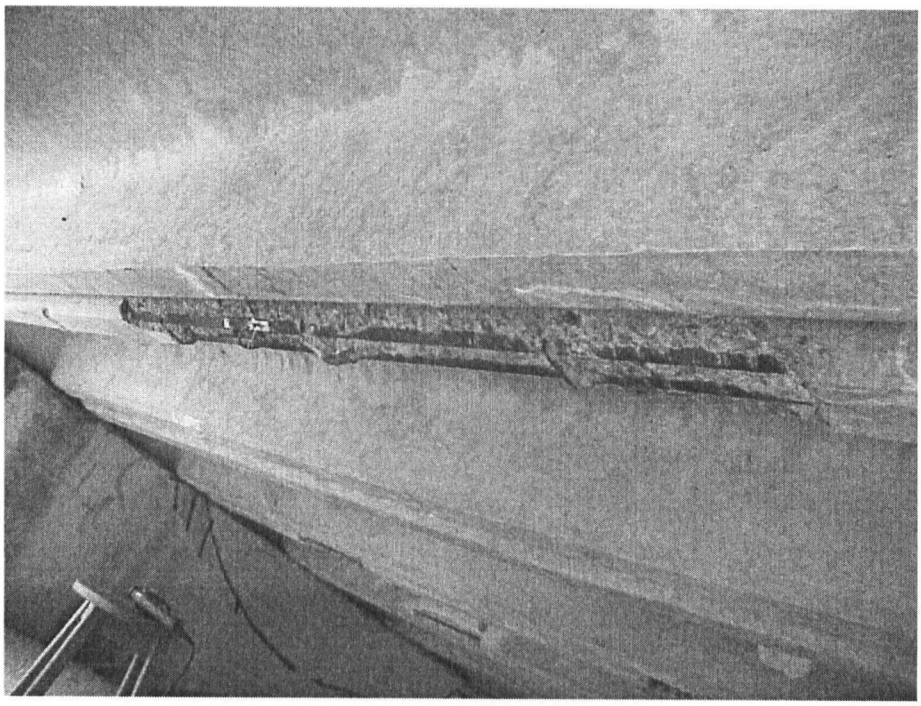

Figure 4.2(a): Longitudinal steel rebar exposed at mid-span.

Figure 4.2(b): Longitudinal and stirrup reinforcement exposed near support section.

Figure 4.2(c): Longitudinal and stirrup reinforcement exposed at support section.

Table 4.1: Properties of FRP Sprayed Beam (60 x 60 x 300 mm) Specimens [62].

Flexural Strength (MPa)		Flexural Toughness Factor (MPa)
	24.56	14.13
	30.42	15.25
	31.01	13.05
	25.98	14.13
	32.93	20.08
	35.62	15.27
	31.26	14.98
	29.52	15.35
	28.11	14.54
Mean	29.93	15.20
COV(%)	10.70	12.30

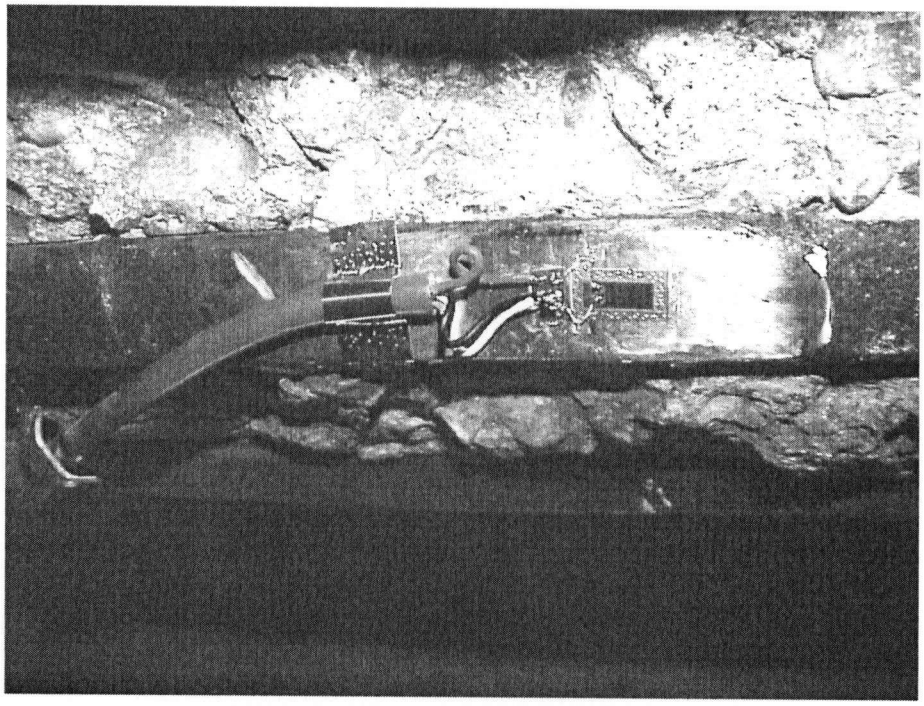

Figure 4.3(a): Strain gauge was mounted on well-prepared steel surface.

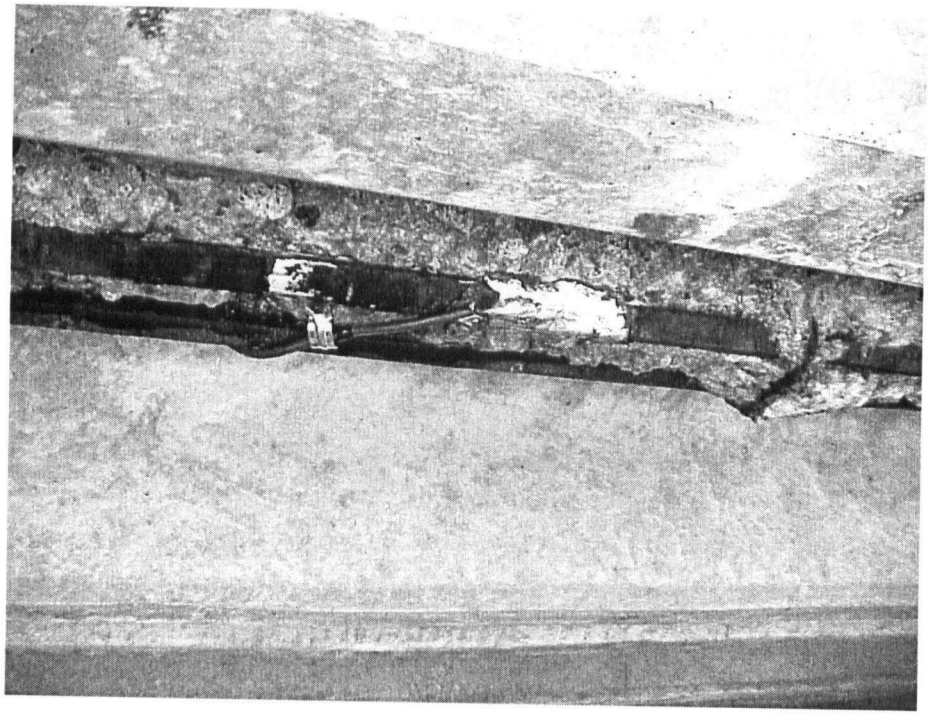

Figure 4.3(b): Strain gauge was protected using waterproof material.

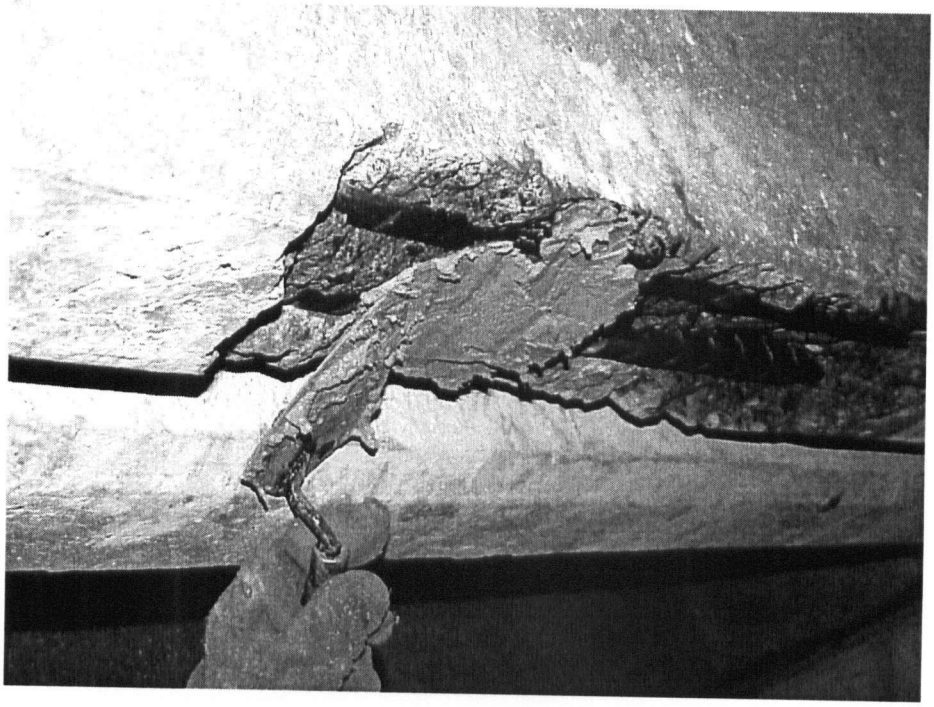

Figure 4.4(a): Applying hybrid fiber reinforced mortar on the damaged surfaces.

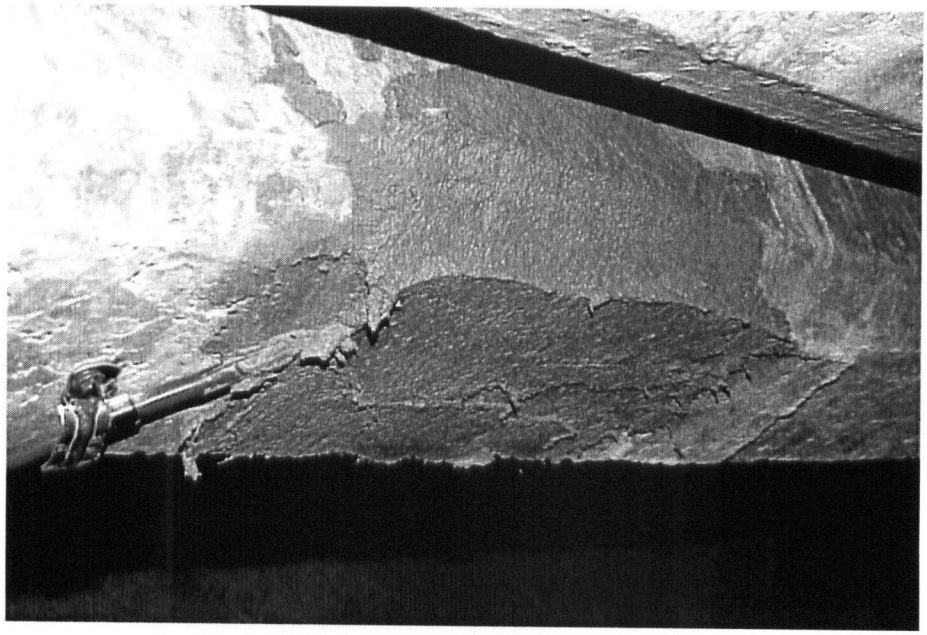

Figure 4.4(b): Applying hybrid fiber reinforced mortar on the damaged surfaces.

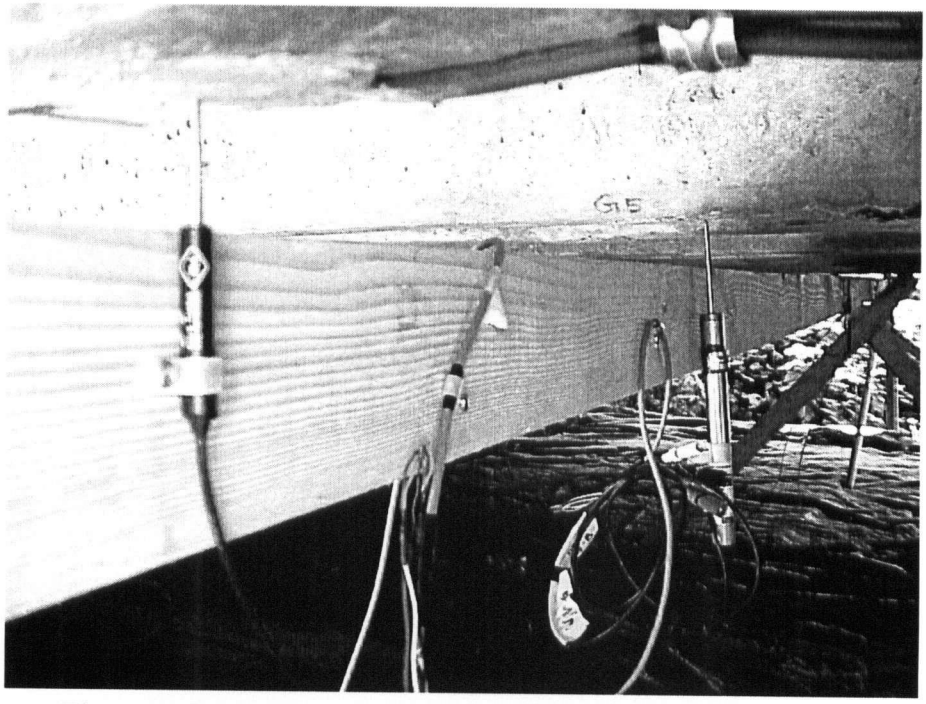

Figure 4.5: Location of six transducers along the mid-span.

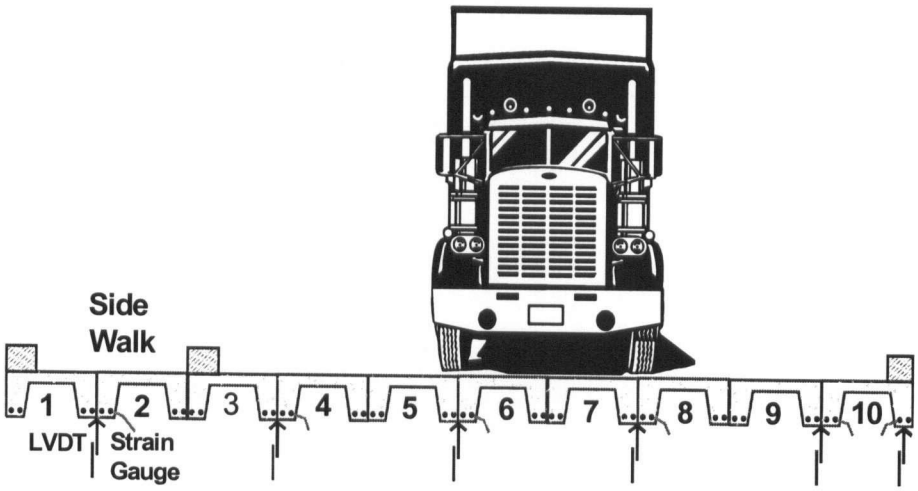

Figure 4.6: Location of six transducers and strain gauges along the mid-span.

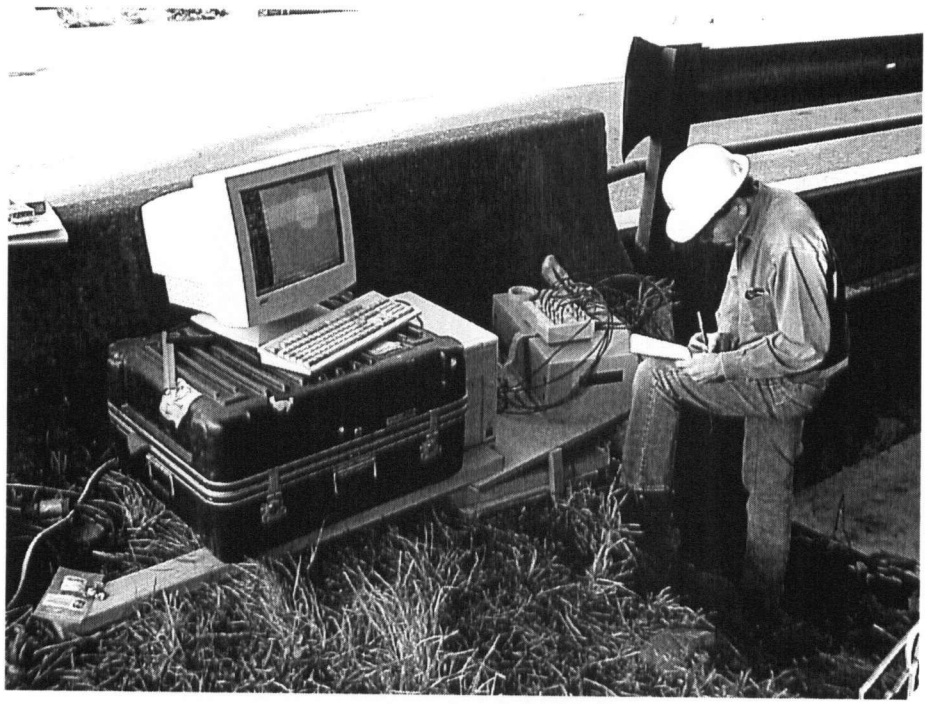

Figure 4.7: Data recorded using a data acquisition system.

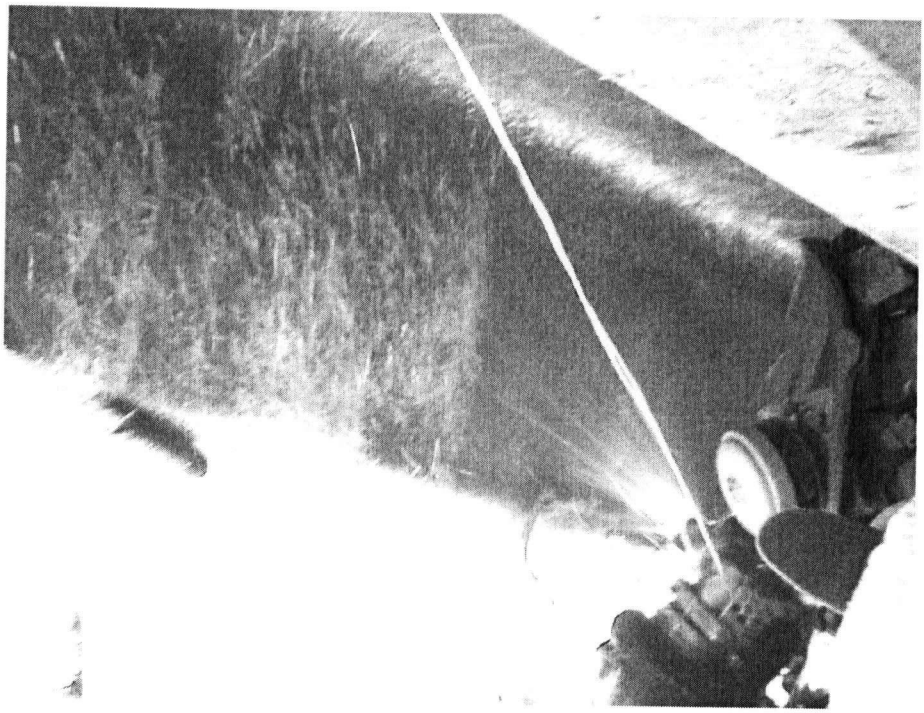

Figure 4.8: Spraying GFRP on the girder legs.

Figure 4.9: Finished surface of sprayed GFRP.

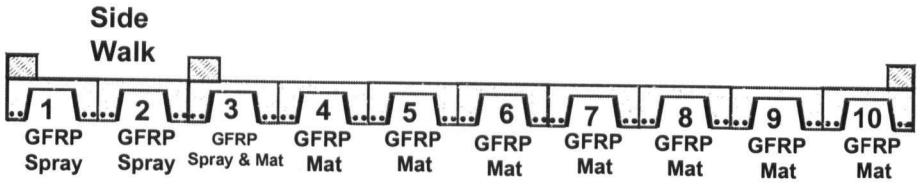

Figure 4.10: Final configuration of sprayed and wrapped girders.

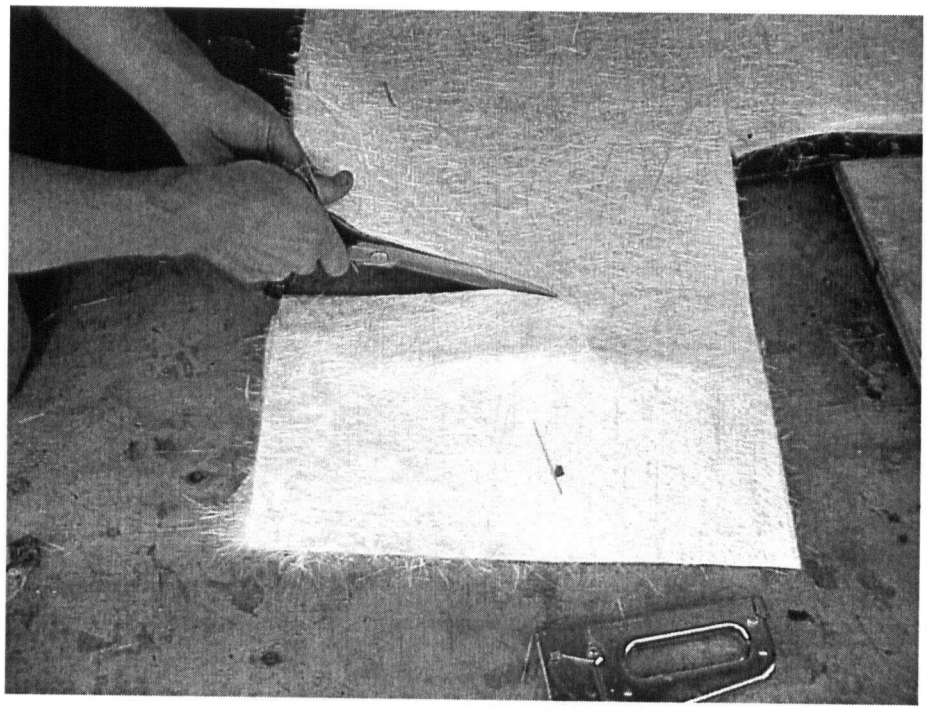

Figure 4.11(a): Cutting the glass fiber fabric to desired dimension.

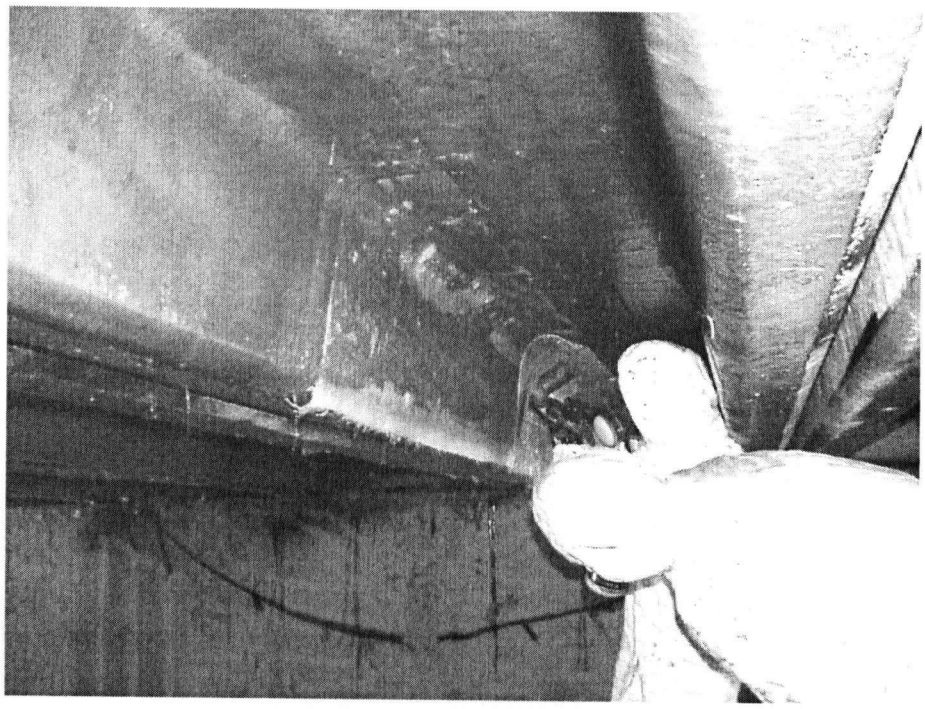

Figure 4.11(b): Placing the GFRP mat on the girder legs.

Figure 4.11(c): The finished surface of the wrapped GFRP mat.

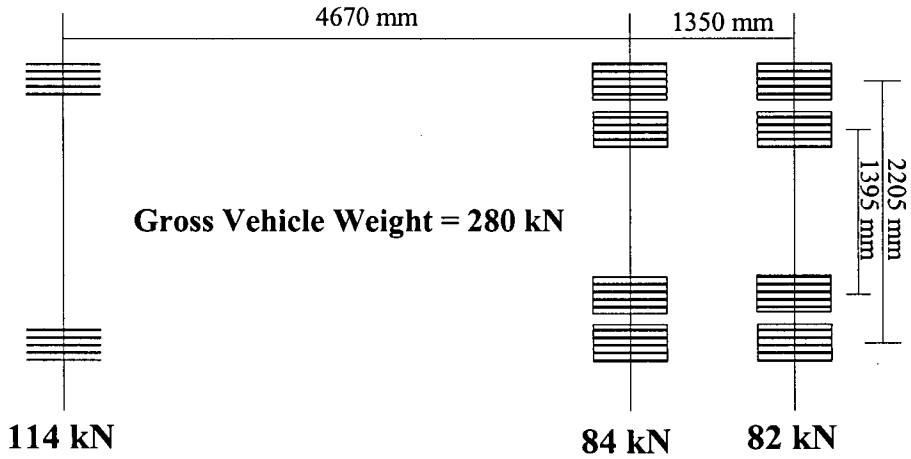

Figure 4.12: Dimensions and weight distribution of the truck.

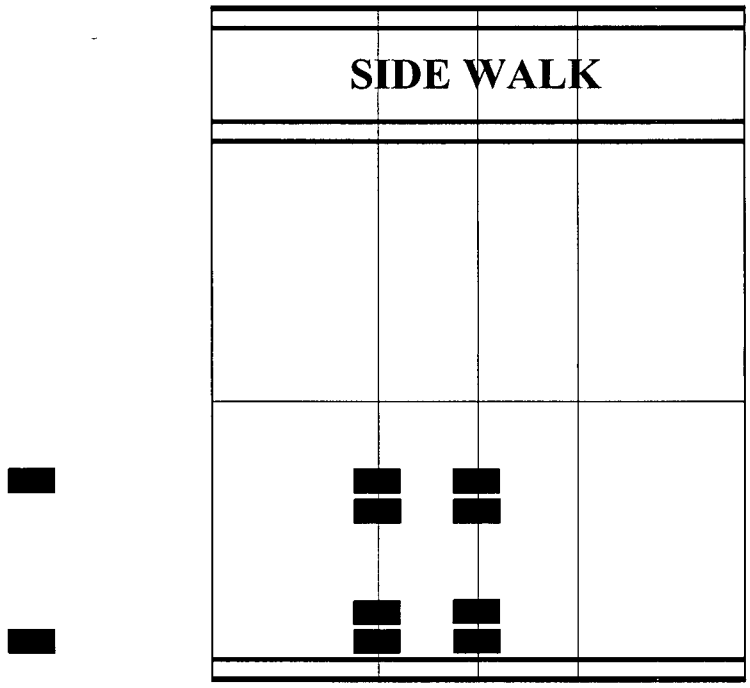

Figure 4.13(a): Position 1, truck placed close to curb with second rear axle at mid-span.

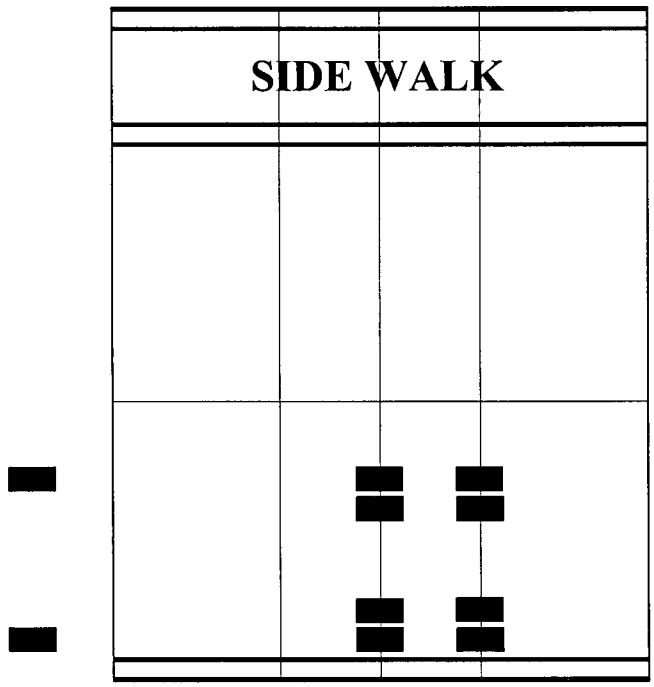

Figure 4.13(b): Position 2, truck placed close to curb with first rear axle at mid-span.

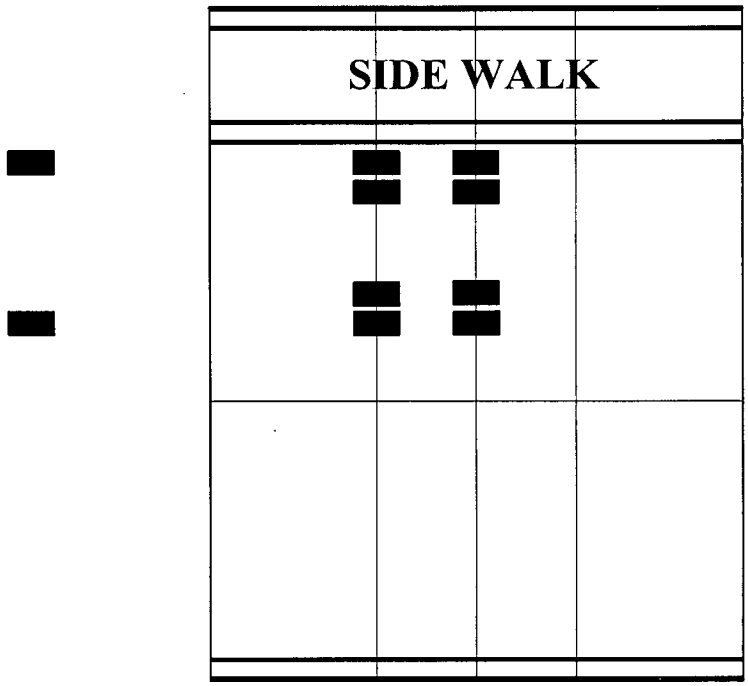

Figure 4.13(c): Position 3, truck placed close to curb with second rear axle at mid-span.

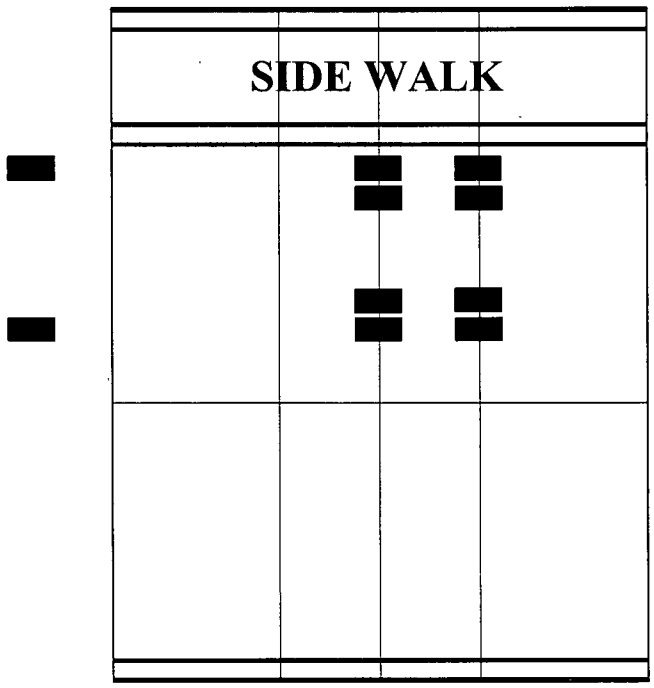

Figure 4.13(d): Position 4, truck placed close to curb with first rear axle at mid-span.

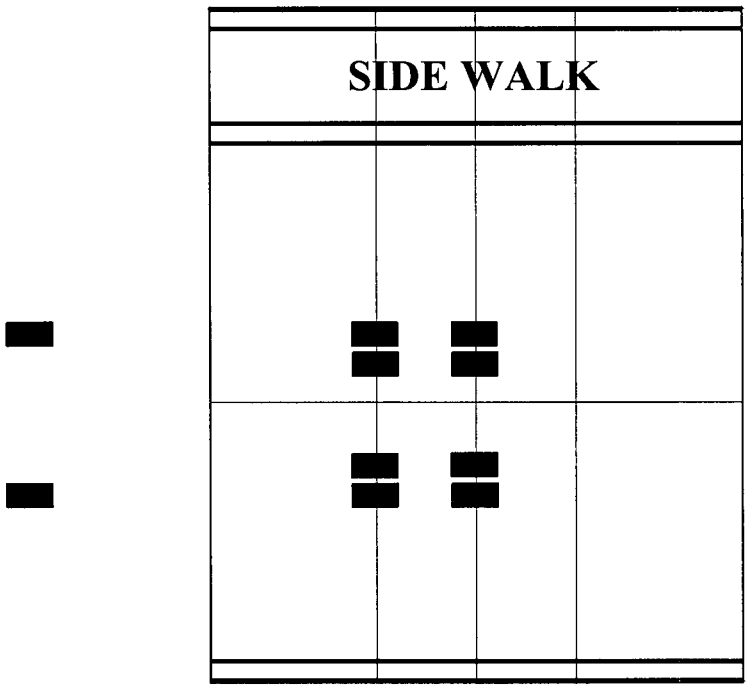

Figure 4.13(e): Position 5, truck placed centrally with second rear axle at mid-span.

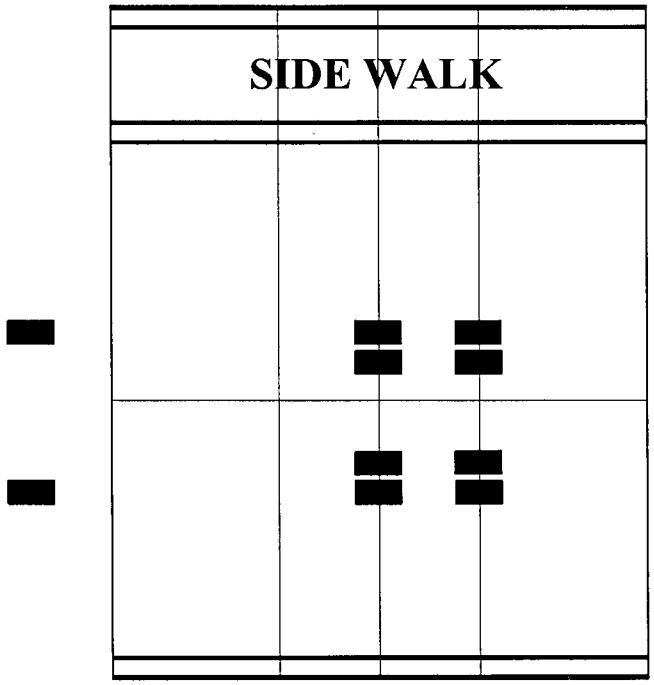

Figure 4.13(f): Position 6, truck placed centrally with first rear axle at mid-span.

5

EXPERIMENTAL RESULTS

5.1 - Static Load Test Results

Identical static tests were conducted on two different occasions on Safe Bridge, before and after the application of GFRP. Due to differences between weights of the loaded truck in two tests, a linear correction factor of 1.12 was used throughout the analysis. Tables 5.1-5.4 and Figures 5.1-5.4 shows the converted recorded values and graphs for the selected girders at different load positions. The maximum strain value observed in the longitudinal steel rebars during testing was 101.8E-6 m/m, and it happened before the application of GFRP. Consequently, after the employment of GFRP that value reduced to 73.65E-6 m/m, and it happened at the same location. Moreover, the maximum girder deflection before application was 1.55 mm compared to 1.21 mm after the application of GFRP. Comparisons of the Safe Bridge strain and deflection

characteristics before and after refurbishment clearly advocate the success of the refurbishment. Most significantly, the GFRP refurbishment reduced the percentage of yield capacity reached due to the 28-ton dead load by 28 %. A reduction of this magnitude greatly prolongs the service life of the Safe Bridge, and demonstrates the benefits of sprayed GFRP as a rehabilitating technique. The load positions 2, 4, and 6 show a bit higher values for strains and deflections and that is due to the fact that there are small load variation between the first rear axle and the second rear axle (84 kN compare to 82 kN). Figures 5.5 and 5.6 compare the performance of the bridge before and after the spray, and they show a considerable improvement in load capacity of the Bridge.

5.2 - Rolling Load Test Results

Figures 5.7 through 5.18 show the measured strains and deflections, both before and after the application of GFRP, plotted against time for each of the respective running load positions, namely ROLL I, ROLL II, and ROLL III. In these figures, only the relevent girders were plotted against time (i.e. the girders directly under the moving truck). A summary of the maximum strains and deflections in the girders for each of the tests is shown in Tables 5.5 through 5.8. The highlighted values in these two tables correspond to the maximum values attained in all three test combined. The maximum recorded strain and defection values occurred in girder 6 for ROLL III truck position, except for one case where girder 8 showed (Table 5.8) to have the maximum deflection. Due to the fact that once again girder 6 had the maximum strain, it is concluded that there must have been some misreading or malfunctioning of the LVDT. Hence, again

girder 6 can be assumed the controlling girder in determining the bridge behaviour. The maximum-recorded strain before application of GFRP was 72.1 micro-strain (Girder 6, ROLL III). The corresponding longitudinal tensile stress associated with this value is approximately 14.42 MPa (E = 200 GPa). This value represents 4.7% of the longitudinal yield capacity assuming a 304 MPa steel [10]. After the refurbishment of GFRP that reduced to 62.7 micro-strain, which corresponds to tensile stress of 12.54 MPa, and 4.1% of the yield capacity. This corresponds to a 13 % reduction in the percent yield capacity reached.

Tables 5.9 and 5.10, compare the performance of the bridge before and after the refurbishment of GFRP for the static and ROLL tests. Hence, once again, it is clear that a significant reduction has occurred in both the maximum strain and deflection values. These results clearly demonstrate the effectiveness of the GFRP rehabilitation technique.

5.3 - Load Test Comparison

As in testing before GFRP refurbishment, strains and deflections under rolling load were found to be smaller than those observed under static-loading conditions. Specifically, maximum strain recorded for both pre and post GFRP were 29.2 and 14.7 % lower than the static load case. Maximum displacement were found to be 13.6 and 18.2 % lower, respectively.

Maximum strain and deflection values reached during loading are dependent on the loading period due to bridge girder stiffness. During the rolling tests, girders were not loaded for periods long enough for and hence lower strains and displacements were recorded. One can conclude therefore that, the service life of the Safe Bridge is even

longer under rolling loads conditions as resulting stresses and deflections will always be smaller.

Assuming rolling load conditions as the loading criteria, GFRP refurbishment of the Safe Bridge can be surmised as reducing maximum strain, and maximum deflection reached under a 28-ton rolling load by 14.7%, and 18.2% respectively.

Table 5.1: Mid-span strains at various load positions before application of GFRP.

Strain on Longitudinal Steel for Six Static Load Positions (E-6 m/m) (Before Application of GFRP)						
	Girder Number					
Static Load Position	2	4	6	8	10a	10b
Load Position 1	0	1.7	16.3	57.6	62.4	51.8
Load Position 2	0	2.7	18.6	58.2	62.8	53.2
Load Position 3	17.3	59.5	42.2	11.5	1	1.9
Load Position 4	17.3	62.4	39.4	11.5	1.9	1.9
Load Position 5	3.8	18.2	83.5	70.1	15.9	9.6
Load Position 6	2.9	17.3	101.8	64.3	16.9	10.6
Maximum Strain in Girder 6 under loading condition 6 = 101.8 μE						

Table 5.2: Mid-span strains at various load positions after application of GFRP.

Strain on Longitudinal Steel for Six Static Load Positions (E-6 m/m) (After Application of GFRP)						
	Girder Number					
Static Load Position	2	4	6	8	10a	10b
Load Position 1	2.1	*	12.5	49.6	54.9	60
Load Position 2	0	*	15.3	59.1	58.1	54.9
Load Position 3	14.7	*	49.6	10	0.9	1.1
Load Position 4	15.8	*	51.7	11.1	0.9	1.1
Load Position 5	2.1	*	72.4	49.6	13.4	8.3
Load Position 6	3.2	*	73.5	62.2	13.4	8.3
* Output Channel for this girder was out						
Maximum Strain in Girder 6 under loading condition 6 = 65.6 μE						

Table 5.3: Mid-span deflections at various load positions before application of GFRP.

Midspan Deflections of Selected Girders for Six Static Load Positions (mm)
(Before Application of GFRP)

Static Load Position	Girder Number 2	4	6	8	10a	10b
Load Position 1	0	0.08	0.35	1.04	1.09	0.86
Load Position 2	0	0.05	0.41	1.09	1.12	0.81
Load Position 3	0.41	1.32	1.09	0.36	0.05	0
Load Position 4	0.53	1.32	1.12	0.3	0.08	0
Load Position 5	0.03	0.43	1.52	1.37	0.36	0.15
Load Position 6	0.08	0.38	1.55	1.37	0.41	0.18

* Output Channel for this girder was out

Maximum Deflection in Girder 6 under loading condition 6 = 1.55 mm

Table 5.4: Mid-span deflections at various load positions after application of GFRP.

Midspan Deflections of Selected Girders for Six Static Load Positions (mm)
(After Application of GFRP)

Static Load Position	Girder Number 2	4	6	8	10a	10b
Load Position 1	0	0.07	0.37	1.02	1.04	0.84
Load Position 2	0	0.08	0.28	1.1	1.1	0.78
Load Position 3	0.34	1.05	0.92	0.27	0.03	0.02
Load Position 4	0.34	1.08	0.99	0.29	0.03	0
Load Position 5	0.06	0.37	1.16	1.11	0.35	0.15
Load Position 6	0.06	0.4	1.21	1.14	0.35	0.17

* Output Channel for this girder was out

Maximum Deflection in Girder 6 under loading condition 6 = 1.08 mm

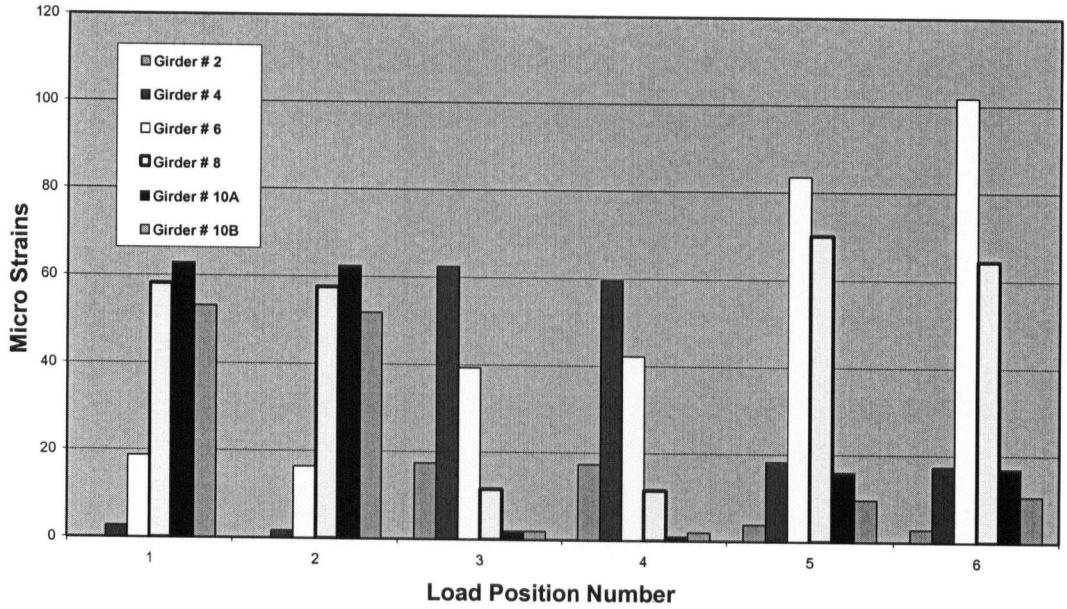

Figure 5.1: Mid-span strains at various load positions before application of GFRP.

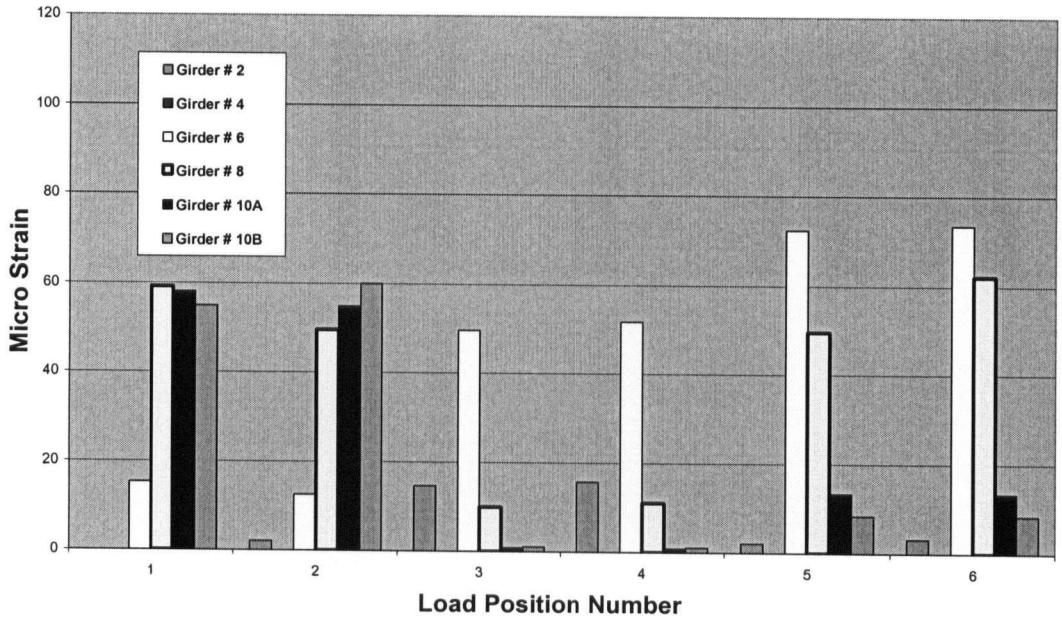

Figure 5.2: Mid-span strains at various load positions after application of GFRP.

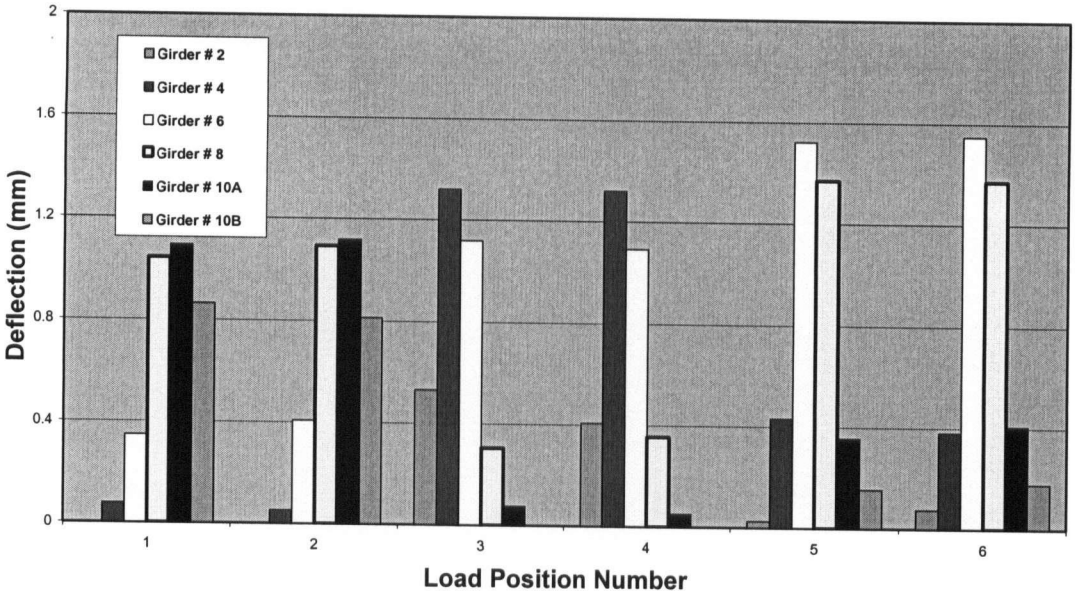

Figure 5.3: Midspan deflections at various load positions before application of GFRP.

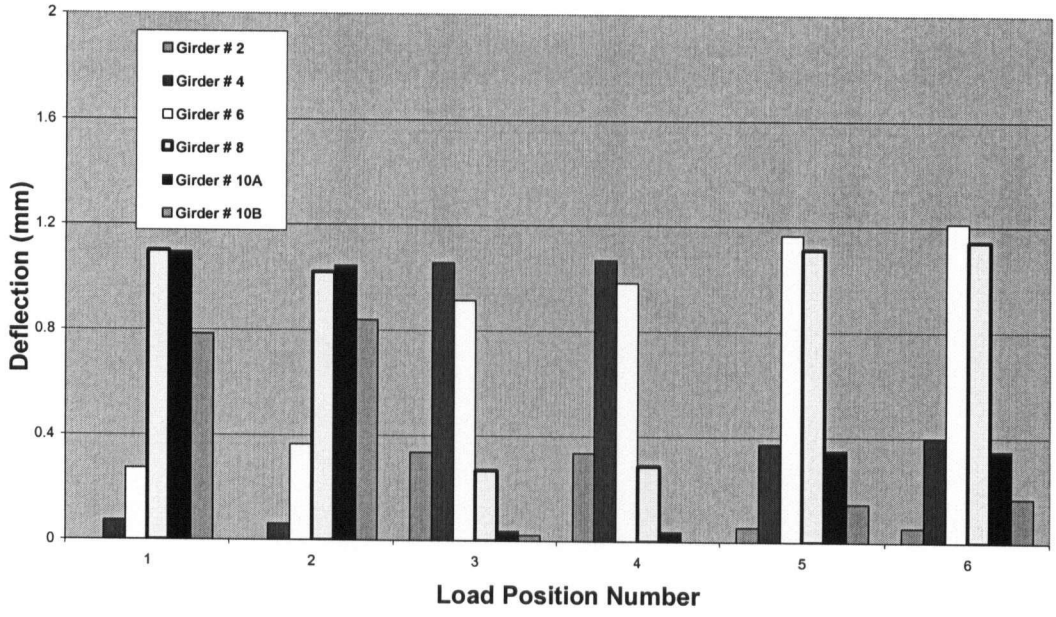

Figure 5.4: Midspan deflections at various load positions after application of GFRP.

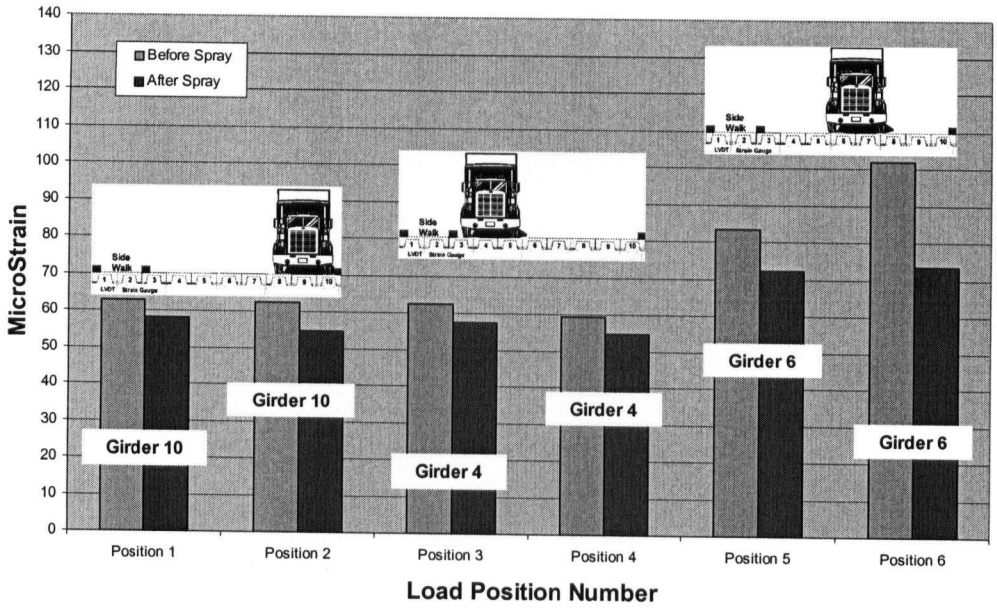

Figure 5.5: Performance of Bridge before and after application of GFRP.

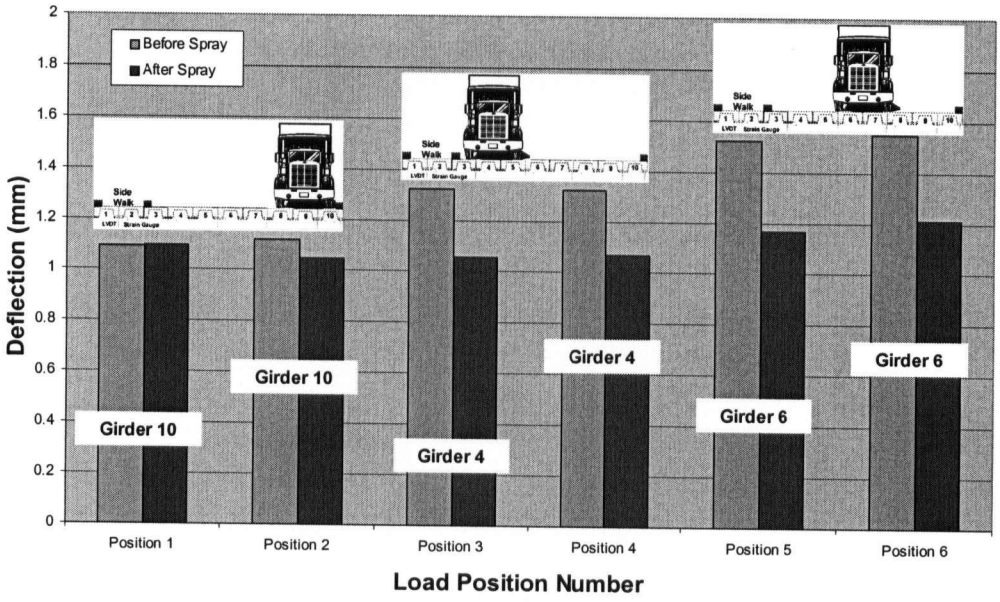

Figure 5.6: Performance of Bridge before and after application of GFRP.

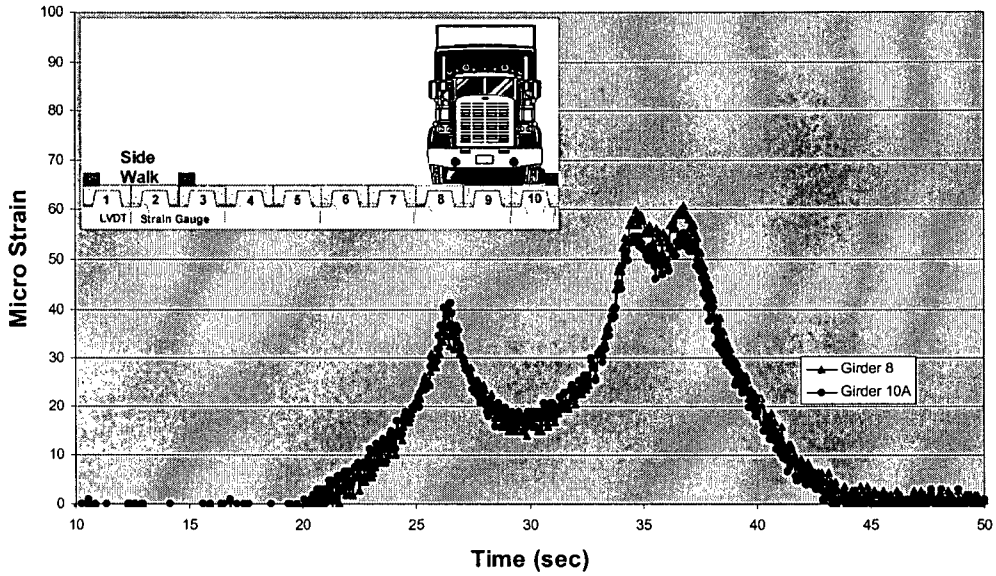

Figure 5.7: Micro strain versus time before the application of GFRP (ROLL I).

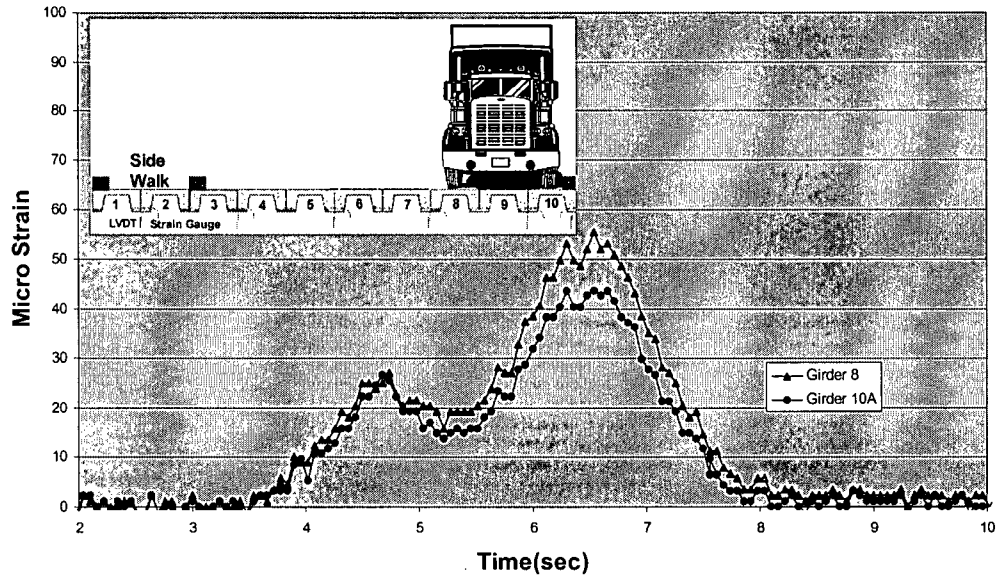

Figure 5.8: Micro strain versus time after the application of GFRP (ROLL I).

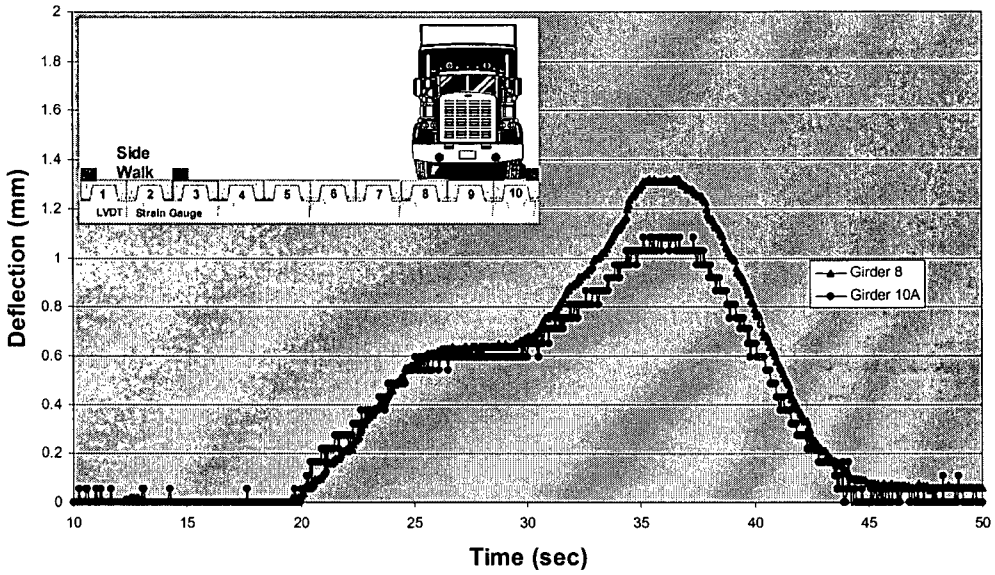

Figure 5.9: Mid-span deflection versus time before the application of GFRP (ROLL I).

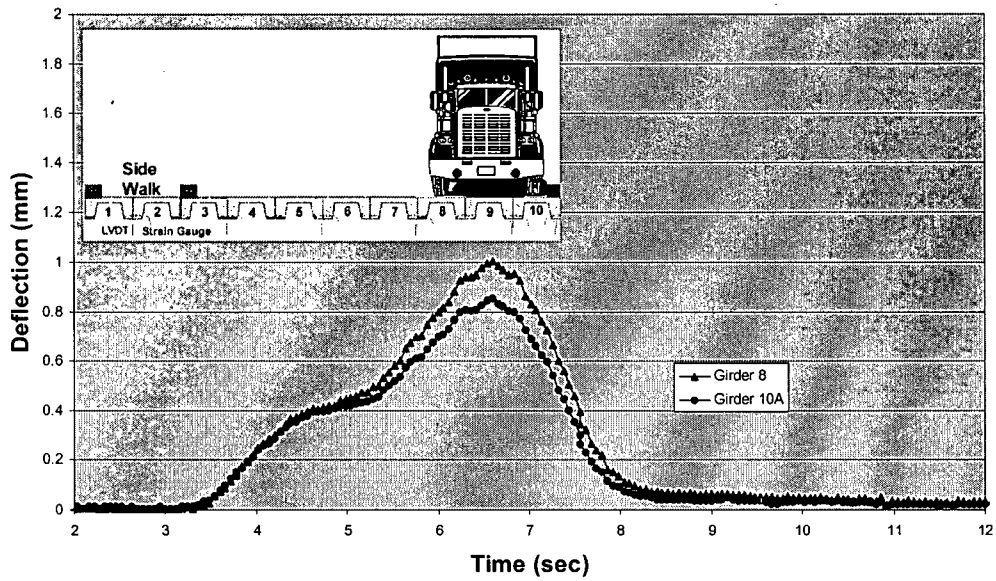

Figure 5.10: Mid-span deflection versus time after the application of GFRP (ROLL I).

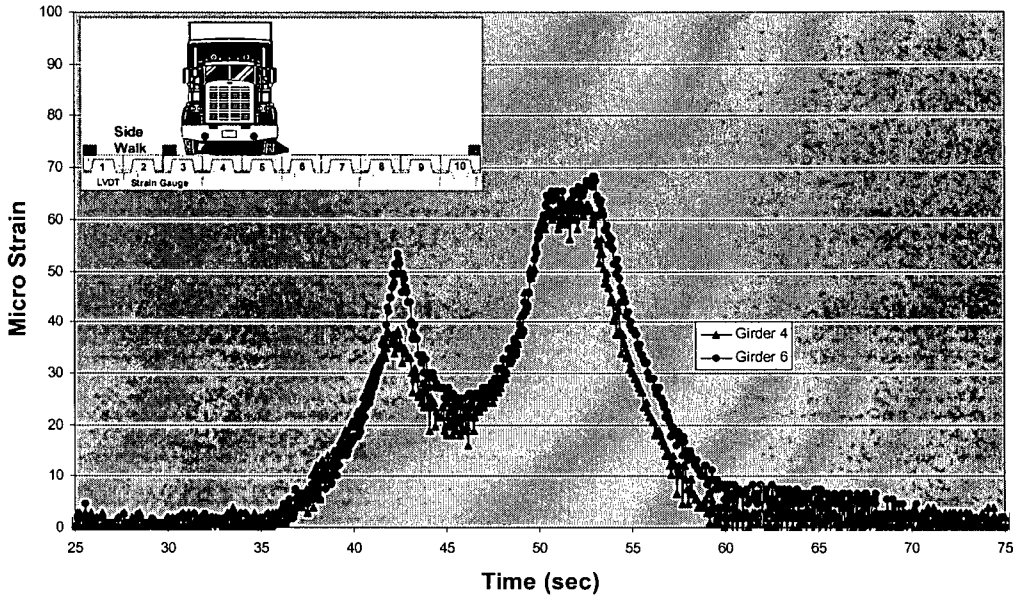

Figure 5.11: Micro strain versus time before the application of GFRP (ROLL II).

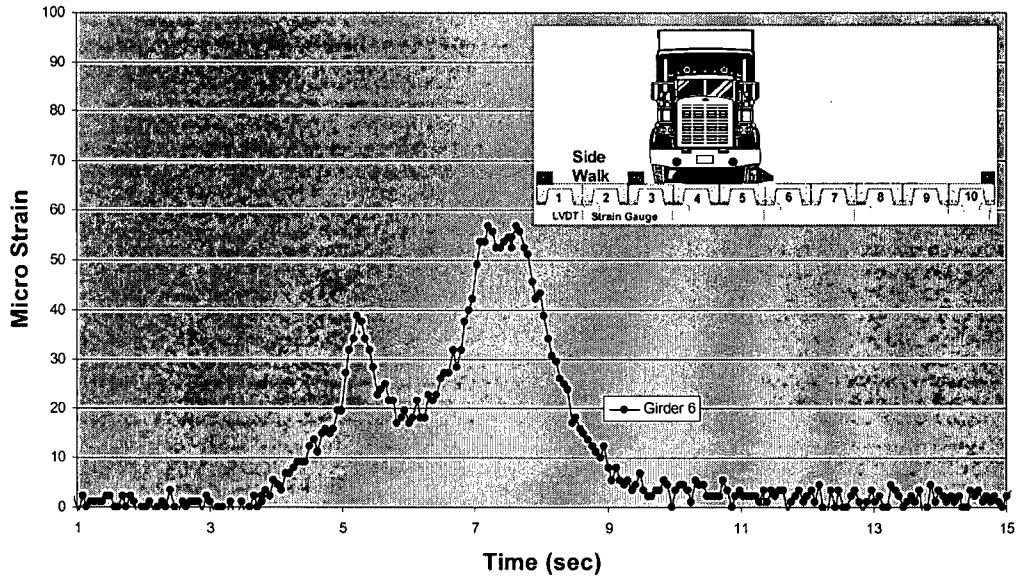

Figure 5.12: Micro strain versus time after the application of GFRP (ROLL II).

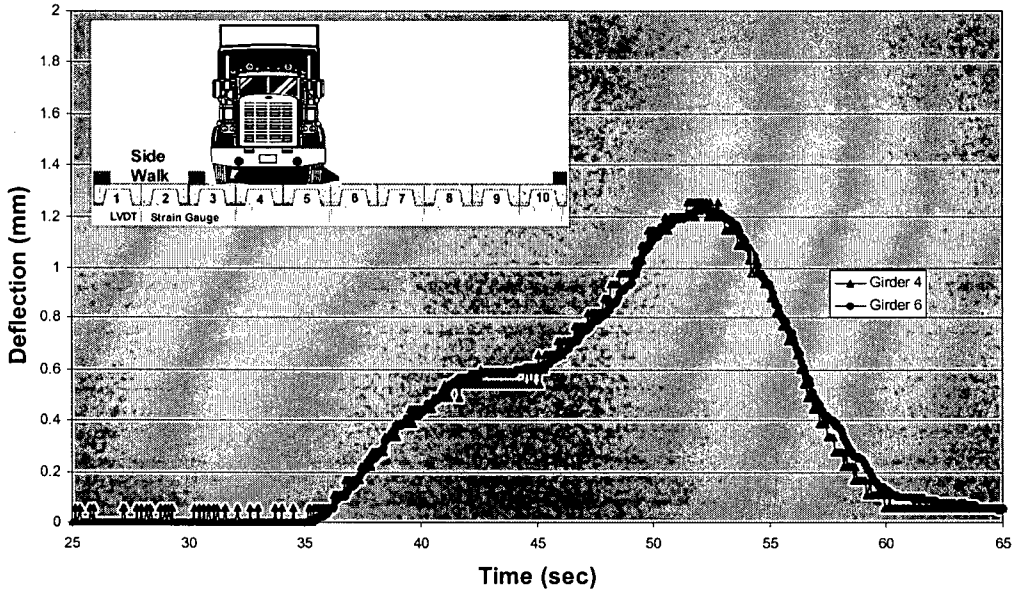

Figure 5.13: Mid-span deflection versus time before the application of GFRP(ROLL II).

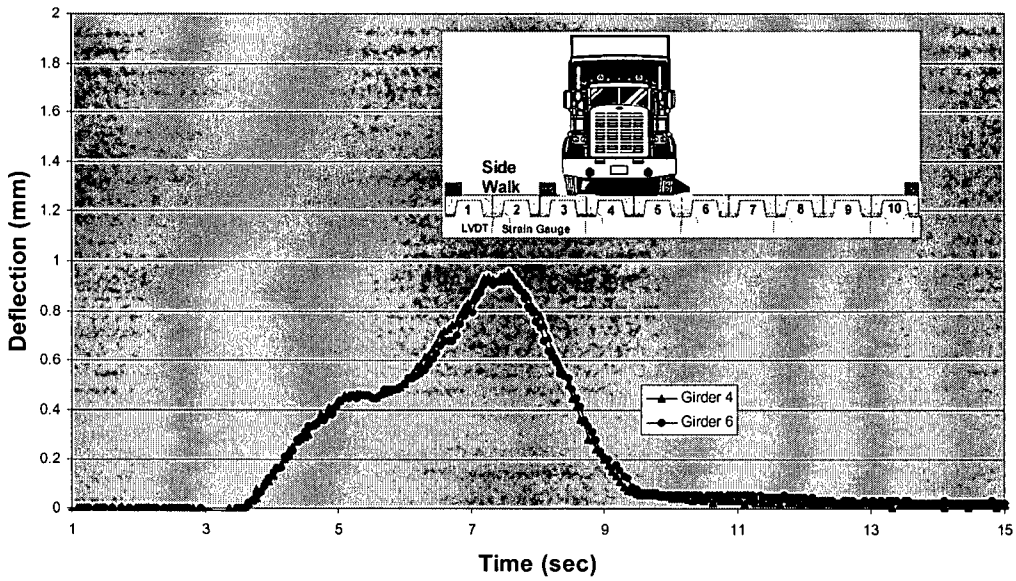

Figure 5.14: Mid-span deflection versus time after the application of GFRP(ROLL II).

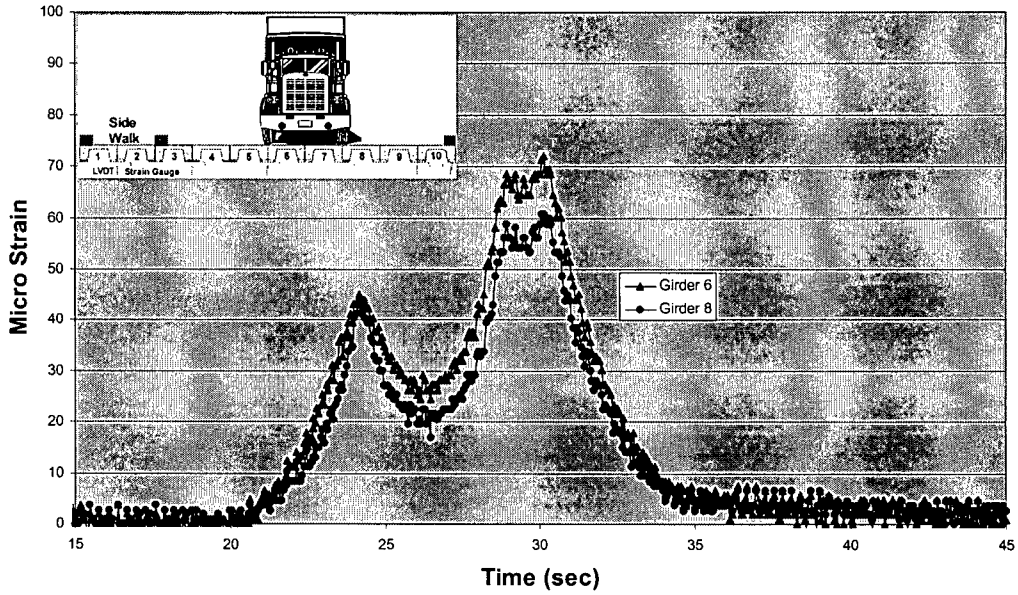

Figure 5.15: Micro strain versus time before the application of GFRP (ROLL III).

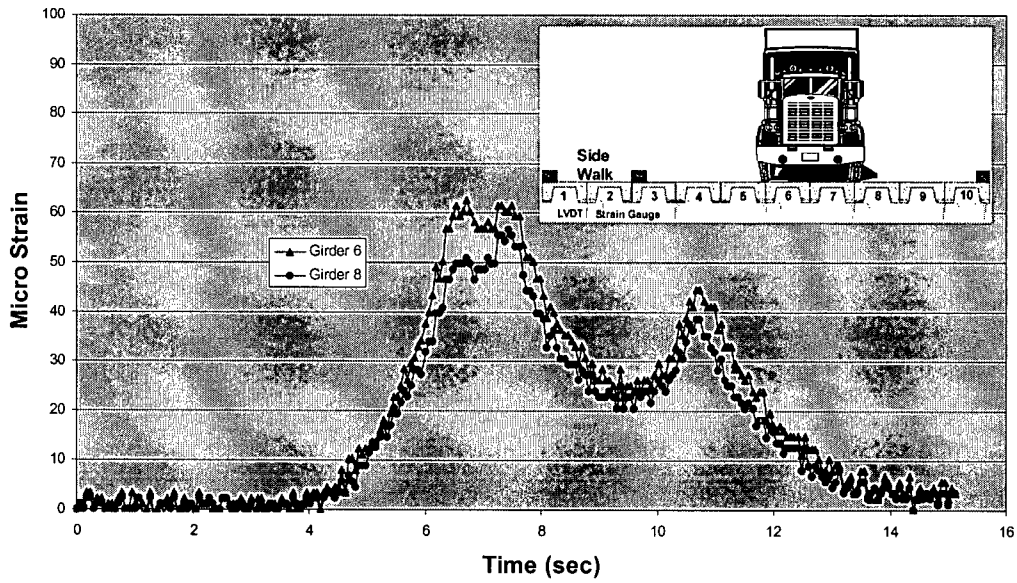

Figure 5.16: Micro strain versus time after the application of GFRP (ROLL III).

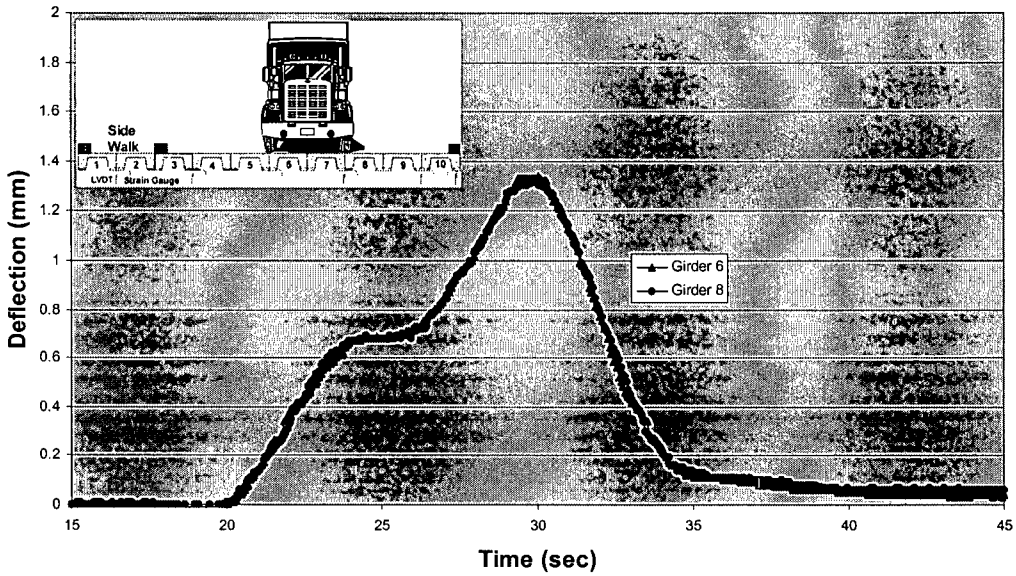

Figure 5.17: Mid-span deflection versus time before application of GFRP (ROLL III).

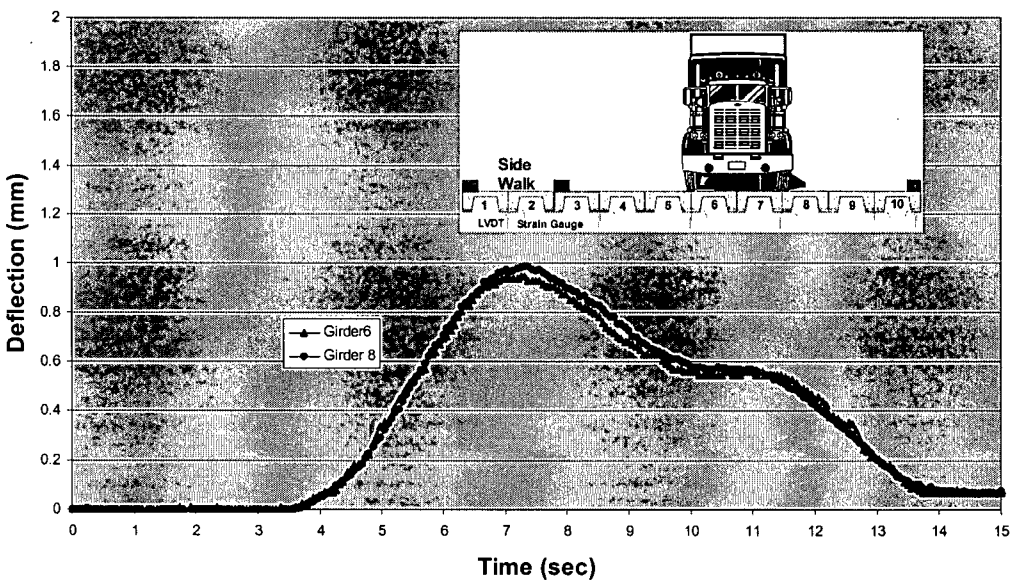

Figure 5.18: Mid-span deflection versus time after application of GFRP (ROLL III).

Table 5.5: Mid-span strains at various ROLL positions before application of GFRP.

	Maximum Strains (E-6 m/m) (Without GFRP) Girder Number					
	2	**4**	**6**	**8**	**10a**	**10b**
Roll Test I	1.9	8.4	25.3	60.8	55.2	44.1
Roll Test II	16.9	63.7	68.3	15.9	6.5	5.8
Roll Test III	6.5	20.5	72.1	60.8	16.9	11.3

Table 5.6: Mid-span strains at various ROLL positions after application of GFRP.

	Maximum Strains (E-6 m/m) (Coated with GFRP) Girder Number					
	2	**4**	**6**	**8**	**10a**	**10b**
Roll Test I	4.4	*	27.3	55.4	43.6	38.8
Roll Test II	13.2	*	57	16.9	3.1	5.4
Roll Test III	7.6	*	62.7	56.7	19.2	14

Table 5.7: Mid-span deflections at various load positions before application of GFRP.

	Maximum Deflections (mm) (Without GFRP) Girder Number					
	2	**4**	**6**	**8**	**10a**	**10b**
Roll Test I	0.02	0.21	0.61	1.32	1.09	0.78
Roll Test II	0.36	1.25	1.23	0.45	0.11	0.08
Roll Test III	0.07	0.06	1.34	1.32	0.11	0.18

Table 5.8: Mid-span deflections at various load positions after application of GFRP.

	Maximum Deflections (mm) (Coated with GFRP) Girder Number					
	2	**4**	**6**	**8**	**10a**	**10b**
Roll Test I	0	0.13	0.5	0.99	0.85	0.6
Roll Test II	0.28	0.95	0.92	0.37	0.08	0.08
Roll Test III	0.06	0.36	0.95	0.99	0.37	0.25

Table 5.9: Comparison of results before and after the application of GFRP for static test.

	Before GFRP Refurbishment	*After GFRP Refurbishment*	*Percent Reduction*
Maximum Strain in Steel Reinforcement (E-6 m/m)	101.8	73.5	28
Maximum Girder Deflection (mm)	1.55	1.21	22
Location of Maximum Deflection	Girder 6	Girder 6	
Load Position of Maximums	Load Position 6	Load Position 6	
Maximum Percentage of Yield Capacity Reached by 28-ton Truck Dead Load (%)	6.7	4.8	28

Table 5.10: Comparison of results before and after application of GFRP for ROLL test.

	Before GFRP Rehabilitation	**After GFRP Rehabilitation**	**Reduction %**
Maximum Strain in Rebars (E-6 m/m)	72.1	62.7	13
Maximum Girder Deflection (mm)	1.34	0.99	26.1
Location of Maximum Strain	Girder # 6	Girder # 6	
Location of Maximum Deflection	Girder # 6	Girder # 8	
ROLL Test of Maximum	ROLL III	ROLL III	
Maximum Percentage of Yield Capacity Reached with a 28-ton Running Load	4.7	4.1	13

6

FINITE ELEMENT ANALYSIS OF THE SAFE BRIDGE

Safe Bridge is the first bridge in the world that has been retrofitted using Sprayed Fiber Reinforced Polymers. This chapter presents the Finite Element analysis of the Safe Bridge prior and after the application of Sprayed GFRP. The finite element models of the Safe Bridge girders were developed for both cases prior and after the application of GFRP. The truck loading was applied to the bridge model at different locations, as in the actual bridge test. The non-linear analyses were carried out using ANSYS [63]. A good match between experimental results and FEM analysis was obtained.

6.1 - Element Description

6.1.1 - Reinforced Concrete

SOLID65 [63] is used for the three-dimensional modeling of concrete with reinforcing bars (rebars). SOLID65 is capable of cracking in tension and crushing in compression. In concrete applications, for example, the solid capability of the element may be used to model the concrete while the rebar capability is available for modeling reinforcement behaviour. The element (Figure 6.1) is defined by eight nodes having three degrees of freedom at each node: translations in the nodal x, y, and z directions. Up to three different rebar specifications may be defined.

The concrete element is similar to the SOLID45 (3-D Structural Solid) element with the addition of special cracking and crushing capabilities. The most important aspect of this element is the treatment of non-linear material properties.

6.1.1.1 - Assumptions and Restrictions

- Cracking is permitted in three orthogonal directions at each integration point.
- If cracking occurs at an integration point, the cracking is modeled through an adjustment of material properties that effectively treats the cracking as a "smeared band" of cracks, rather than discrete cracks.
- The concrete material is assumed to be initially isotropic.

- Whenever the reinforcement capability of the element is used, the reinforcement is assumed to be "smeared" throughout the element.

- In addition to cracking and crushing, the concrete may also undergo plasticity, with the Drucker-Prager failure surface being most commonly used [63]. In this case, the plasticity is considered before the cracking and crushing checks are performed.

6.1.1.2 - Description

SOLID65 permits the presence of four different materials within each element; one matrix material (e.g. concrete) and up to three independent reinforcing materials. The concrete material is capable of directional integration point cracking and crushing besides including plastic and creep behaviour. The reinforcement (which also includes creep and plasticity) has uniaxial stiffness only and is assumed to be smeared throughout the element. Directional orientation is accomplished through user specified angles.

6.1.1.2.1 - Linear Behaviour - General

The stress-strain matrix [D] used for this element is defined as [63]:

$$[D] = \left(1 - \sum_{i=1}^{N_r} V_i^R\right)[D^c] + \sum_{i=1}^{N_r} V_i^R [D^r]_i \tag{1}$$

where:

V_i^R = ratio of the volume of reinforcing material i to the total volume of the element

$[D^r]_i$ = stress-strain matrix for reinforcement i

$[D^c]$ = stress-strain matrix for concrete

N_r = number of reinforcing materials

6.1.1.2.2 - Nonlinear Behaviour - Concrete

As mentioned previously, the matrix material (e.g. concrete) is capable of plasticity, creep, cracking and crushing. This material model predicts elastic behaviour, cracking behaviour or crushing behaviour. If elastic behaviour is predicted, the concrete is treated as a linear elastic material (discussed above). If cracking or crushing behaviour is predicted, the elastic, stress-strain matrix is adjusted as discussed below for each failure mode.

6.1.1.2.2.1 -Modeling of a Crack

The presence of a crack at an integration point is represented through modification of the stress-strain relations by introducing a plane of weakness in a direction normal to the crack face. Also, a shear transfer coefficient β_t is introduced which represents a shear strength reduction factor for those subsequent loads which induce sliding (shear) across the crack face. The stress-strain relations for a material that has cracked in one direction only become:

$$[D_c^{ck}] = \frac{E}{(1+\nu)} \begin{bmatrix} \frac{R^t(1+\nu)}{E} & 0 & 0 & 0 & 0 & 0 \\ 0 & \frac{1}{1-\nu} & \frac{\nu}{1-\nu} & 0 & 0 & 0 \\ 0 & \frac{\nu}{1-\nu} & \frac{1}{1-\nu} & 0 & 0 & 0 \\ 0 & 0 & 0 & \frac{\beta_t}{2} & 0 & 0 \\ 0 & 0 & 0 & 0 & \frac{1}{2} & 0 \\ 0 & 0 & 0 & 0 & 0 & \frac{\beta_t}{2} \end{bmatrix} \quad (2)$$

where the superscript 'ck' signifies that the stress-strain relations refer to a coordinate system parallel to principal stress directions. R^t is the slope (secant modulus). R^t works with adaptive descent and diminishes to 0.0 as the solution converges.

If the crack closes, then all compressive stresses normal to the crack plane are transmitted across the crack and only a shear transfer coefficient β_c for a closed crack is introduced. Then $[D_c^{ck}]$ can be expressed as

$$[D_c^{ck}] = \frac{E}{(1+\nu)(1-2\nu)} \begin{bmatrix} (1-\nu) & \nu & \nu & 0 & 0 & 0 \\ \nu & 1-\nu & \nu & 0 & 0 & 0 \\ \nu & \nu & 1-\nu & 0 & 0 & 0 \\ 0 & 0 & 0 & \beta_c \frac{(1-2\nu)}{2} & 0 & 0 \\ 0 & 0 & 0 & 0 & \frac{(1-2\nu)}{2} & 0 \\ 0 & 0 & 0 & 0 & 0 & \beta_c \frac{(1-2\nu)}{2} \end{bmatrix} \quad (3)$$

The stress-strain relations for concrete that has cracked in two directions are:

$$[D_c^{ck}] = E\begin{bmatrix} \frac{R^t}{E} & 0 & 0 & 0 & 0 & 0 \\ 0 & \frac{R^t}{E} & 0 & 0 & 0 & 0 \\ 0 & 0 & 1 & 0 & 0 & 0 \\ 0 & 0 & 0 & \frac{\beta_t}{2(1+\nu)} & 0 & 0 \\ 0 & 0 & 0 & 0 & \frac{\beta_t}{2(1+\nu)} & 0 \\ 0 & 0 & 0 & 0 & 0 & \frac{\beta_t}{2(1+\nu)} \end{bmatrix} \tag{4}$$

If both directions reclose,

$$[D_c^{ck}] = \frac{E}{(1+\nu)(1-2\nu)}\begin{bmatrix} (1-\nu) & \nu & \nu & 0 & 0 & 0 \\ \nu & 1-\nu & \nu & 0 & 0 & 0 \\ \nu & \nu & 1-\nu & 0 & 0 & 0 \\ 0 & 0 & 0 & \beta_c\frac{(1-2\nu)}{2} & 0 & 0 \\ 0 & 0 & 0 & 0 & \frac{(1-2\nu)}{2} & 0 \\ 0 & 0 & 0 & 0 & 0 & \beta_c\frac{(1-2\nu)}{2} \end{bmatrix} \tag{5}$$

The stress-strain relations for concrete that has cracked in all three directions are:

$$[D_c^{ck}] = E\begin{bmatrix} \frac{R^t}{E} & 0 & 0 & 0 & 0 & 0 \\ 0 & \frac{R^t}{E} & 0 & 0 & 0 & 0 \\ 0 & 0 & 1 & 0 & 0 & 0 \\ 0 & 0 & 0 & \frac{\beta_t}{2(1+\nu)} & 0 & 0 \\ 0 & 0 & 0 & 0 & \frac{\beta_t}{2(1+\nu)} & 0 \\ 0 & 0 & 0 & 0 & 0 & \frac{\beta_t}{2(1+\nu)} \end{bmatrix} \tag{6}$$

If all three cracks reclose, Equation (5) is followed. In total there are 16 possible combinations of crack arrangement and appropriate changes in stress-strain relationships are incorporated in SOLID65. A note is output if $1 > \beta_c > \beta_t > 0$ are not true.

6.1.1.2.2.2 - Modeling of Crushing

If the material at an integration point fails in uniaxial, biaxial, or triaxial compression, the material is assumed to crush at that point. In SOLID65, crushing is defined as the complete deterioration of the structural integrity of the material (e.g. material spalling). Under conditions where crushing has occurred, material strength is assumed to have degraded to an extent such that the contribution to the stiffness of an element at the integration point in question can be ignored.

A LINK8 element was used to model (Figure 6.2) the steel reinforcement. The three-dimensional spar element is a uniaxial tension-compression element with three degrees of freedom at each node: translations in the nodal x, y, and z directions. Plasticity, creep, swelling, stress stiffening, and large deflection capabilities are included. For more details please refer to *ANSYS, Inc. Theory Reference Section 14.65*.

6.1.2 - Glass Fiber Reinforced Polymers

SHELL43 is used to model the GFRP layers (Figure 6.3). SHELL43 is well suited to model linear, warped, moderately-thick shell structures. The element has six degrees of freedom at each node: translations in the nodal x, y, and z directions and rotations about the nodal x, y, and z axes. The deformation shapes are linear in both in-plane directions. For the out-of-plane motion, it uses a mixed interpolation of tensorial components. The element has plasticity, creep, stress stiffening, large deflection, and large strain capabilities.

6.1.3 – Contact Surface between GFRP and Concrete

To model the contact surface between GFRP and concrete, CONTA174 and TARGE170 were used. CONTA174 is used to represent contact and sliding between 3-D "target" surfaces (TARGE170) and a deformable surface, defined by this element. This element has three degrees of freedom at each node: translations in the nodal x, y, and z directions. This element is located on the surfaces of 3-D solid or shell elements with midside nodes. It has the same geometric characteristics as the solid or shell element face with which it is connected (Figure 6.4). Contact occurs when the element surface penetrates one of the target segment elements (TARGE170) on a specified target surface. Coulomb and shear stress friction is allowed. TARGE170 is used to represent various 3-D "target" surfaces for the associated contact elements (CONTA174). The contact elements themselves overlay the solid elements describing the boundary of a deformable body and are potentially in contact with the target surface, defined by TARGE170. This target surface is discretized by a set of target segment elements (TARGE170) and is paired with its associated contact surface via a shared real constant set. It is possible to impose any translational or rotational displacement on the target segment element. One can also impose forces and moments on target elements (Figure 6.5).

6.2 - MATERIAL PROPERTIES

6.2.1 - Concrete

FEM modeling for concrete is a challenging task. Concrete is a quasi-brittle material and has different behavior in compression and tension. The tensile strength of concrete is

typically 8-15% of the compressive strength [64]. Figure 6.6 shows a typical stress-strain curve for normal weight concrete [65].

As seen in the Figure 6.6, the stress-strain curve for concrete is linearly elastic up to about 30 percent of the maximum compressive strength. Beyond this point, the stress increases gradually up to the maximum compressive strength. And after that, the curve moves down into a softening region, and finally crushing failure occurs at an ultimate strain, ε_{cu} . In tension, the stress-strain curve for concrete is approximately linearly elastic up to the maximum tensile strength. Beyond this point, the concrete cracks and the stress decreases to zero [65].

6.2.1.1 Concrete Input Data

ANSYS requires the following input data for material properties:

Modulus of Elasticity (E_c)

Ultimate uniaxial compressive strength (f'_c)

Ultimate uniaxial tensile strength (modulus of rupture, f_r)

Poisson's ratio (ν)

Shear transfer coefficient (β_c)

Compressive uniaxial stress-strain relationship

According to the Canadian code CSA Standard A23.3-94 Clause 8.6.2.3, it is permissible to take the modulus of elasticity, E_c, of normal density concrete with compressive strength between 20 and 40 MPa as

$$E_c = 4500\sqrt{f'_c} \tag{7}$$

And according to Clause 8.6.4 of CSA Standard A23.3-94, the modulus of rupture of concrete, f_r, shall be taken as,

$$f_r = 0.6\,\lambda\,\sqrt{f'_c} \tag{8}$$

the factor λ was chosen as 1.0 (i.e. for normal concrete, based on the Clause 8.6.5 of CSA Standard A23.3-94) and E_c , and f_r are in MPa. Poisson's ratio for concrete was assumed to be 0.2 [65].

The shear transfer coefficient, β_c , represents conditions at the crack face. The value of β_c ranges from 0.0 to 1.0, with 0.0 representing a complete loss of shear transfer and 1.0 representing no loss of shear transfer (*ANSYS 1998*). The value of β_c used in many studies of reinforced concrete structures, however, varied between 0.05 and 0.25 [65].

6.2.1.2 Failure Criteria for Concrete

ANSYS concrete element is capable of predicting failure in concrete materials. Cracking and crushing failures are accounted for. To define a failure surface for concrete, ultimate tensile and compressive strengths are needed. Figure 6.7 represents the 3-D failure surface for states of stress that are biaxial or nearly biaxial. If the most significant nonzero principal stresses are in the σ_{xp} or σ_{yp}, directions, the three surfaces represented are for σ_{zp} slightly greater than zero, σ_{zp} equal to zero, and σ_{zp} slightly less than zero. Although the three surfaces, shown as projection on the σ_{xp}-σ_{yp} plane, are nearly equivalent and the 3-D failure surface is continuous, the mode of material failure is a function of the sign of σ_{zp}. For example, if σ_{xp} and σ_{yp} are both negative (compressive) and σ_{zp} is slightly positive (tensile), cracking would be predicted in a direction

perpendicular to σ_{zp} direction. However, if σ_{zp} is zero or slightly negative, the material is assumed to crush (*ANSYS 1998*).

In a concrete element, cracking occurs when the principal tensile stress in any direction lies outside the failure surface. After cracking, the elastic modulus of the concrete element is set to zero in the direction parallel to the principal tensile stress direction. Crushing occurs when all principal stresses are compressive and lie outside the failure surface; afterward, the elastic modulus is set to zero in all directions (*ANSYS 1998*), and the element effectively disappears.

6.2.2 - Steel Reinforcement

Steel reinforcement for the concrete girders was chosen as typical steel reinforcing bars. The steel reinforcement in this study was chosen to be an elastic-perfectly plastic material and identical in tension and compression. Figure 6.8 shows the stress-strain relationship used in this study. Material properties for the steel i.e. elastic modulus of elasticity, yield stress, and Poisson's ratio was based on Banthia et al. [10]. To be on the conservative side, the lower limit value was chosen for the yield stress.

Elastic modulus of elasticity, E_s = 200,000 MPa

Yield stress, f_y = 304 MPa

Poisson's ratio, ν = 0.3

6.2.3 - Sprayed FRP Composites

Sprayed FRP composites are materials that consist of two components. One component is the reinforcement that is embedded randomly in the second component, a continuous

polymer called the matrix. The reinforcing material is in the form of fibers, i.e., carbon and glass, which are characteristically stiffer and stronger than the matrix. The sprayed FRP composites unlike the continuous fiber reinforced polymers are isotropic materials; that is, their properties are the same in all directions. Sprayed glass fiber reinforced polymer was used for shear reinforcement on the Safe Bridge because of its superior strain at failure. Linear elastic properties of the FRP composites were assumed throughout this study.

6.3 - Finite Element Modeling

Due to the complex behaviour of reinforced concrete, which is both non-homogeneous and anisotropic, the modeling of concrete structures has been a difficult challenge in the finite element analysis. Normally, the behaviour of reinforced concrete beams is studied by full-scale experimental testing. Then, the results are compared to theoretical calculations that approximate deflection and internal stress/strain distributions within the beams. With the recent addition of concrete element in FEM, it can also be used to model the behaviour numerically to confirm these calculations, as well as to provide a valuable supplement to the laboratory analysis, particularly in parametric studies.

In this study, ANSYS with the capability of concrete element (SOLID65) was used to model the Safe Bridge. The concrete element in ANSYS is capable of the three-dimensional modeling of solids with or without reinforcing bars (rebars). The solid is capable of cracking in tension, crushing in compression, plastic deformation, and creep. Finite element analysis, as used in structural engineering, determines the overall

behaviour of a structure by dividing it into a number of simple elements, each of which has well-defined mechanical and physical properties.

6.3.1 - Bridge Modeling and Analysis Assumptions

In order to analyze all the load locations on the bridge deck without changing the mesh, the load for each set of dual tires was lumped and assumed to occur at the center of the dual tires, as shown in Figure 6.9. Therefore, truck configuration shown in Figure 6.9 was used in all FE analyses.

6.3.2 - Finite Element Discretization

To model the bridge, a 3-Dimensional FEM model was constructed. The bridge structure was categorically analyzed using a properly selected combination of finite elements. Although the bridge is symmetric in the transverse direction, the loading conditions were asymmetric. Therefore, a 3-Dimensional model for the entire bridge was required. An isometric view of FEM model is shown in Figure 6.10.

In the actual bridge, the concrete girders had exhibited extensive shear cracking. Therefore the elastic modulus of the girders was modified slightly to simulate their cracked state. The modulus of elasticity of the deck was calculated using the Clause 8.6.4 of CSA Standard A23.3-94 ($E_c = 4500 \sqrt{f'_c}$), where f'_c is the concrete compressive strength in MPa. The bonding of the GFRP materials to the damaged concrete surfaces prevented the cracks from opening when bridge was subjected to loading, and tended to stiffen the girders. The repaired girders were estimated to be 25-30% stiffer than the damaged girders.

The FEM analyses were conducted through implementation of the ANSYS 7.0 finite element computer program. The FEM model consisted of five different 3 dimensional elements, namely, SOLID65, LINK8, SHELL41, CONTA174, and TARGE170. The number of each elements used in the FEM model is summarized in Table 6.1. For the FEM model, 9917 3-D, eight node concrete elements were used to model the girders, and 4000 structural 3-D Link elements were used to model the steel reinforcing bars. The bonded GFRP were represented with 1597 3-D Shell elements, and finally 2797 3-D Contact elements were used to bond concrete surface to The GFRP surface.

A comprehensive series of three-dimensional FEM analyses were conducted on the bridge structure. The dynamic analysis studies included the frequency analyses to establish the dynamic characteristics of the bridge. A parametric study was also conducted to quantify the effects of varying several cross section characteristics and mechanical properties of the GFRP on the structural responses of bridge girders.

6.4 - Frequency Analysis

To establish the dynamic characteristic of the Bridge, a FEM modal analysis were undertaken. Although the bridge under our study was rigid and short (very low period), by setting up the strain gauges at higher sensitivity for the retrofitted bridge, the free vibration characteristics were captured after the bridge was excited by the heavy truck brakes. The first 20 natural frequencies and the corresponding mode shape for the bridge were determined using the subspace iteration method [63] and are presented in Tables 6.2 and 6.3 before and after the application of GFRP. The first vibration mode shape was

identified as the symmetric flexural mode having an axis of symmetry about midspan as shown in Figures 6.11 and 6.12 for before and after the application of GFRP.

The natural period measured from the experimental test for retrofitted bridge was 0.045 seconds, which agreed very well with the FEM result of 0.0466 seconds.

6.5 - Static Analysis

The results from the static FEM analysis before the application of GFRP are presented in Figures 6.13-6.24 for six static load position discussed earlier. Figures 6.25-6.26 show the comparison of the maximum deflection and stresses for all six positions for field test and ANSYS results. A very good correlation of the FEM results with experimental measurements for both girder deflections and reinforcement steel stresses was noted. The reinforcing steel stresses obtained from the FEM analysis for load position 6, are somehow lower than the results obtained from the field tests. This can be attributed to the malfunctioning of the device because as it is seen for load position 5 which is similar to the load position 6 the reading difference is quite a bit, which is unlikely. Therefore, the reading value of 101.8E-6 m/m in the experimental test appears to be an anomaly.

The results of the FEM analysis after the application of GFRP are presented on Figures 6.27-6.38. The FEM results are in good agreement with the static load test for both girder deflection and reinforcing steel stresses. Moreover, the average decrease in midspan deflection and steel reinforcing stresses predicted by FEM analysis is equal to 24%. This is approximately equal to the actual recorded decrease in the field. Finally, Figures 6.39-6.40 show the comparison between the FEM results and the field test results after the application of sprayed GFRP. The results show an excellent correlation

between the site results and ANSYS. Due to malfunctioning of the recording device the strain values for girder 4 were not recorded. Once again, as in the pre-application of GFRP results, the most discrepancy in results are for the tensile stress values for girder 6, which can be due to some corrosive damage to the rebars inside it.

6.6 - Parametric Study

The reinforced concrete bridge span considered in this study is a representative of hundreds of other similar structures in MOTH bridge inventory. Thus, a parametric study to assess the effects of changing the GFRP modulus of elasticity and cross sectional area on the maximum midspan deflection and reinforcing steel stresses of Girder 6 (the most critical girder) was performed for the static field loading conditions. The results show that increase of either parameter will cause the decrease in both reinforcing steel stresses and girder deflections. These responses are attributed to the downward shifting of the neutral axis resulting in a decrease in reinforcing steel stresses and an increase in the flexural rigidity, EI (for the decrease in girder deflections).

The effect of varying the modulus of elasticity of the GFRP on the girder deflections and steel reinforcing bar stresses are shown in Figures 6.41-6.42. It can be concluded that a 7 times increase in modulus of elasticity can reduce the maximum deflection by 60%, and the maximum reinforcing steel stresses by 58%. Therefore, girders repaired with a higher strength material will exhibit a greater ultimate flexural capacity. Figures 6.43-6.44 show the effects of increasing the GFRP cross sectional area on reducing both the maximum girder deflection and reinforcing steel stresses for the static load tests. Although the main function of the applied GFRP was to improve the shear capacity of

the girders, it also had some effects on reducing the midspan deflections and rebar stresses, the results show the maximum girder deflection can be reduced by as much as 25%, and the maximum reinforcing steel stress by as much as 30%. However, as can be seen from these figures, an increase in the thickness of GFRP coating does not have as significant effect as the GFRP modulus of elasticity.

6.7 – Ultimate Bridge Capacity

To investigate the maximum load that the bridge is capable of handling before and after the retrofitting, the bridge was modeled once again. The loading conditions were assumed symmetric. Figure 6.45 shows the isometric view of FEM model. In this figure one can carefully see the two types of concrete element one without reinforcement (gray colored) and other with smeared reinforcement (dark colored). The sprayed GFRP layer is also shown (dark blue elements). The load deflection responses for the bridge are plotted in Figure 6.46. The numerical model predicts a maximum load of 598 kN before the retrofit and 766 kN after the retrofit. That shows an increase of 28 % over the maximum load capacity before the failure. It is clear from the numerical model that the response of the model is linear until the first crack has formed at approximately 280 kN, which corresponds to truck load of almost 38 tons (as was mentioned before, only the rear axles of truck is considered for this short span bridge). After the occurrence of cracking the load is carried out partially by the reinforcement until yielding of reinforcing bar took place, which is at 590 kN for the conventional bridge, and 707 kN

for the retrofitted bridge. That is again an indication of almost 20% improvement, and from there on it reaches to the maximum load of 766 kN before the GFRP layers fail. The ANSYS program records a crack pattern at each applied load step. Figure 6.47 shows the crack patterns for concrete before failure.

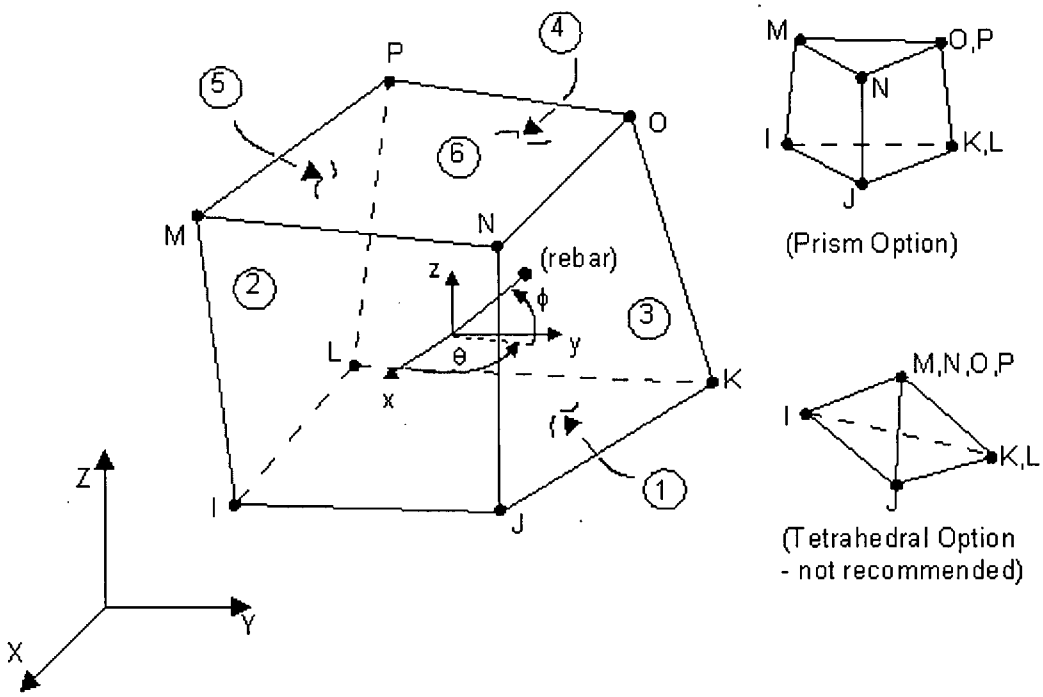

Figure 6.1: SOLID65 3-D Reinforced Concrete Solid [63].

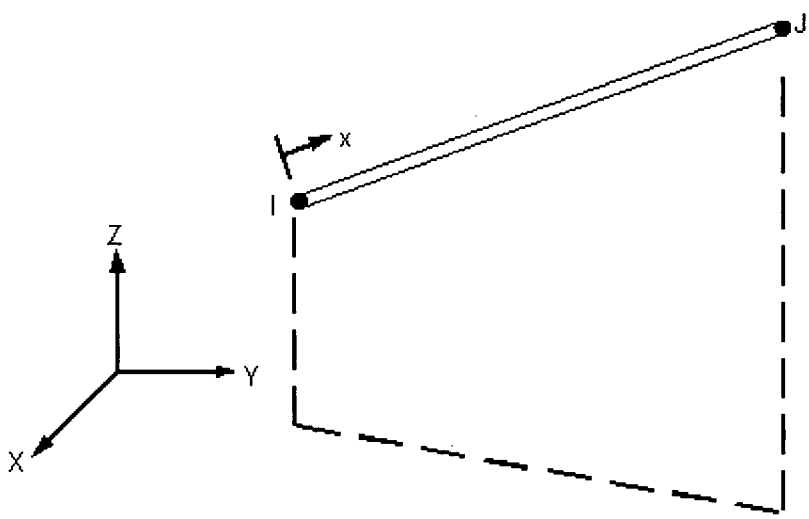

Figure 6.2: LINK8 3-D Spar [63].

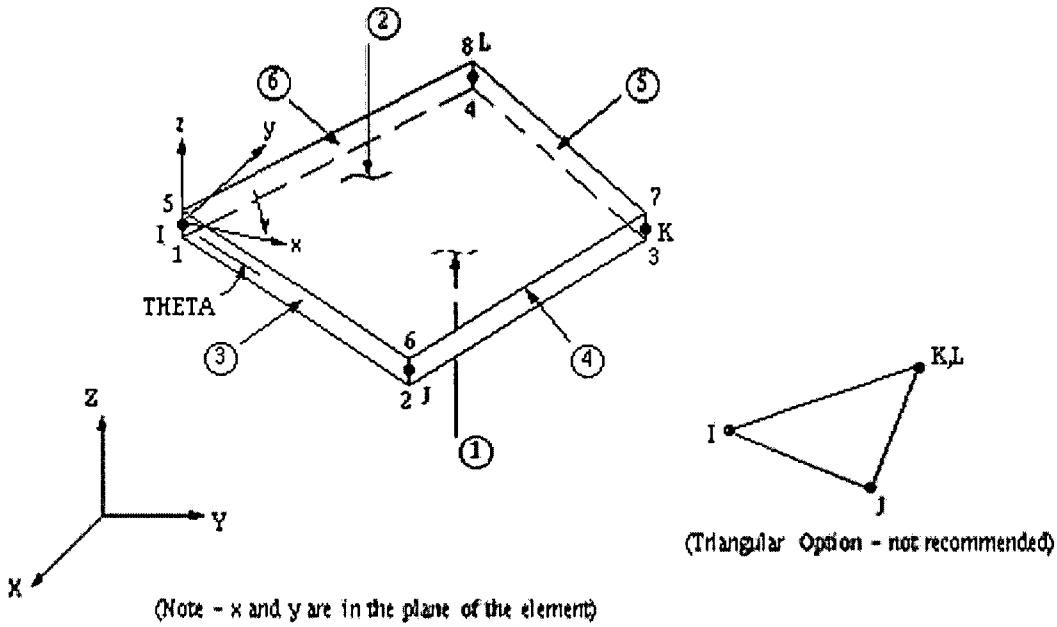

Figure 6.3: SHELL43 Plastic Large Strain Shell [63].

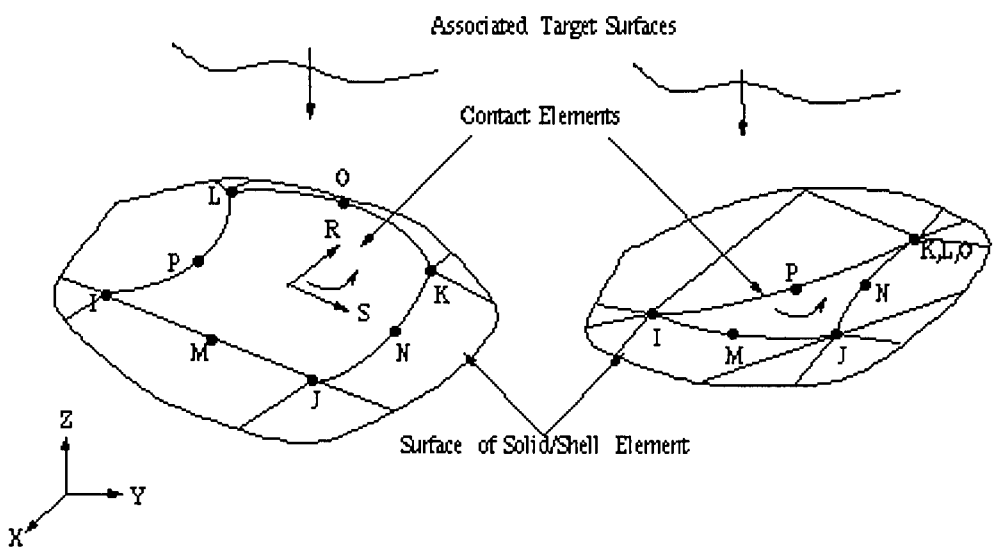

Figure 6.4: CONTA174 3-D Surface-to-Surface Contact Element (8 nodes) [63].

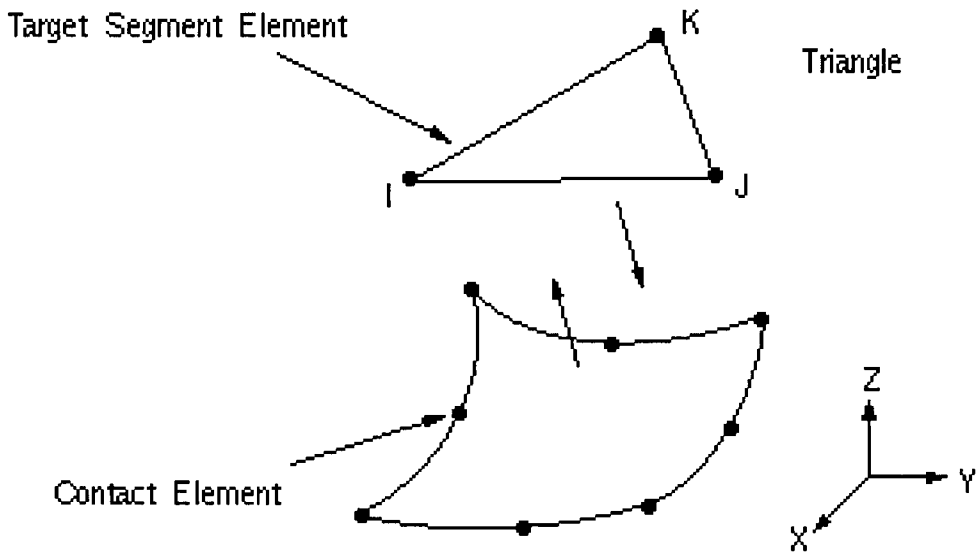

Figure 6.5: TARGE170 Target Surface Element [63].

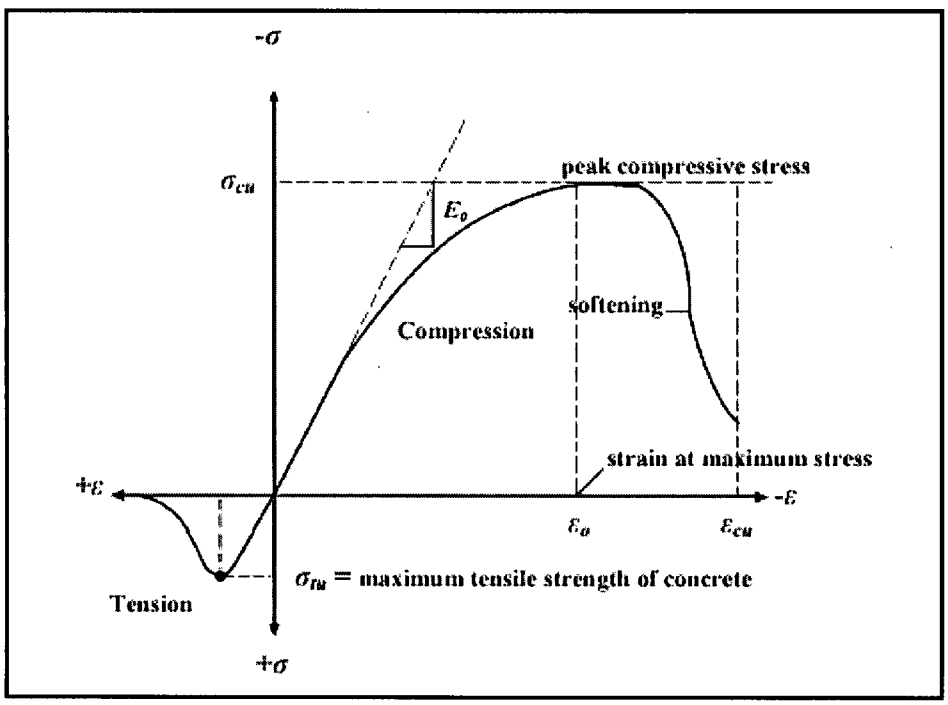

Figure 6.6: Typical uniaxial compressive and tensile stress-strain curve for concrete [65].

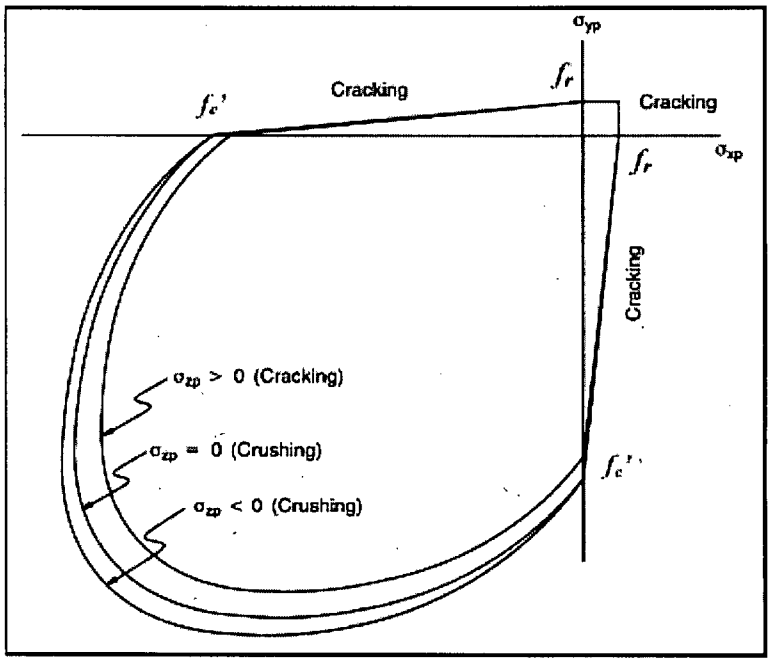

Figure 6.7: Failure Surface in Principal Stress Space σ_{zp} close to zero [63].

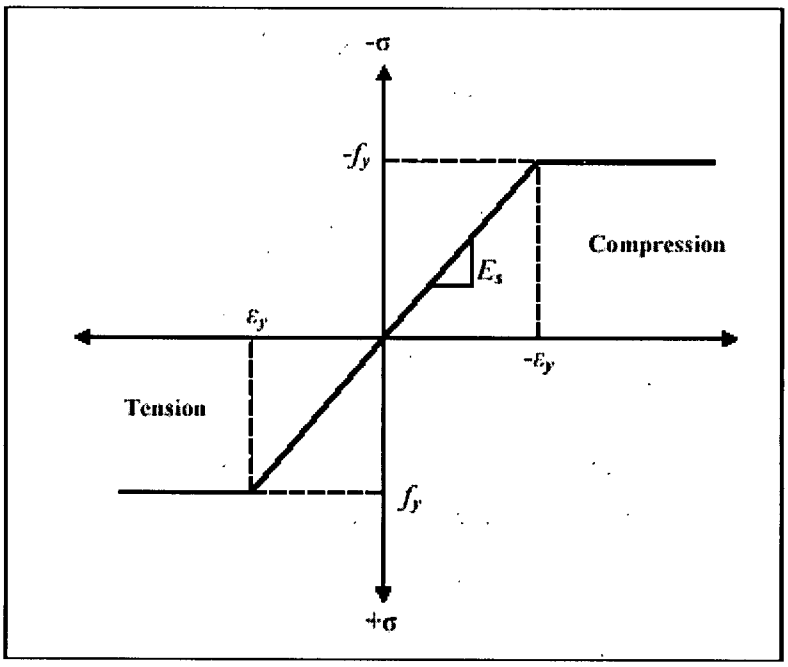

Figure 6.8: Stress-strain curve for steel reinforcement [63].

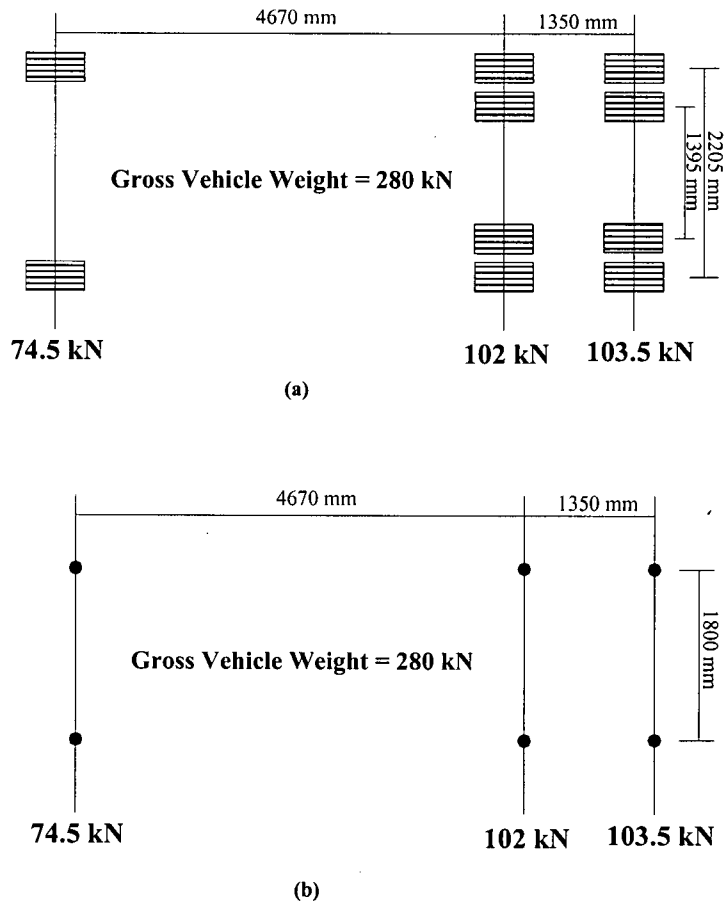

Figure 6.9: Truckload simplification: (a) and (b) show configurations of the dump truck and the simplified truck, respectively.

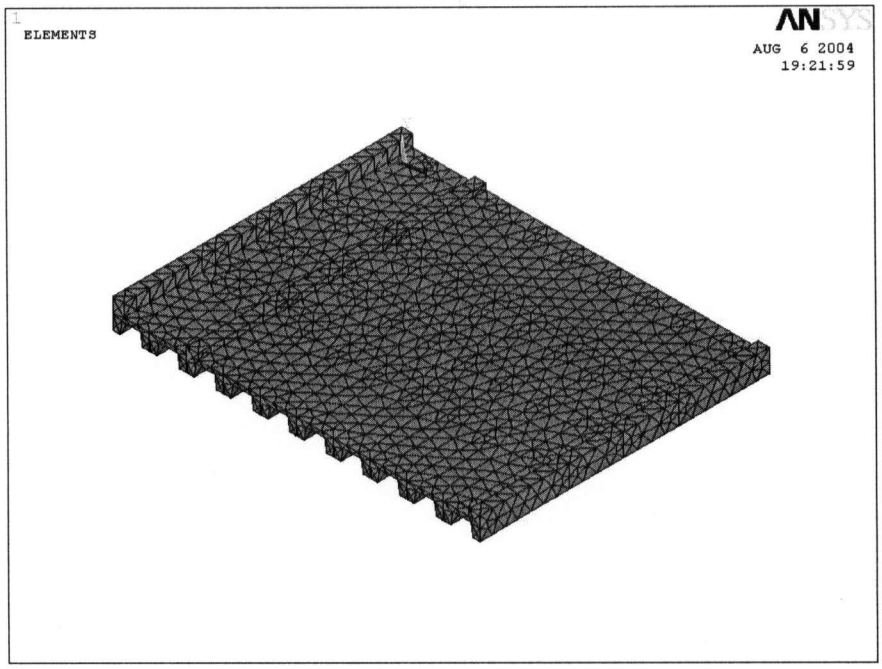

Figure 6.10: An isometric view of the finite element model of the bridge.

Table 6.1: Summary of the number of elements used in the bridge model.

Type of Element	No. of Elements
Concrete (SOLID65)	9917
Steel Bar (LINK8)	4000
Sprayed GFRP (SHELL41)	1597
Contact Elements	2797
Total	**18311**

Table 6.2: Natural circular frequency, natural frequency and natural period for the first twenty modes extracted from the FEM frequency analysis before application of GFRP.

Mode number	Natural frequency (Hz)	Frequency (rad/s)	Natural period (s)
1	21.48	134.97	0.0466
2	32.82	206.22	0.0305
3	45.64	286.76	0.0219
4	65.55	411.88	0.0153
5	67.90	426.60	0.0147
6	68.11	427.92	0.0147
7	83.37	523.83	0.0120
8	85.59	537.74	0.0117
9	97.03	609.62	0.0103
10	102.65	644.95	0.0097
11	121.20	761.50	0.0083
12	125.77	790.21	0.0080
13	132.35	831.56	0.0076
14	140.07	880.06	0.0071
15	143.41	901.05	0.0070
16	153.34	963.44	0.0065
17	158.46	995.60	0.0063
18	178.91	1124.09	0.0056
19	180.22	1132.32	0.0055
20	183.58	1153.43	0.0054

Table 6.3: Natural circular frequency, natural frequency and natural period for the first twenty modes extracted from the FEM frequency analysis after application of GFRP.

Mode number	Natural frequency (Hz)	Frequency (rad/s)	Natural period (s)
1	23.88	150.03	0.0419
2	36.48	229.23	0.0274
3	50.73	318.75	0.0197
4	72.87	457.83	0.0137
5	75.47	474.20	0.0132
6	75.71	475.67	0.0132
7	92.68	582.28	0.0108
8	95.14	597.74	0.0105
9	107.85	677.62	0.0093
10	114.11	716.95	0.0088
11	134.72	846.45	0.0074
12	139.81	878.43	0.0072
13	147.12	924.35	0.0068
14	155.70	978.26	0.0064
15	159.41	1001.57	0.0063
16	170.45	1070.94	0.0059
17	176.14	1106.69	0.0057
18	198.87	1249.50	0.0050
19	200.33	1258.67	0.0050
20	204.06	1282.11	0.0049

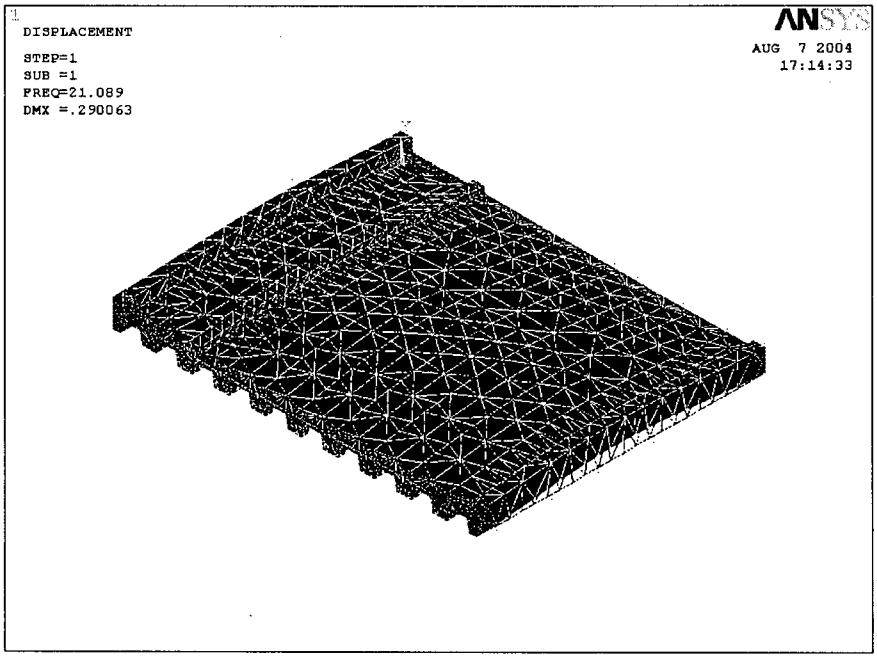

Figure 6.11: Mode shape corresponding to fundamental vibration frequency before the application of GFRP.

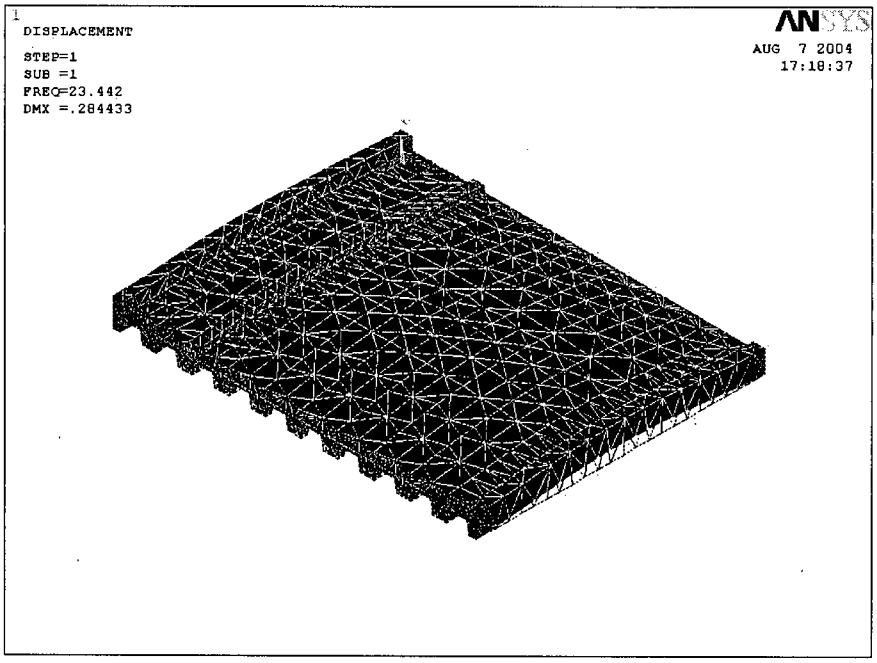

Figure 6.12: Mode shape corresponding to fundamental vibration frequency after the application of GFRP.

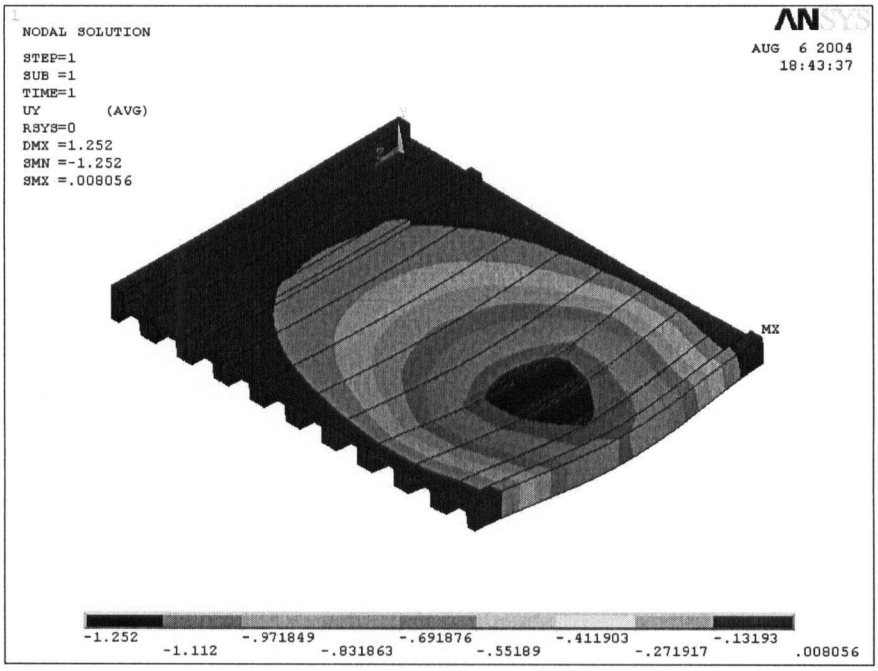

Figure 6.13: Deflection under static load position 1, before the application of GFRP.

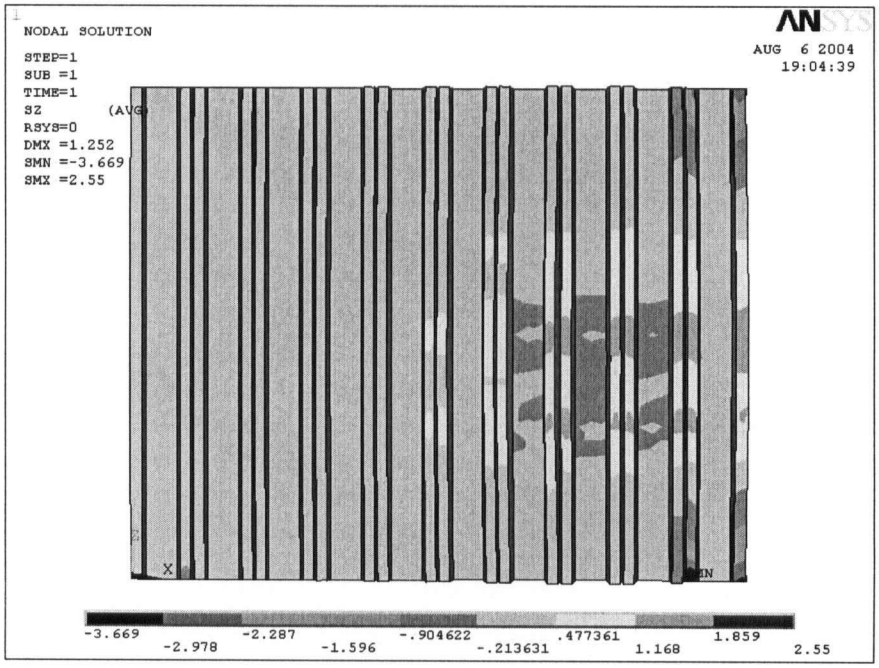

Figure 6.14: Stress distribution under static load position 1, before application of GFRP.

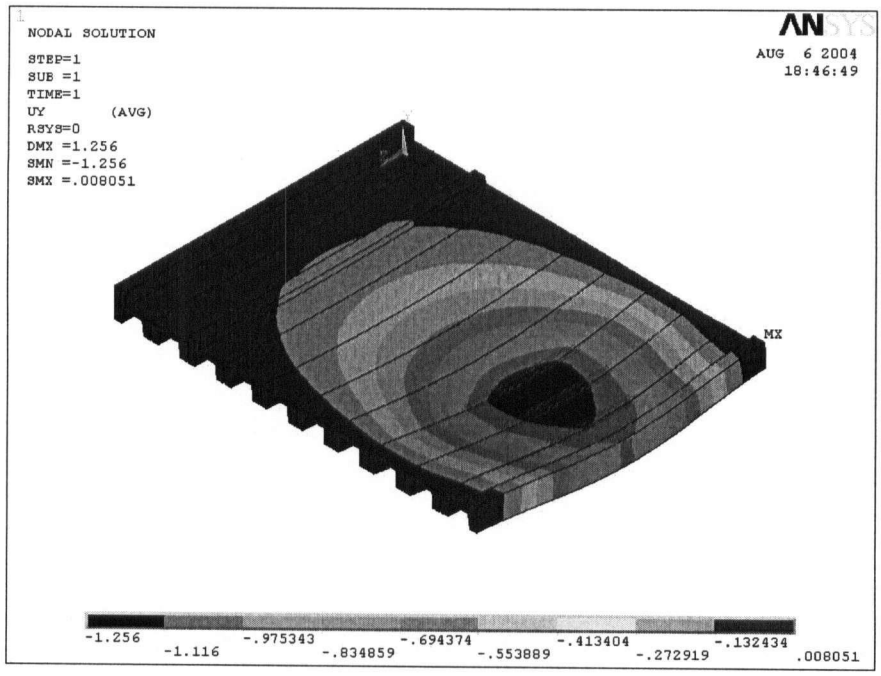

Figure 6.15: Deflection under static load position 2, before the application of GFRP.

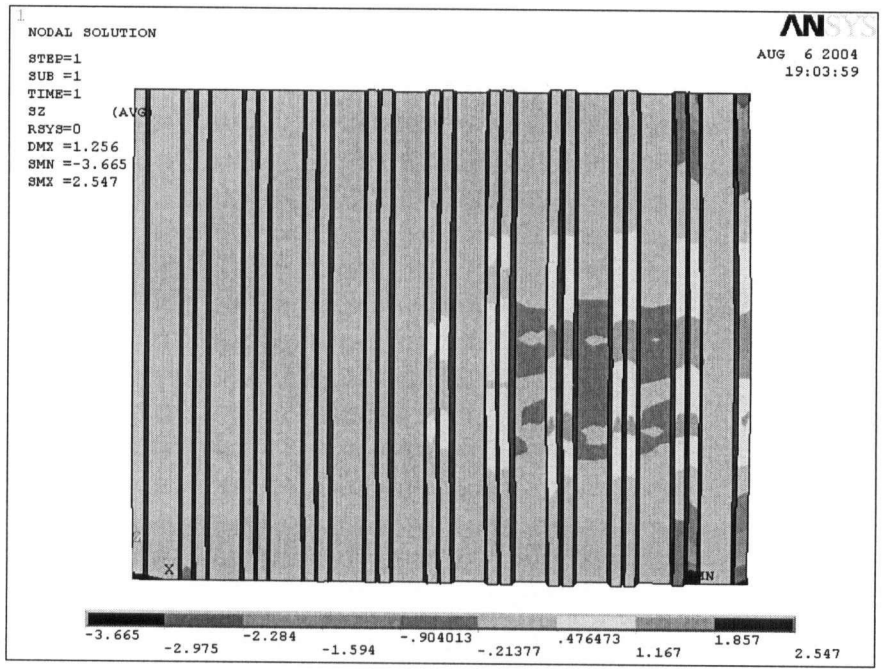

Figure 6.16: Stress distribution under static load position 2, before application of GFRP.

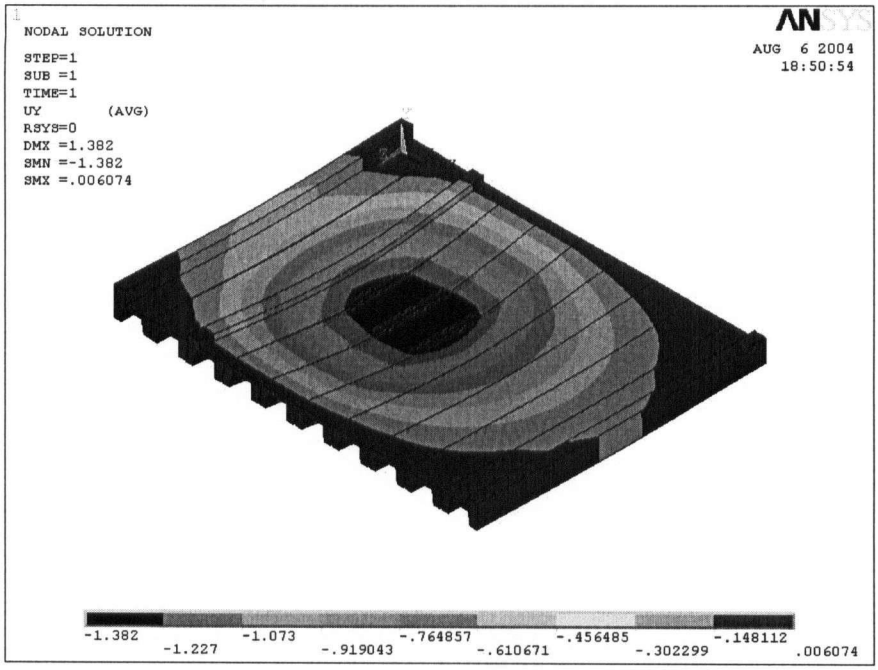

Figure 6.17: Deflection under static load position 3, before the application of GFRP.

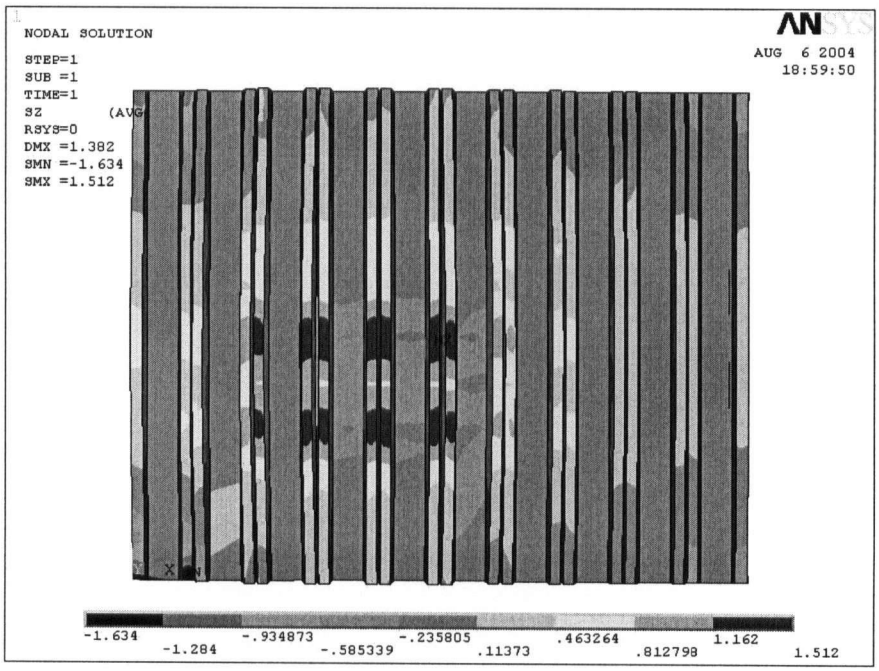

Figure 6.18: Stress distribution under static load position 3, before application of GFRP.

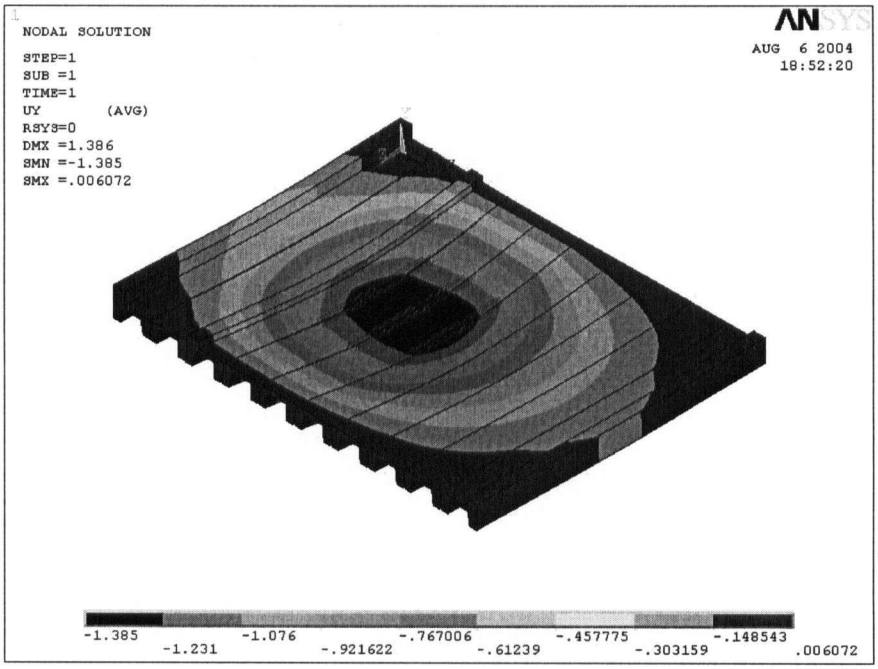

Figure 6.19: Deflection under static load position 4, before the application of GFRP.

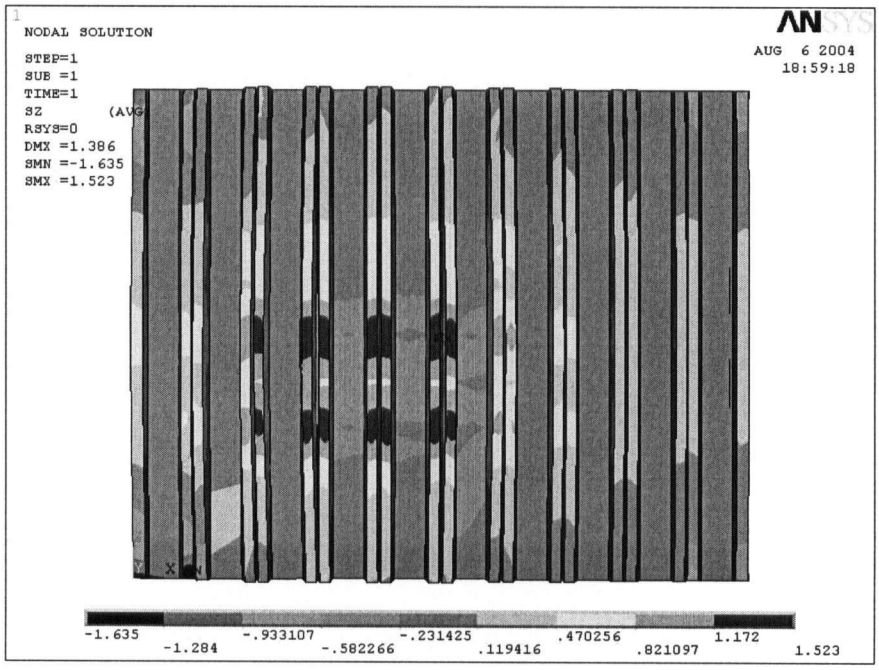

Figure 6.20: Stress distribution under static load position 4, before application of GFRP.

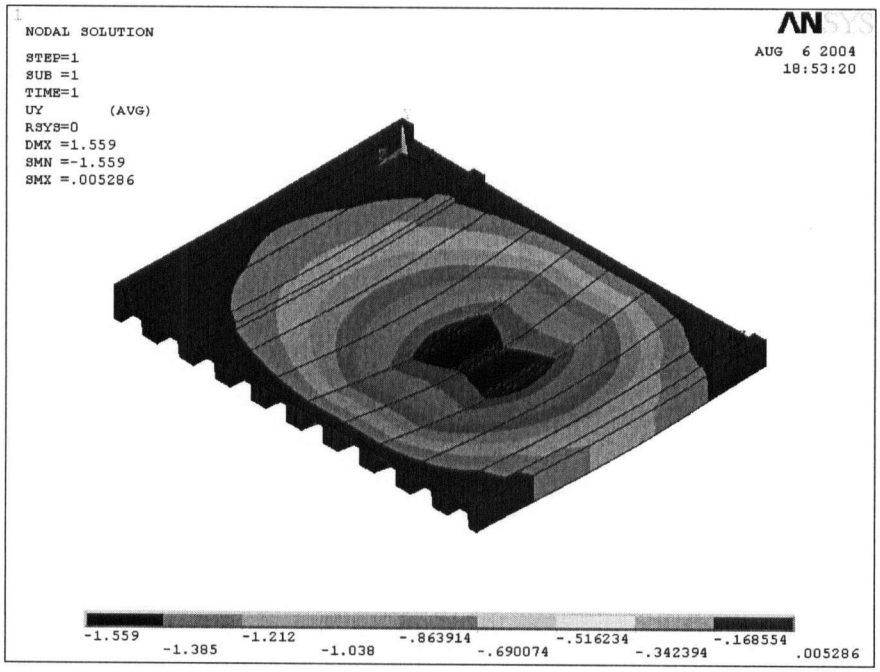

Figure 6.21: Deflection under static load position 5, before the application of GFRP.

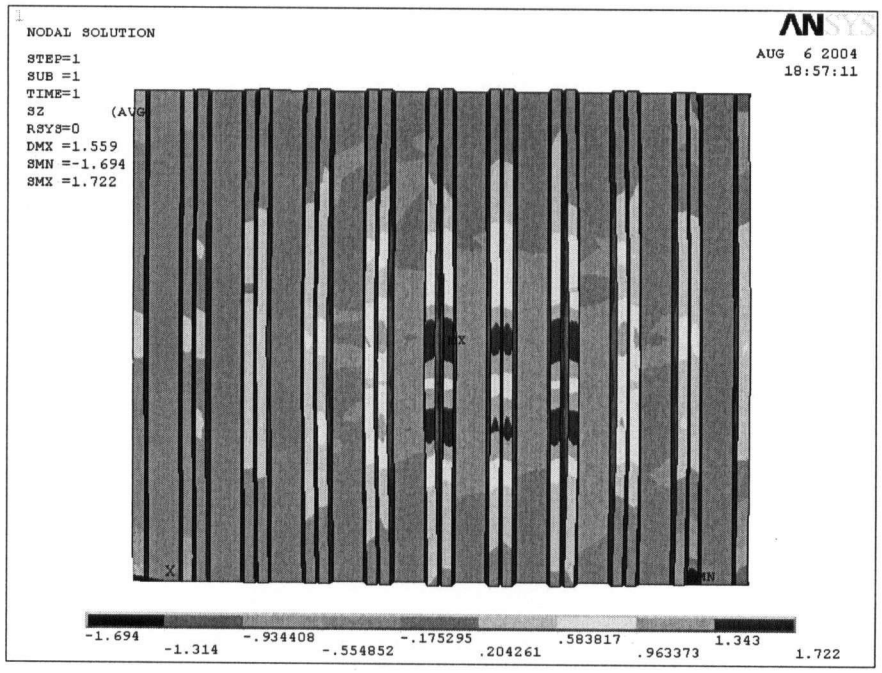

Figure 6.22: Stress distribution under static load position 5, before application of GFRP.

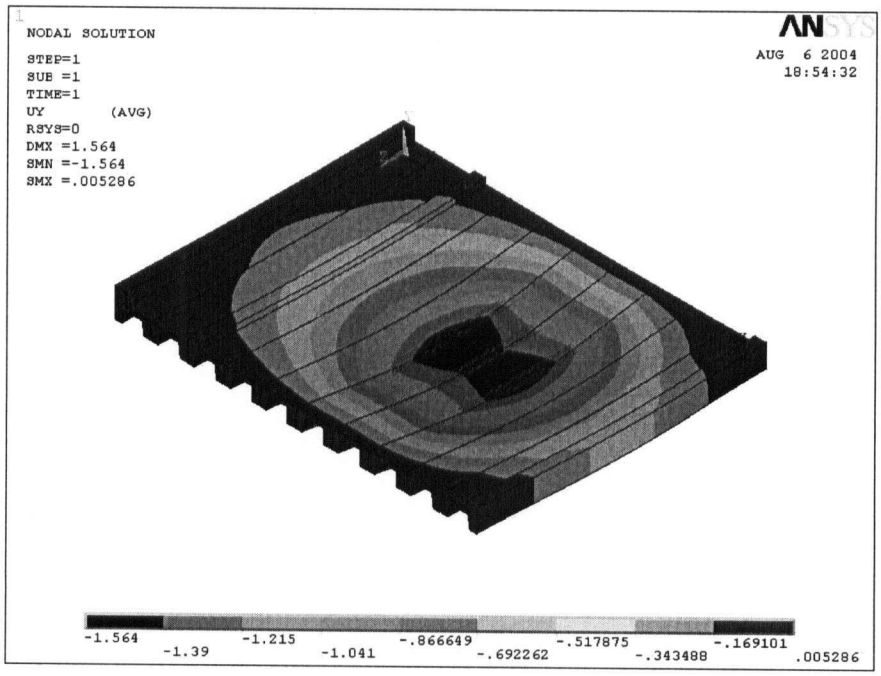

Figure 6.23: Deflection under static load position 6, before the application of GFRP.

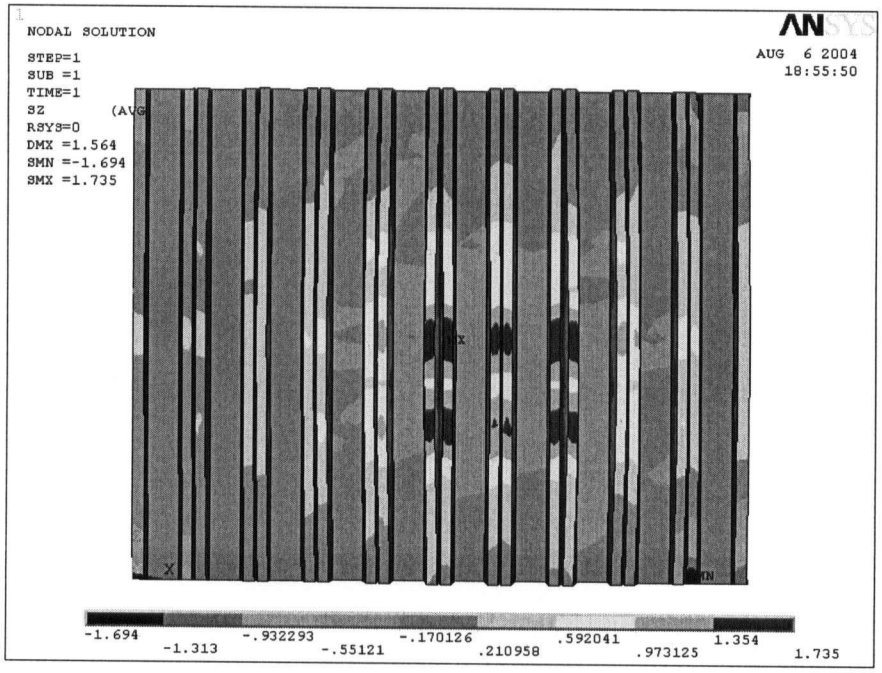

Figure 6.24: Stress distribution under static load position 6, before application of GFRP.

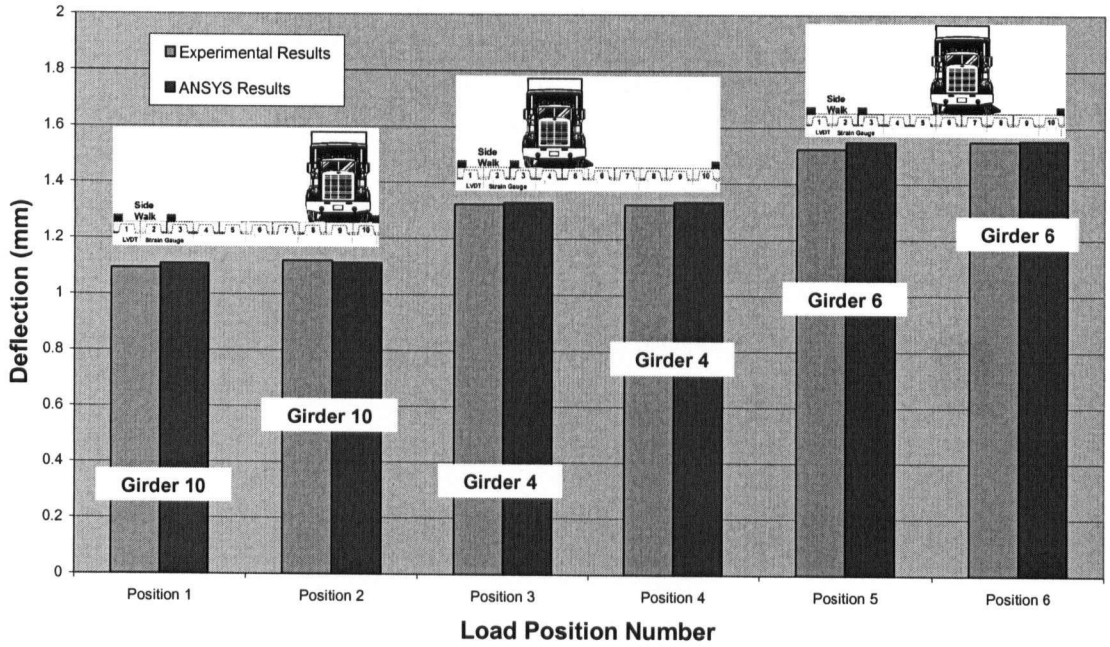

Figure 6.25: Comparison between the experimental and ANSYS results before the application of GFRP.

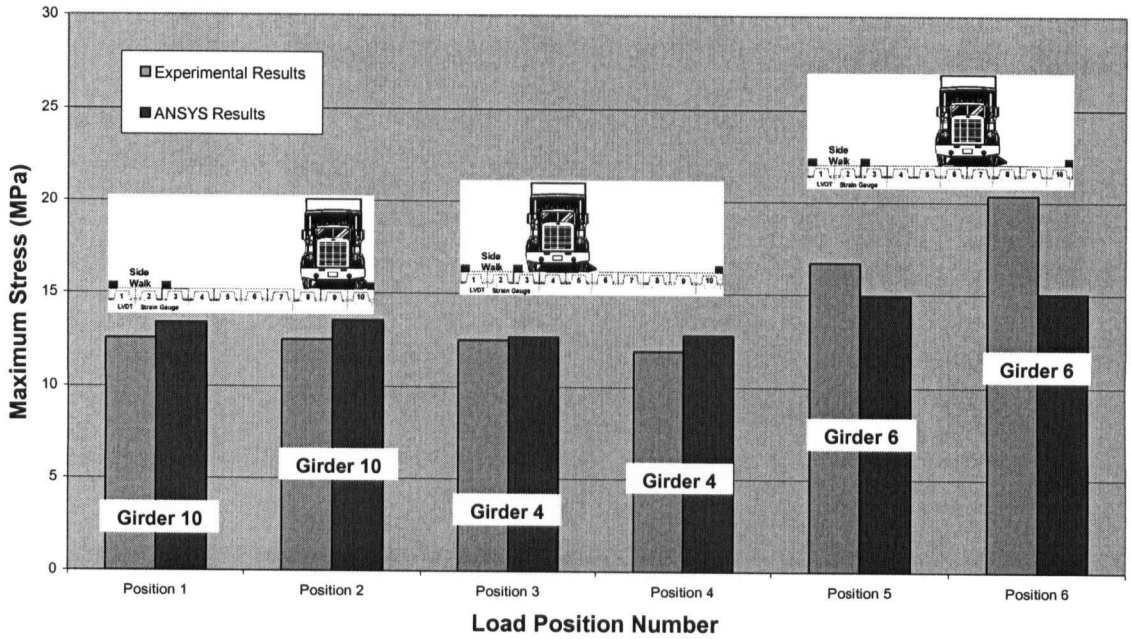

Figure 6.26: Comparison between the experimental and ANSYS results *before the* application of GFRP.

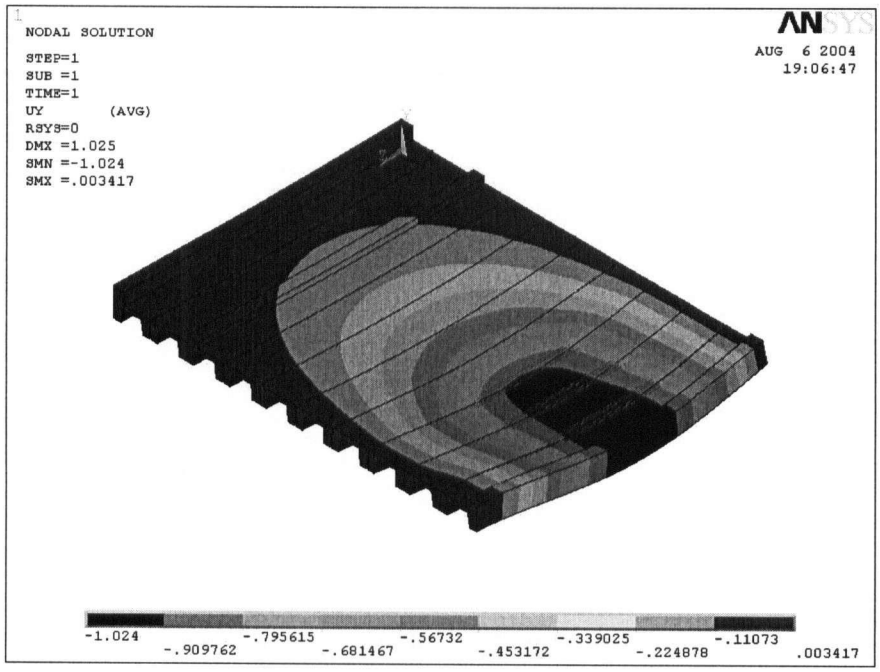

Figure 6.27: Deflection under static load position 1, after the application of GFRP.

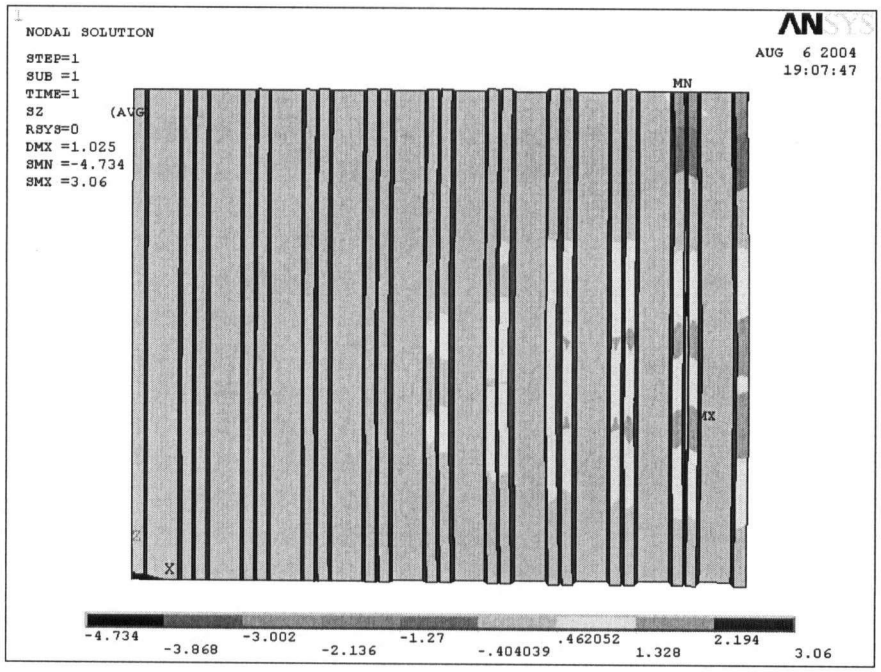

Figure 6.28: Stress distribution under static load position 1, after application of GFRP.

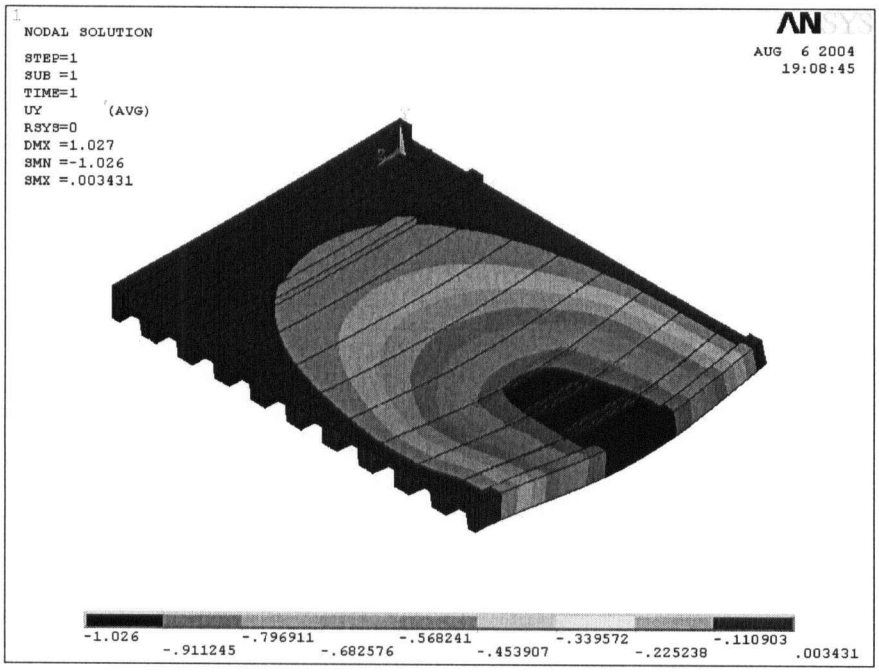

Figure 6.29: Deflection under static load position 2, after the application of GFRP.

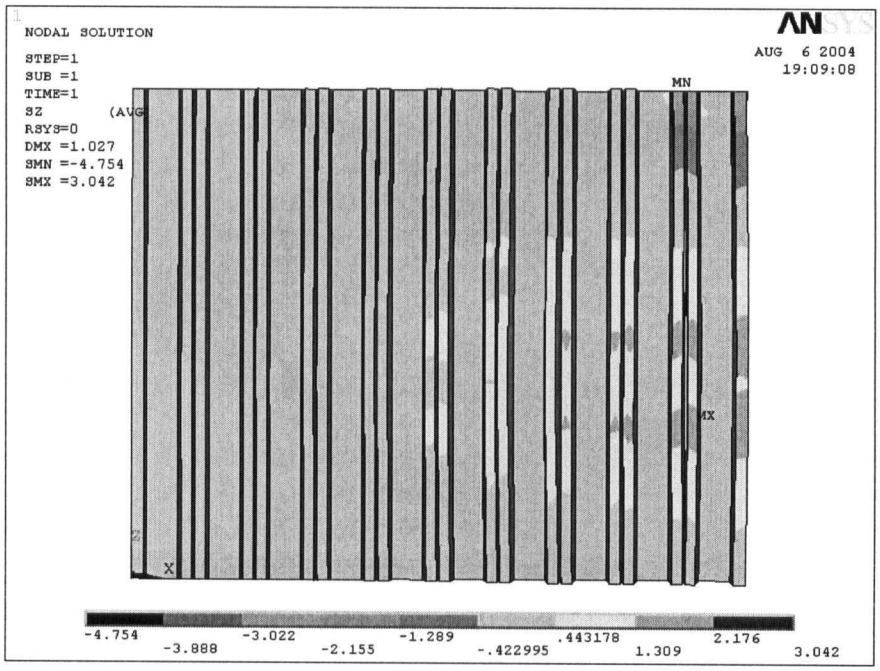

Figure 6.30: Stress distribution under static load position 2, after application of GFRP.

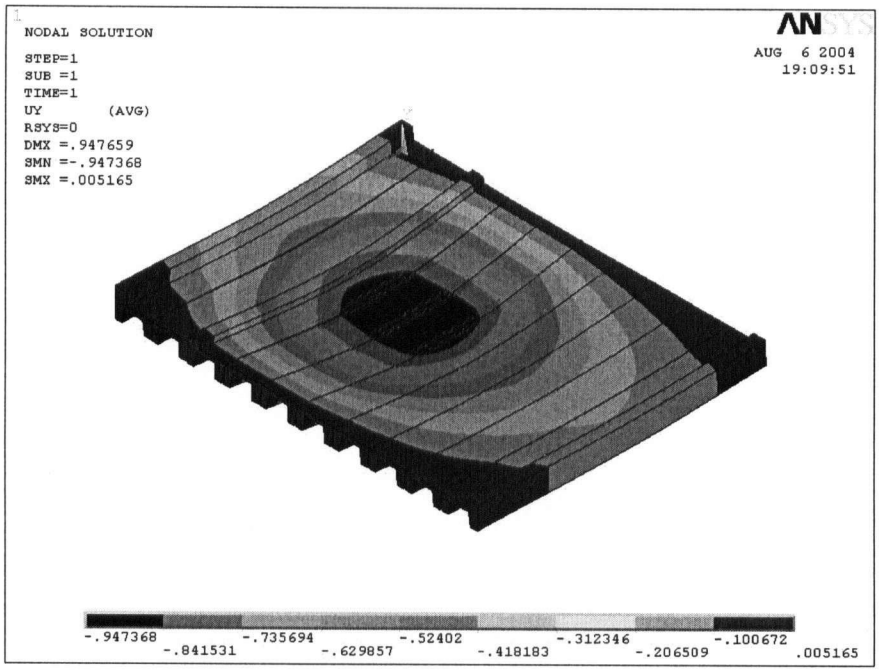

Figure 6.31: Deflection under static load position 3, after the application of GFRP.

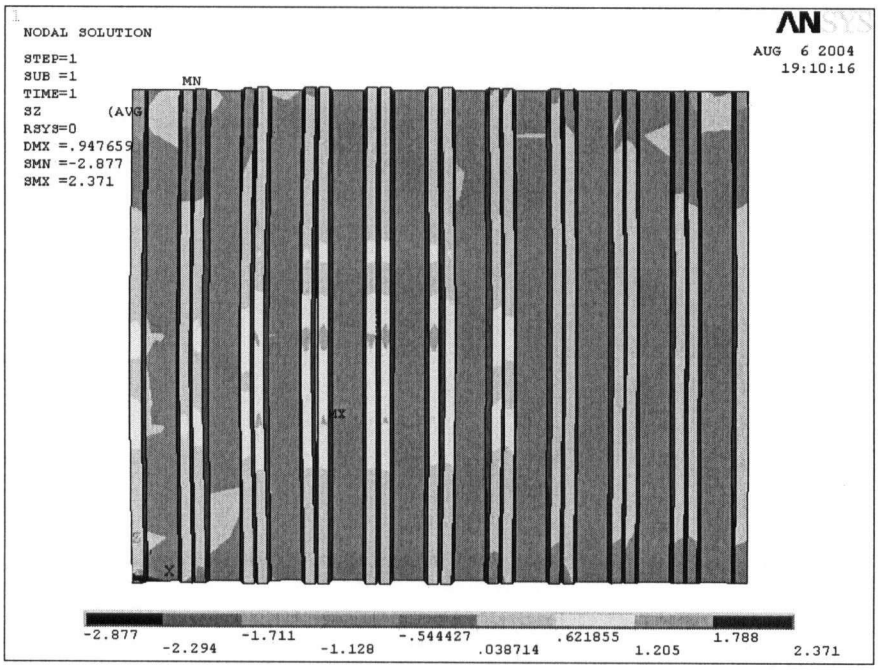

Figure 6.32: Stress distribution under static load position 3, after application of GFRP.

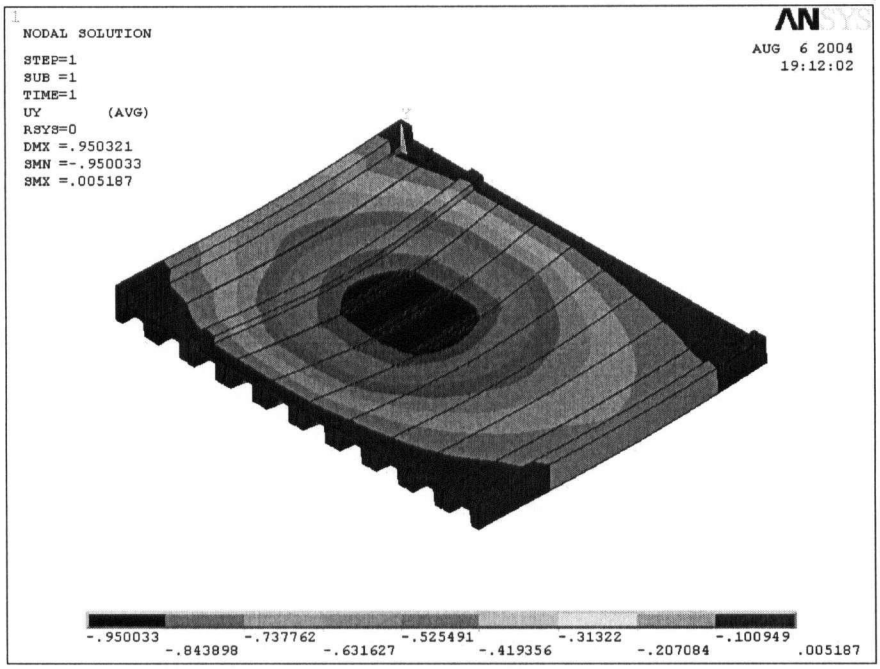

Figure 6.33: Deflection under static load position 4, after the application of GFRP.

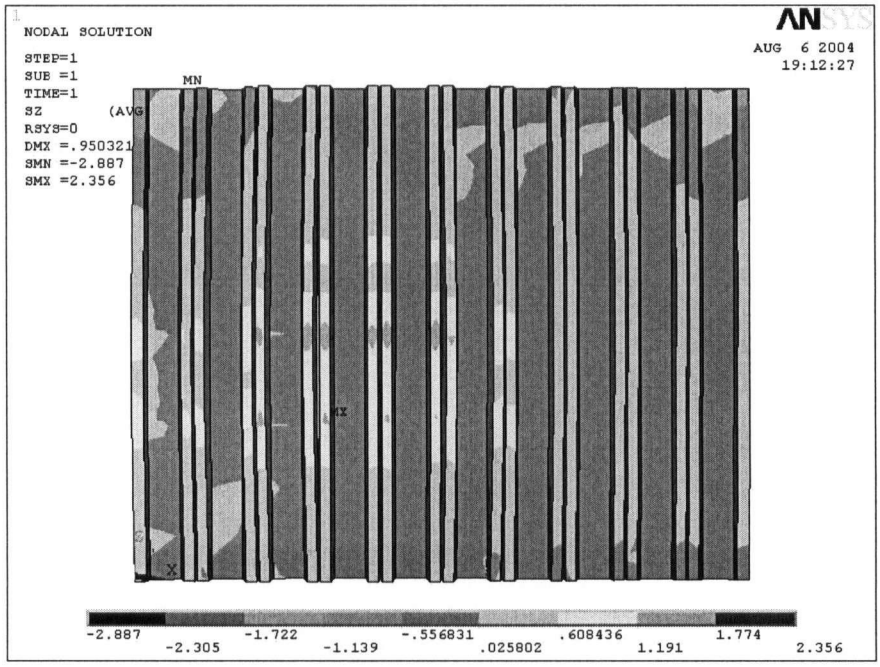

Figure 6.34: Stress distribution under static load position 4, after application of GFRP.

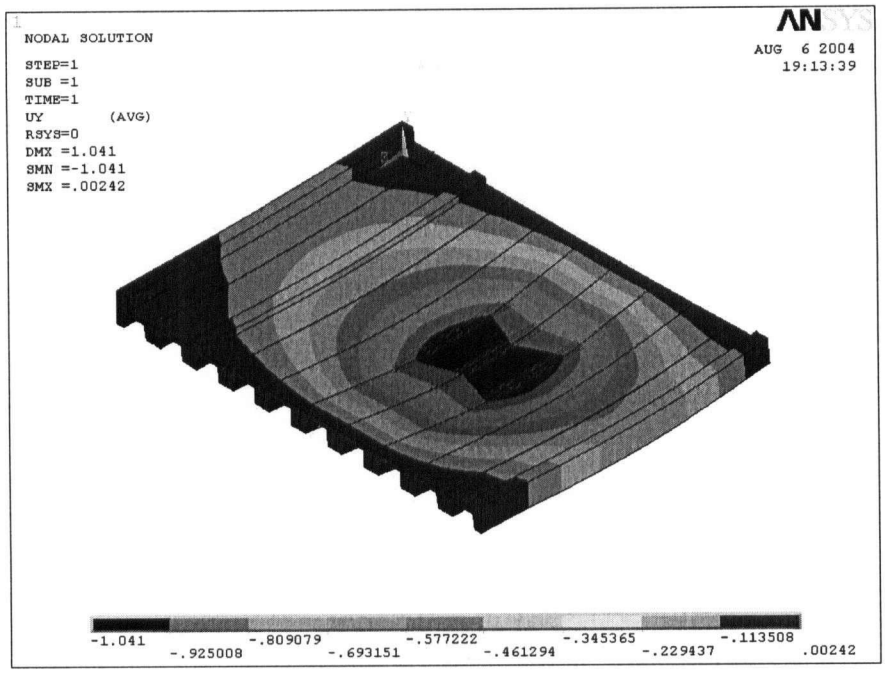

Figure 6.35: Deflection under static load position 5, after the application of GFRP.

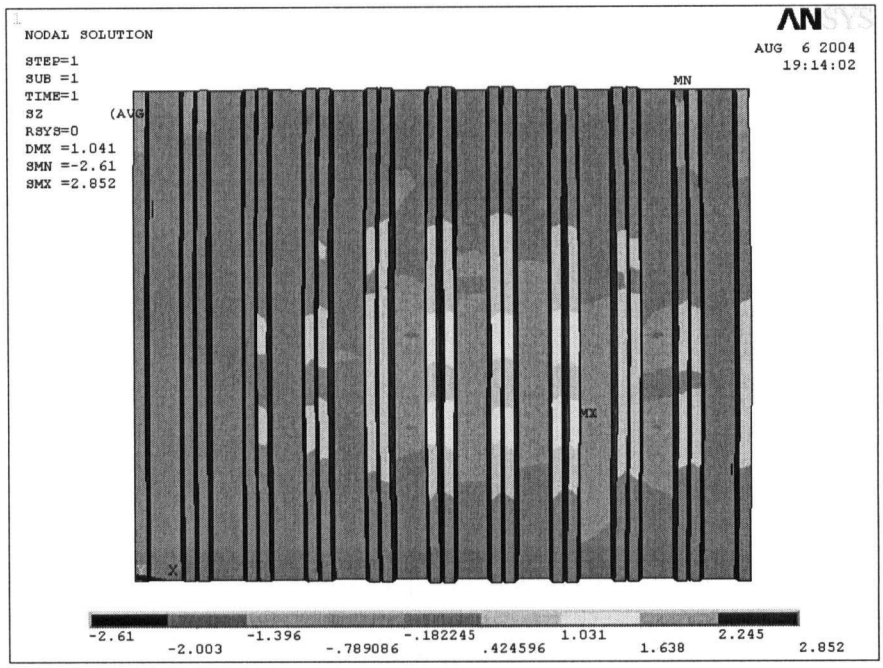

Figure 6.36: Stress distribution under static load position 5, after application of GFRP.

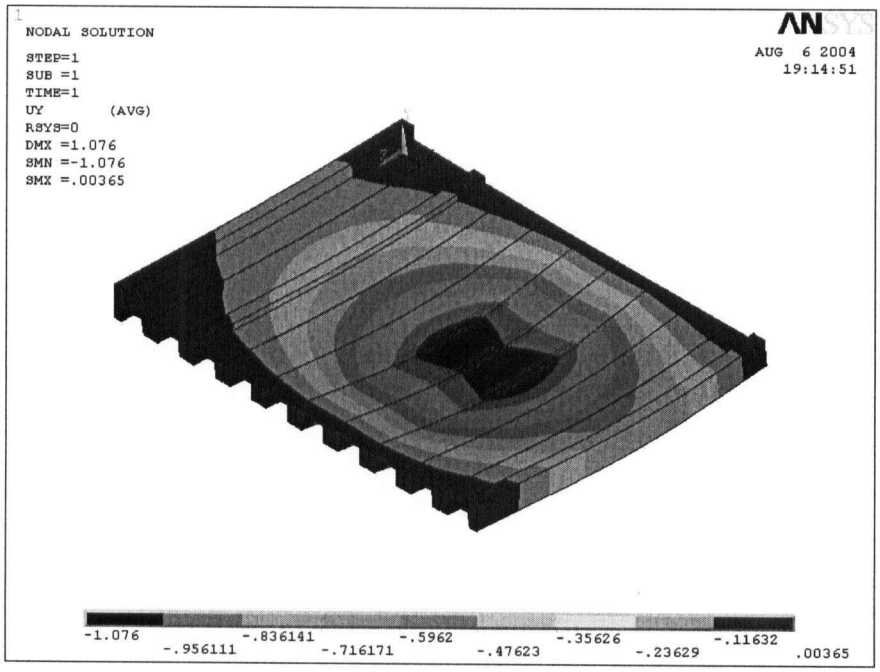

Figure 6.37: Deflection under static load position 6, after the application of GFRP.

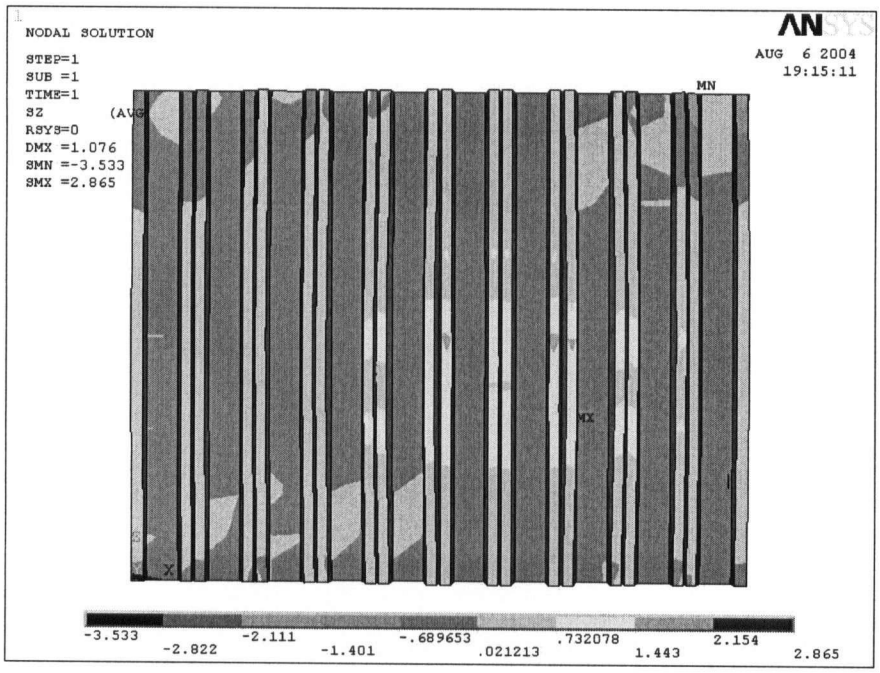

Figure 6.38: Stress distribution under static load position 6, after application of GFRP.

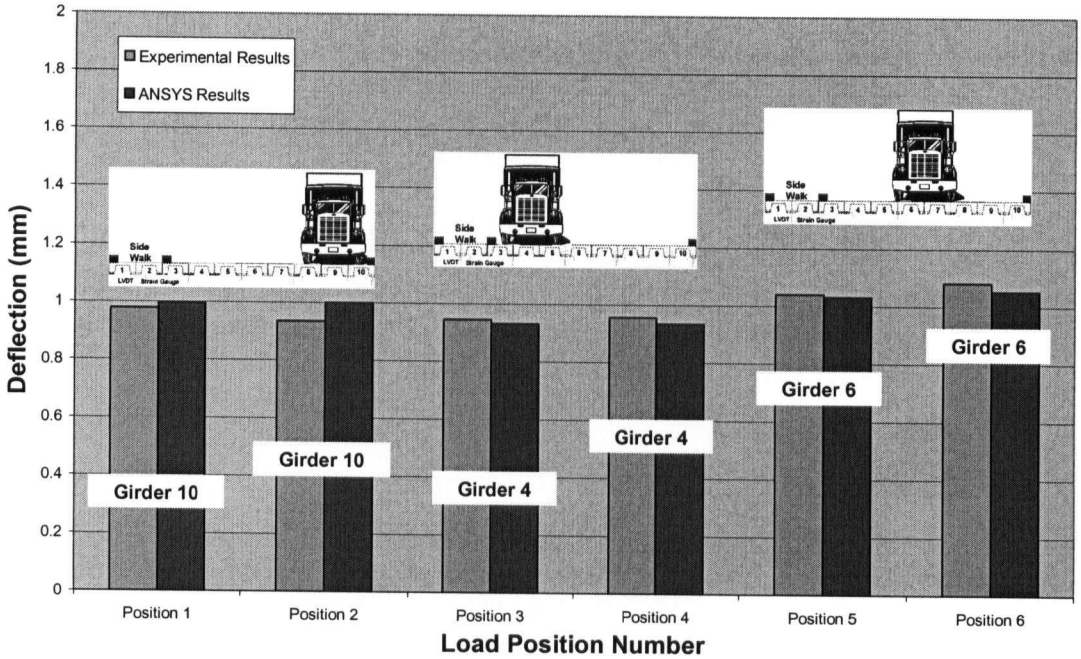

Figure 6.39: Comparison between the experimental and ANSYS results after the application of GFRP.

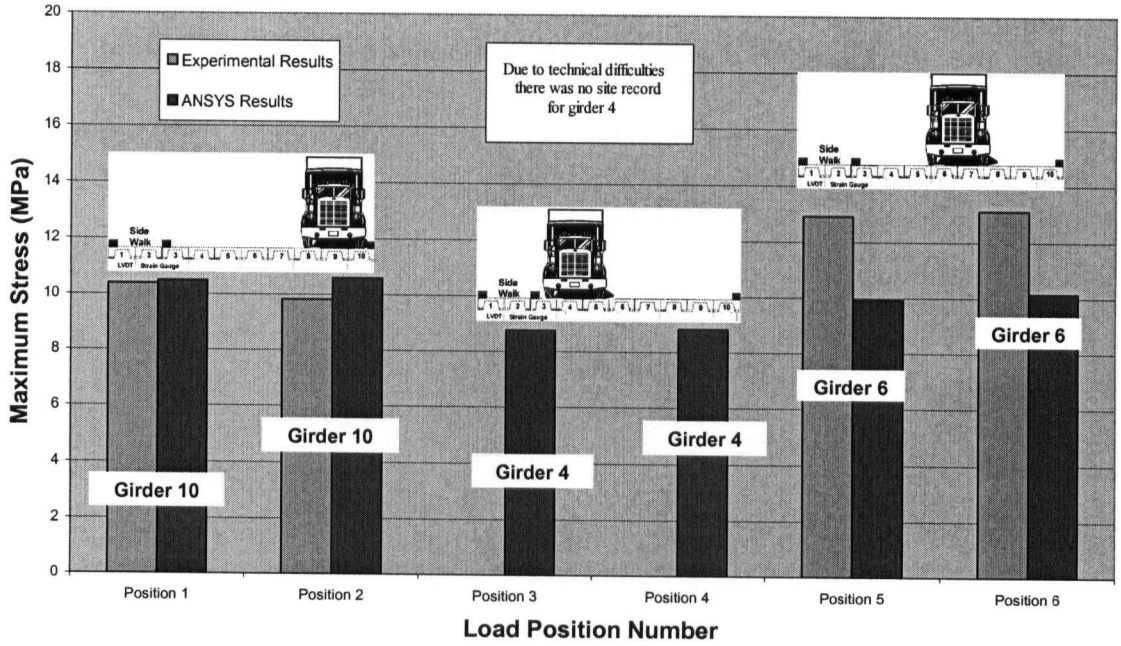

Figure 6.40: Comparison between the experimental and ANSYS results after the application of GFRP.

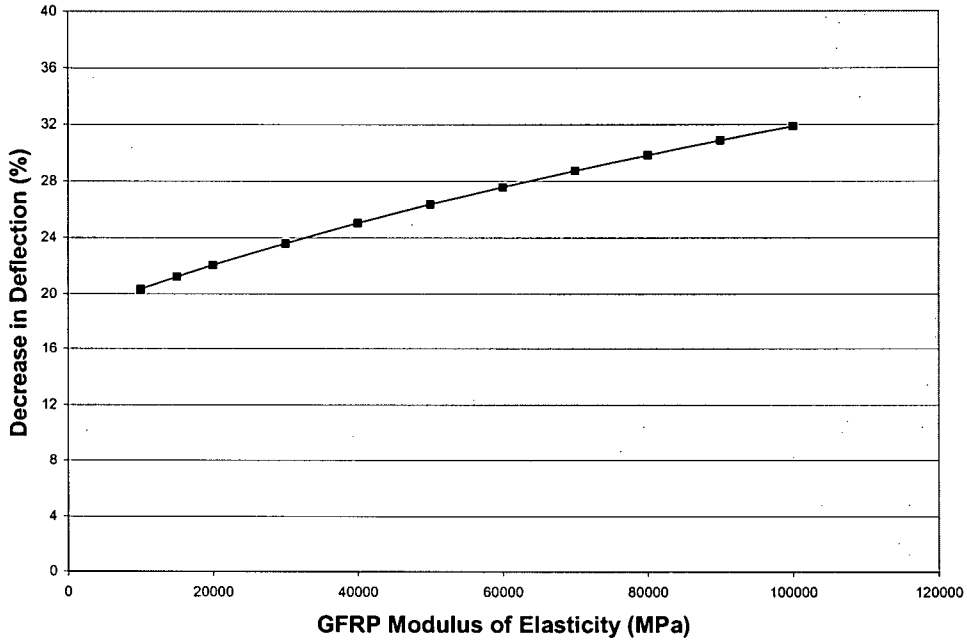

Figure 6.41: Effect of GFRP modulus of elasticity on reduction of maximum girder deflection (girder 6).

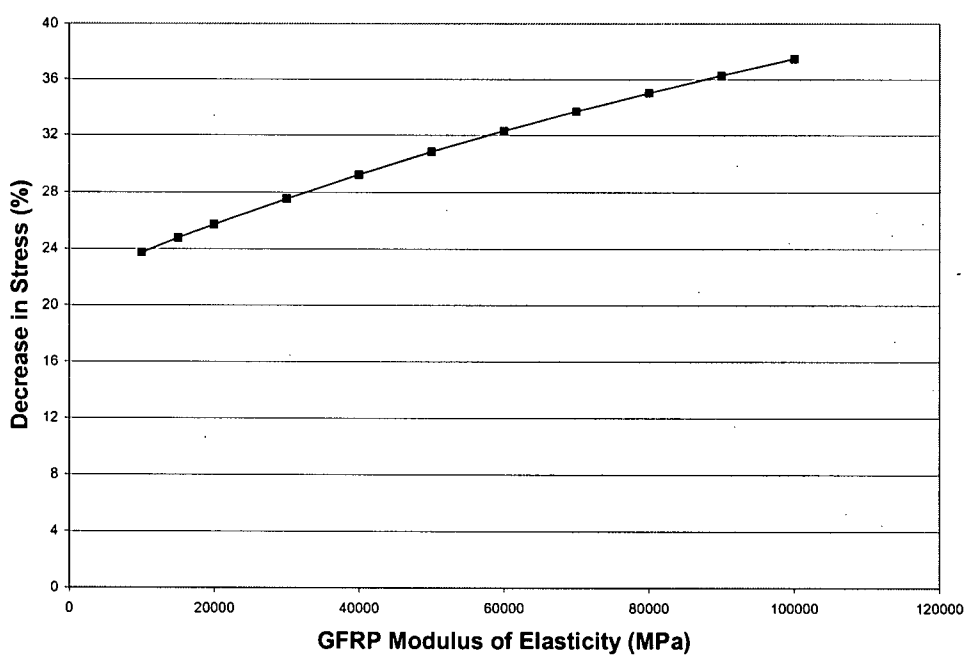

Figure 6.42: Effect of GFRP modulus of elasticity on reduction of maximum stress in reinforcing steel (girder 6).

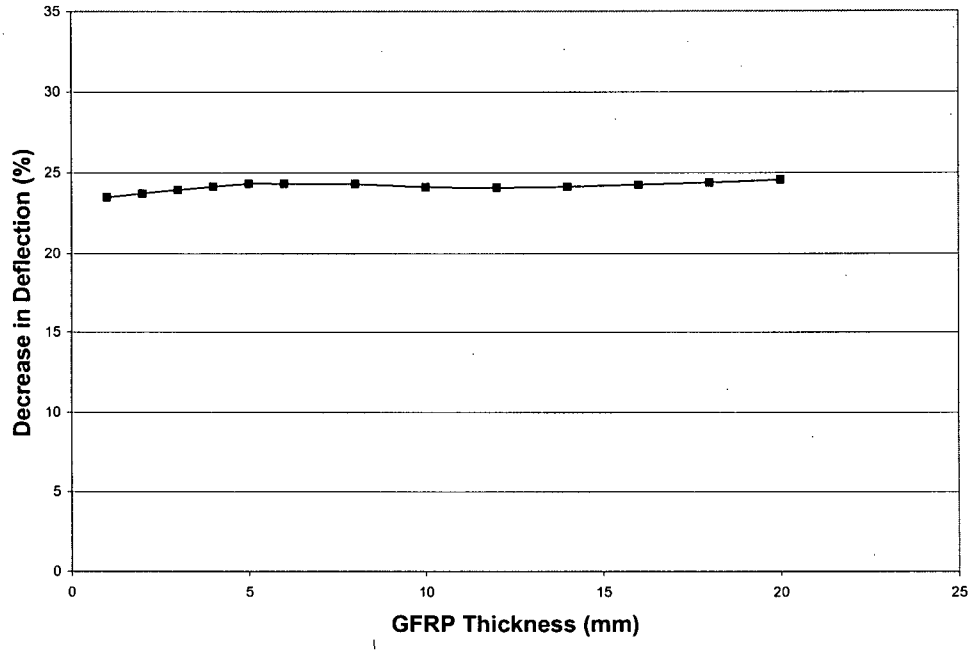

Figure 6.43: Effect of GFRP thickness on reduction of maximum girder deflection (girder 6).

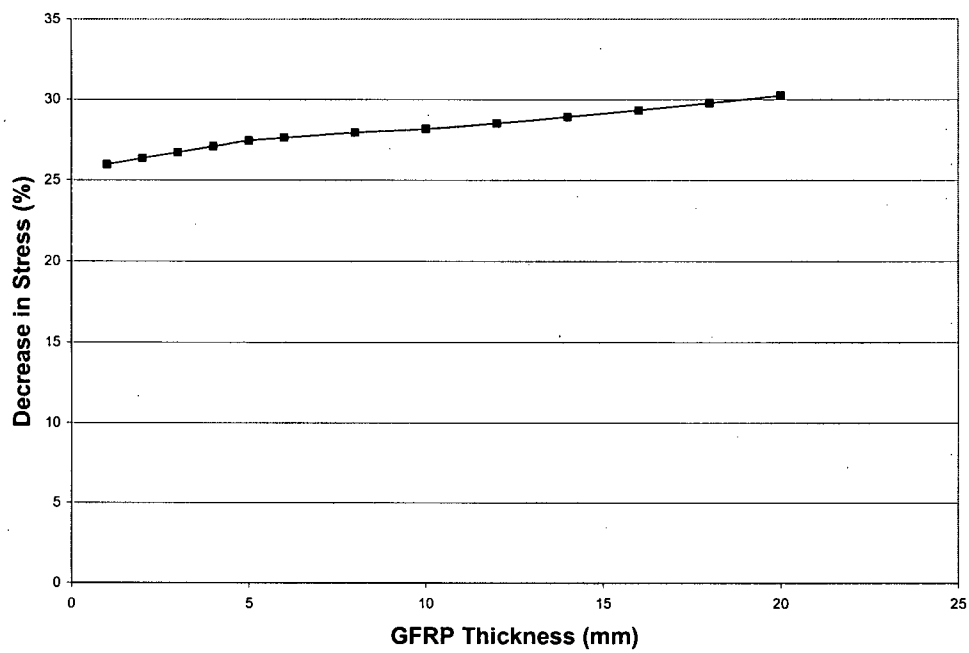

Figure 6.44: Effect of GFRP thickness on reduction of maximum stress in reinforcing steel (girder 6).

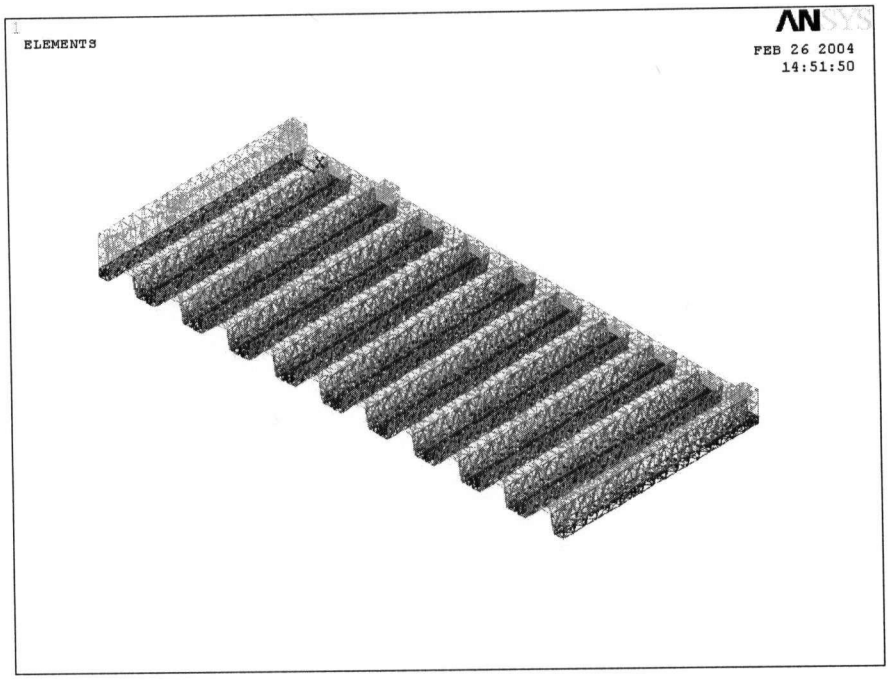

Figure 6.45: An isometric view of the finite element model using the transverse symmetry.

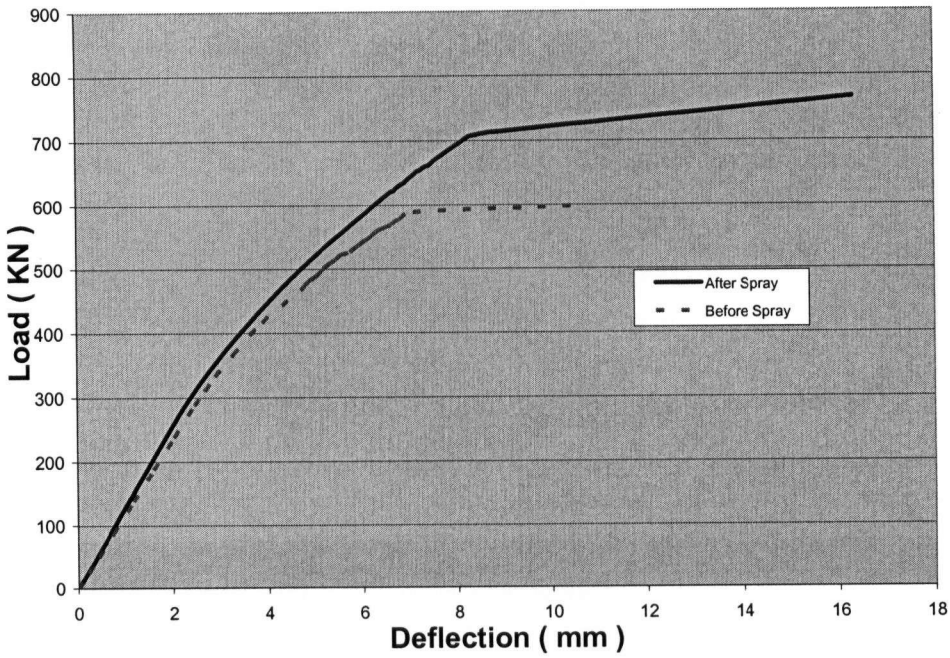

Figure 6.46: Load deflection response for the Safe bridge.

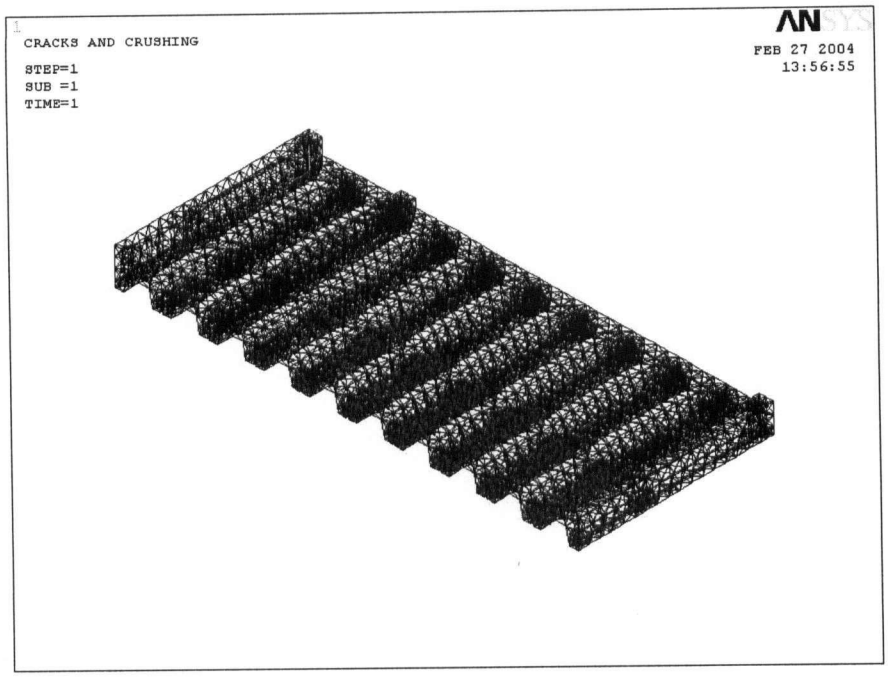

Figure 6.47: Crack patterns for the Safe bridge.

7

FINITE ELEMENT ANALYSIS OF FULL-SCALE SPECIMENS

In order to validate our numerical modeling, three full scale reinforced concrete bridge channel beams which were already tested experimentally by Andrew Boyd [12] at UBC were selected for analysis. These beams came from an existing but badly deteriorated bridge that required complete replacement after approximately 50 years of service. The Ministry of Transportation and Highways of British Columbia supplied three girders for testing.

7.1 – Experimental Testing of MOTH Beam

7.1.1 – Beam Description

The beams cross section shown schematically in Figure 7.1. These beams were cast from a structural lightweight aggregate concrete with a core compressive strength of 35 MPa. It was discovered [12] that all of the reinforcing steel present was in imperial bar sizes with tensile strengths ranging from 304 MPa to 408 MPa. The steel reinforcements contained in these sections is shown in Figure 7.2, again with all sizes being indicated using imperial bar sizes. The shear stirrups were spaced at varying intervals along the length of the beam, ranging from a minimum spacing of 125 mm at the ends of the beam to a maximum spacing of 760 mm at the midspan.

7.1.2 - Specimen Preparation

After patching the three channel beams supplied, one was rehabilitated with the sprayed GFRP technique (Figure 7.3); a second was retrofitted using a commercially available continuous glass fiber fabric system (Figure 7.4). This latter approach utilized the MBrace® system produced by Master Builder Technologies. The third specimen was to be tested in its original state to serve as a control specimen [12].

7.1.3 – Experimental Setup and Results

All three of the beams were tested under third-point loading using four large hydraulic jacks as load actuators. Figure 7.5 shows a schematic diagram of the test setup. LVDTs were used to record the deflection of the beam, while load cells provided the load

information. Figure 7.6 shows the actual load deflection curves for the three beams tested.

7.2 – Finite Element Modeling of MOTH Beam

7.2.1 – Element Description

7.2.1.1 – Reinforced Concrete

As explained previously, reinforced concrete is modeled using SOLID65 with smeared reinforcement LINK8.

7.2.1.2 – Sprayed Glass Fiber Reinforced Polymers

SOLID45 is used to model the sprayed GFRP layer (Figure 7.7). SOLID45 is used for the three-dimensional modeling of solid structures. The element is defined by eight nodes having three degrees of freedom at each node: translations in the nodal x, y, and z directions. The element has plasticity, creep, swelling, stress stiffening, large deflection, and large strain capabilities.

7.2.1.3 – Wrapped Glass Fiber Reinforced Polymers

SOLID46 was used to model the wrapped GFRP layer (Figure 7.8). SOLID46 is a layered version of the 8-node structural solid (SOLID45) designed to model layered thick shells or solids. The element allows up to 250 different material layers. If more than 250 layers are required, a user-input constitutive matrix option is available. The element may also be stacked as an alternative approach. The element has three degrees

of freedom at each node: translations in the nodal x, y, and z directions. See Section 14.46 of the *ANSYS Theory Reference* for details of this element.

7.2.2 – Material Properties

7.2.2.1 – Concrete and Steel Reinforcement

The material properties for concrete were the same as defined previously, except here the compressive strength of concrete was taken to be 35 MPa, and consequently the other properties were changed accordingly based on the defined formulae (*Section 6.2.1.1*). Steel Reinforcements had the same properties as discussed before (*Section 6.2.2*).

7.2.2.2 – Sprayed GFRP Composites

As stated by Boyd [12] for a nominal GFRP thickness of 8 mm and 48 mm fibers the composite had an ultimate strength of 108 MPa, and modulus of elasticity of 11.8 GPa. The Poisson's Ratio was chosen to be 0.27 for sprayed GFRP, and it is assumed to be isotropic.

7.2.2.3 – Wrapped GFRP Composites

GFRP composites are materials that consist of two constituents. The constituents are combined at a macroscopic level and are not soluble in each other. One constituent is the reinforcement that is embedded in the second constituent, a continuous polymer called the matrix [68]. The reinforcing material is in the form of glass fibers, which are typically stiffer and stronger than the matrix. The GFRP composites are anisotropic

materials. That means their properties are not the same in all directions. The unidirectional lamina has three mutually orthogonal planes of material properties (i.e., *xy*, *xz*, and *yz* planes). The *xyz* coordinate axes are referred to as the principal material coordinates where the *x* direction is the same as the fiber direction, and the *y* and *z* directions are perpendicular to the *x* direction. It is a so-called especially orthotropic material [68-69]. In this study, the especially orthotropic material is also transversely isotropic, where the properties of the GFRP composites are nearly the same in any direction perpendicular to the fibers. Thus, the properties in the *y* direction are the same as those in the *z* direction. Glass fiber reinforced polymer was used for shear reinforcement on the Safe Bridge because of its greater strain capacity.

Input data needed for the FRP composites in the finite element models are as follows:

- Number of layers
- Thickness of each layer
- Orientation of the fiber direction for each layer
- Elastic modulus of the FRP composite in three directions (E_x, E_y and E_z)
- Shear modulus of the FRP composite for the three planes (G_{xy}, G_{yz} and G_{xz})
- Major Poisson's ratios for the three planes (ν_{xy}, ν_{yz} and ν_{xz})

Note that a local coordinate system for the GFRP layered solid elements is defined where the *x* direction is the same as the fiber direction, while the *y* and *z* directions are perpendicular to the *x* direction.

The properties of isotropic materials, such as elastic modulus and Poisson's ratio, are identical in all directions; therefore no subscripts are required. This is not the case with especially orthotropic materials. Subscripts are needed to define properties in the various directions.

The various thicknesses of the FRP composites create discontinuities, which are not difficult to simulate in the finite element analysis. Layers may develop high stress concentrations at local areas and, as a result, the solution may have difficulties to converge. Thus, a consistent overall thickness of GFRP composite was used in the models to eliminate discontinuities. Wrapped GFRP was taken as an orthotropic material. The material properties for the wrapped GFRP was selected from Kachlakev report [44], and as he noted the ultimate strength for GFRP is 600 MPa, modulus of elasticity in three directions are 20.7, 6.89, 6.89 GPa, the major Poisson's ratio in three directions are 0.26, 0.26, 0.3, and the shear modulus in three directions are 1.52, 1.52, 2.65 GPa.

7.2.3 – FEM Modeling

7.2.3.1 – Geometry

The dimensions of the full-scaled beams were as specified in Figure 7.1, and the length of the beam was 6.7 meters. By taking advantage of the symmetry of the beam, a quarter of the beam was used for modeling. This approach reduced computational time and computer disk space requirement significantly. The quarter of the entire model is shown in Figures 7.9 and 7.10.

Ideally, the bond strength between the concrete and sprayed GFRP should be considered. However, in this study, perfect bond between materials was assumed due to the fact that the sprayed and wrapped GFRP were extended over the supports, which is unlikely to happen during the retrofits of existing bridges. To provide the perfect bond, the solid element for the GFRP was connected between nodes of each adjacent concrete solid element, so the two materials shared the same nodes. The same approach was adopted for the wrapped GFRP composites. The high strength of the epoxy used to attach GFRP sheets to the experimental beams supported the perfect bond assumption.

7.2.3.2 – Finite Element Discretization

As an initial step, a finite element analysis involves meshing of the model. In other words, the model is divided into a number of small elements, and after loading, stress and strain are calculated at integration points of these small elements [66]. An important step in finite element modeling is the selection of the mesh density. A convergence of results is obtained when an adequate number of elements are used in a model. This is practically accomplished when an increase in the mesh density has a negligible effect on the results [67]. Therefore, for this analysis a convergence study was carried out to determine an appropriate mesh density. Tables 7.1 through 7.3 show the number of elements used for each material for the three cases of control beam, sprayed GFRP beam and wrapped GFRP beam.

7.3 – Load-Deflection Results

Deflections are measured at midspan at the center of the bottom face of the beam. Figure 7.11 shows the load deflection plots for the control, sprayed GFRP, and wrapped GFRP beams.

7.4 – Comparison of Experimental and Numerical Results

In general, the load deflection plots for the beams from the finite element analyses agree quite well with the experimental data. The finite element load-deflection plots in the linear range are somewhat stiffer than the experimental plots. After first cracking, the stiffness of the finite element models is again higher than that of the experimental beams. There are several effects that may cause the higher stiffnesses in the finite element models. First, microcracks are present in the concrete for the experimental beams, and could be produced by drying shrinkage in the concrete and/or handling of the beams. On the other hand, the finite element models do not include the microcracks. The microcracks reduce the stiffness of the experimental beams. Next, perfect bond between the concrete and steel reinforcing is assumed in the finite element analyses, but the assumption would not be true for the experimental beams. As bond slip occurs, the composite action between the concrete and steel reinforcing is lost. Thus, the overall stiffness of the experimental beams is expected to be lower than that for the finite element models.

Table 7.4 shows comparisons between the ultimate loads of the experimental beams and the final loads from the finite element models. The final loads for the finite element

models are the last applied load steps before the solution diverges due to numerous cracks and large deflections. It is seen that the ANSYS models underestimate the strengths of the control and sprayed GFRP beams, as anticipated. Toughening mechanisms at the crack faces [70] (e.g. the grain bridging process, interlocking between the cracked faces, crack tips blunted by voids, and the crack branching process) may also to some extent extend the failures of the experimental beams before complete collapse. The finite element models do not have these mechanisms. Finally, the material properties assumed in this study may not be accurate. In the experiment, the failure modes for the beams were as predicted. The control beam failed due to yielding of the flexural reinforcement. For both of the retrofitted beams, the event corresponding to the failure point was tensile fracture of the GFRP in tension zone at the bottom of the member [12]. Crack patterns, deflection, and stress distribution (Figure 7.12-7.14) obtained from the finite element analyses at the last converged load step and the failure modes of the experimental beams agree very well.

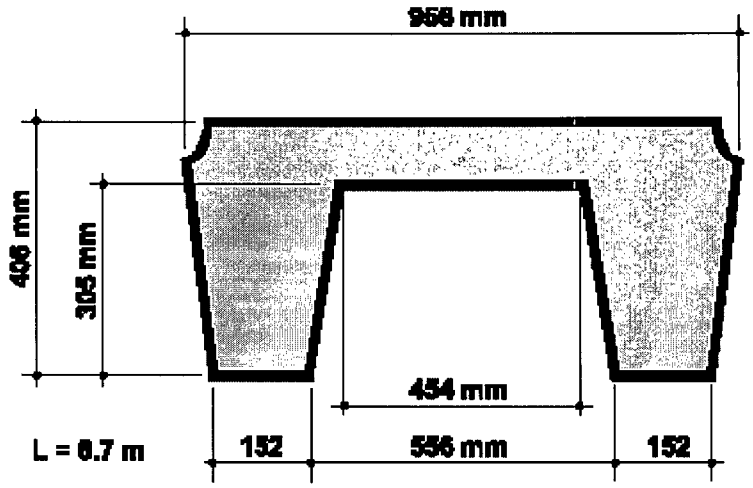

Figure 7.1: MOTH channel beam dimensions [12].

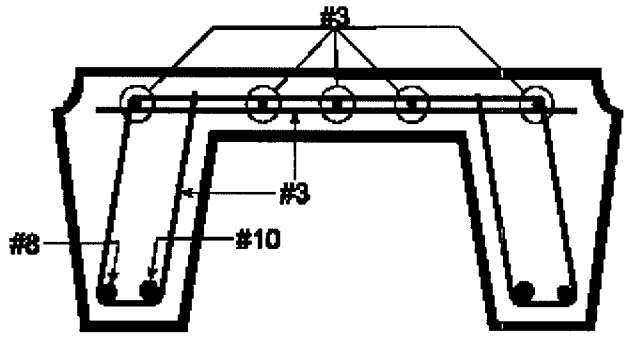

Figure 7.2: MOTH channel beam reinforcement details [12].

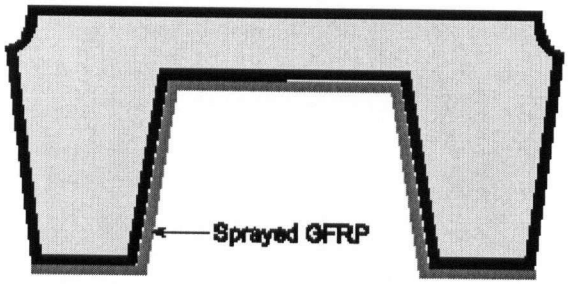

Figure 7.3: MOTH channel beam sprayed GFRP locations [12].

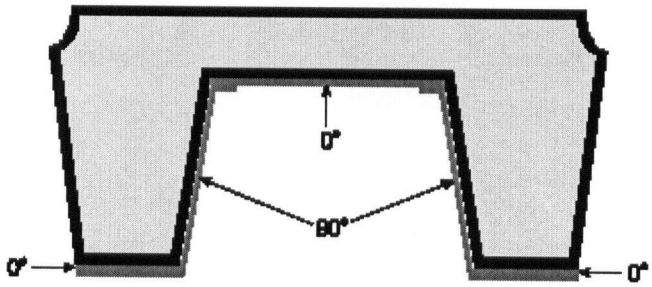

Figure 7.4: MOTH channel beam wrapped specimen fabric orientation [12].

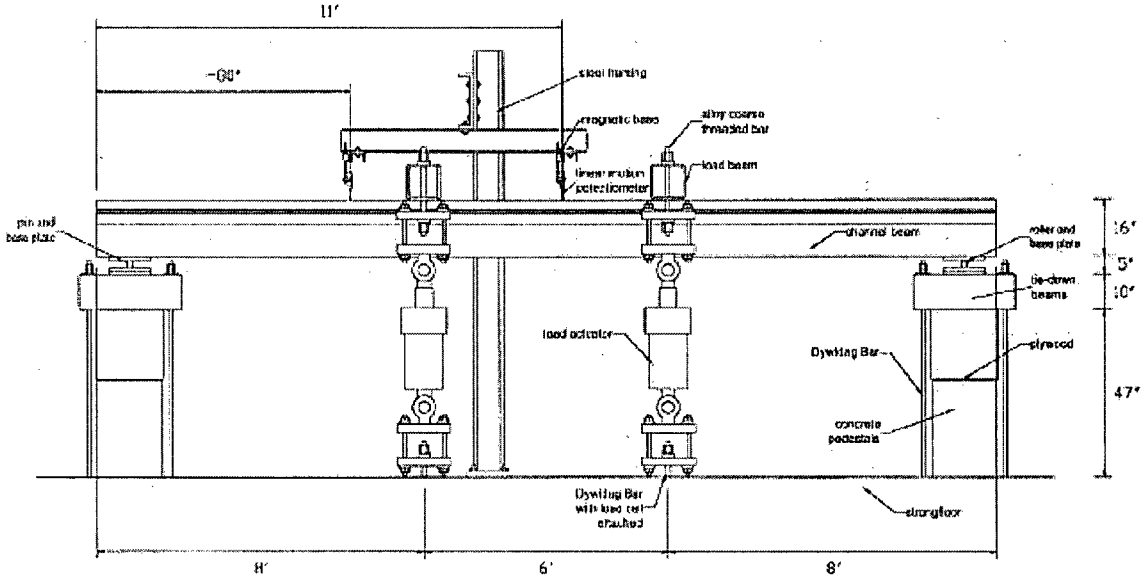

Figure 7.5: Schematic of MOTH channel beam test setup [12].

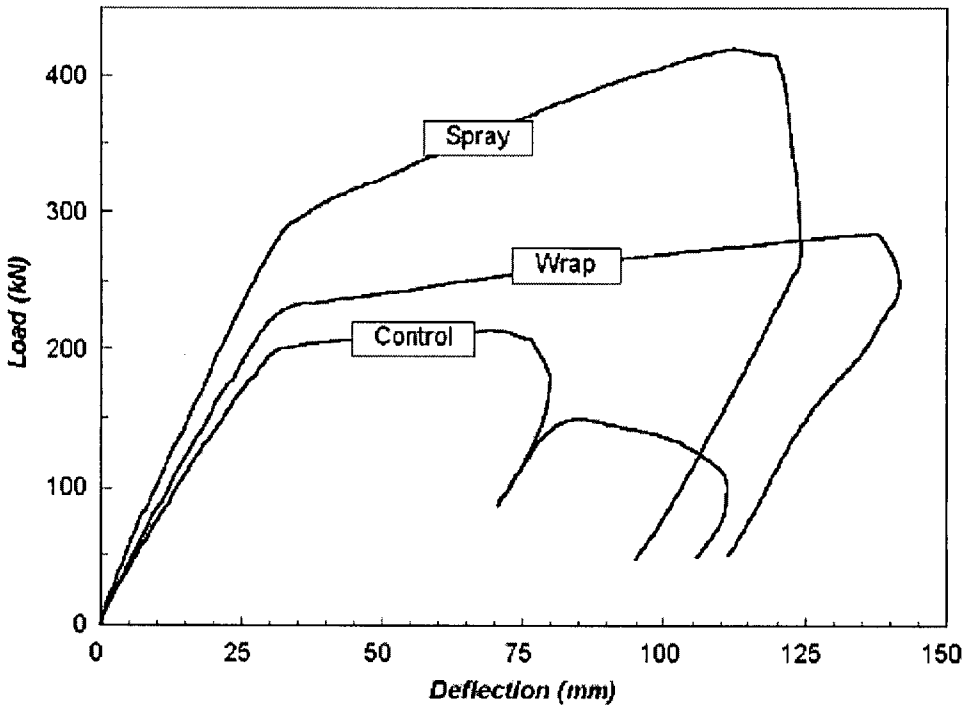

Figure 7.6: MOTH channel beam – load deflection curves [12].

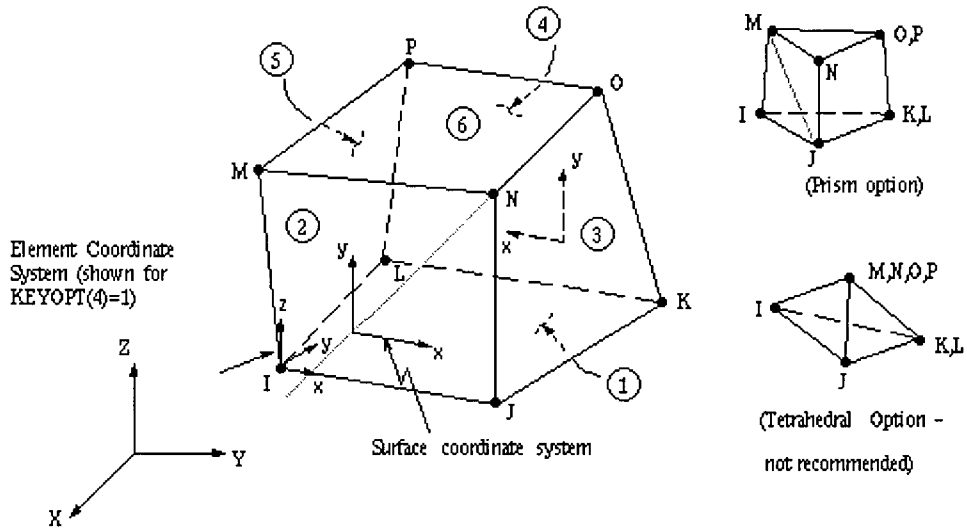

Figure 7.7: SOLID45 3-D Structural Solid [63].

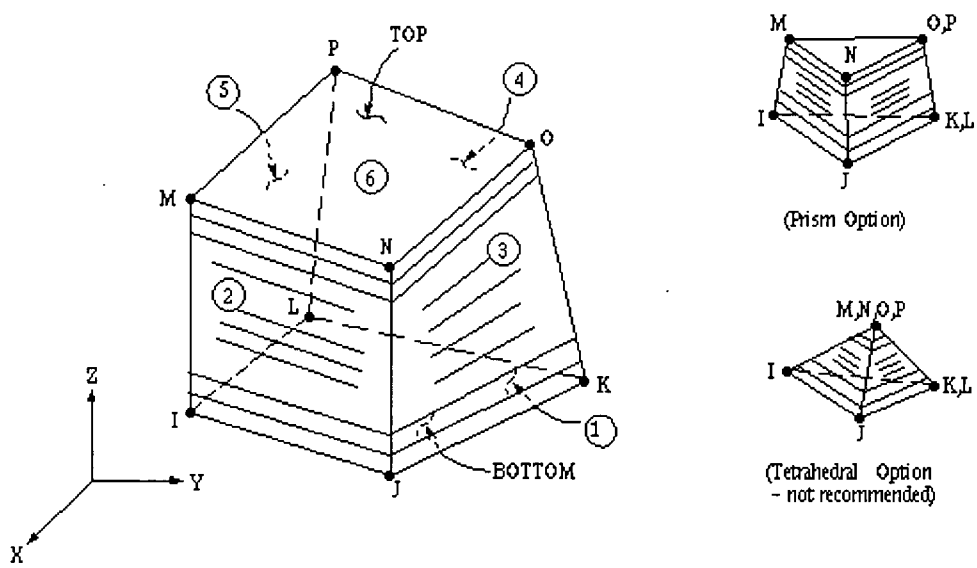

Figure 7.8: SOLID46 3-D Layered Structural Solid [63].

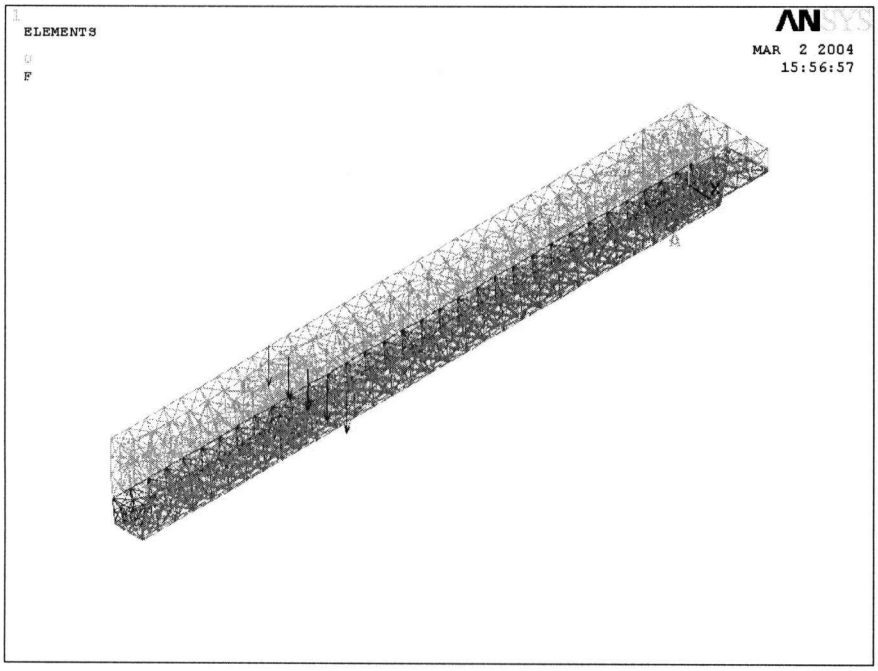

Figure 7.9: Use of a quarter beam model.

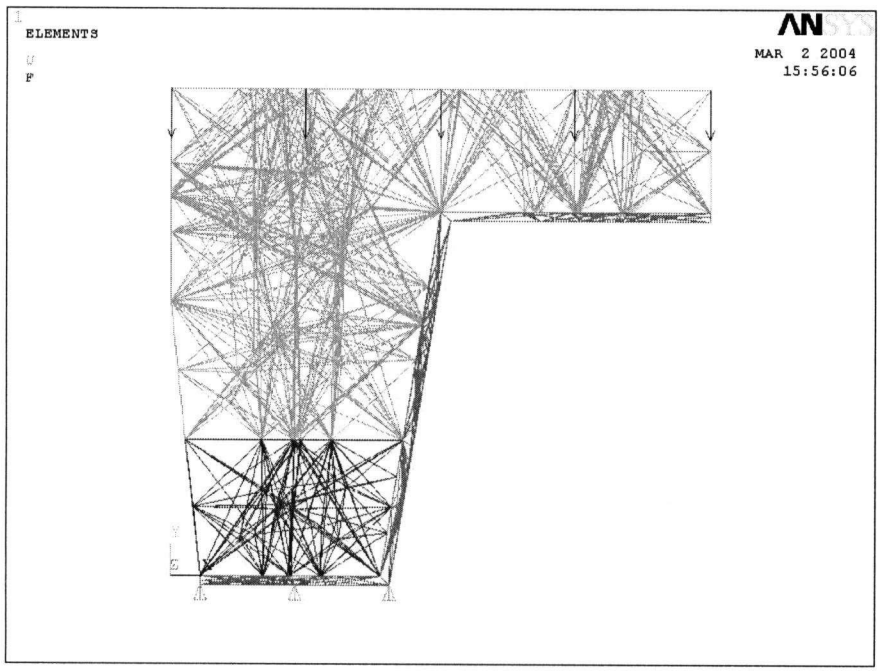

Figure 7.10: Cross-section of quarter beam model.

Table 7.1: Number of elements used in the control beam.

Type of Element	Number of Elements
Plain Concrete (SOLID65)	**1717**
Reinforced Concrete (SOLID65)	**598**
Total	**2315**

Table 7.2: Number of elements used in the sprayed GFRP beam.

Type of Element	Number of Elements
Plain Concrete (SOLID65)	**1912**
Reinforced Concrete (SOLID65)	**517**
Sprayed GFRP (SOLID45)	**1461**
Total	**3890**

Table 7.3: Number of elements used in the wrapped GFRP beam.

Type of Element	Number of Elements
Plain Concrete (SOLID65)	**1912**
Reinforced Concrete (SOLID65)	**517**
Wrapped GFRP (SOLID46)	**1580**
Total	**4009**

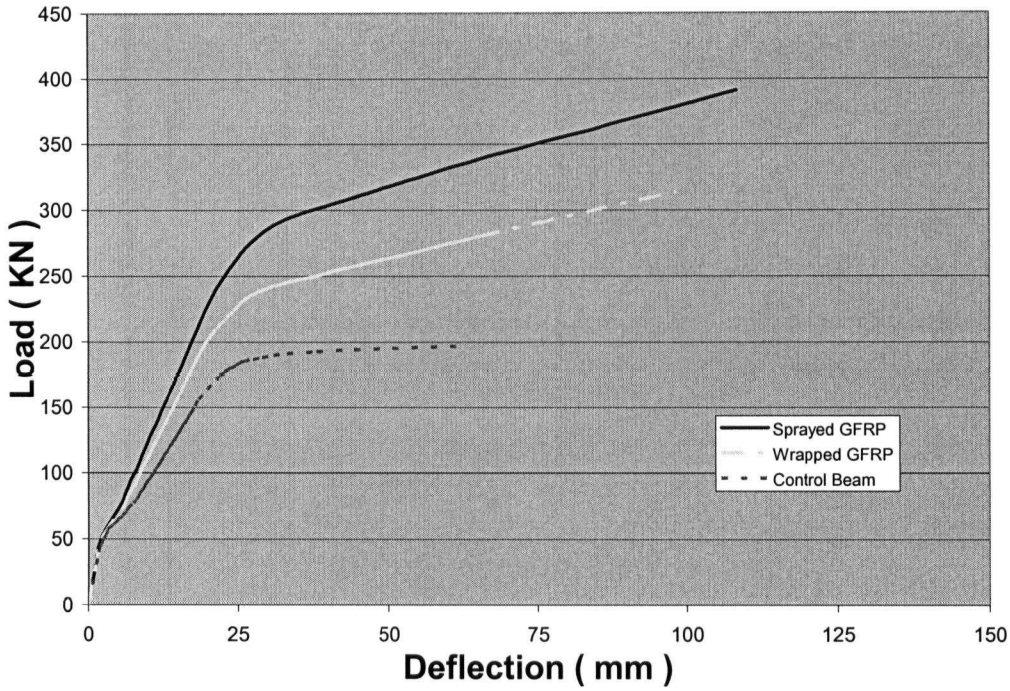

Figure 7.11: FEM Load – Deflection plot.

Table 7.4: Comparison between experimental ultimate loads and FEM final loads.

Beams	Ultimate Load (kN) from Experiment, Failure Mode	Percent Gain over Control Beam % (Experiment)	Final Load (kN) from FEM	Percent Gain over Control Beam % (FEM)	Percent Difference %
Control Beam	214	.....	197	.....	-7.9
Sprayed GFRP	419	96	391	98	-6.7
Wrapped GFRP	284	33	314	59	10.5

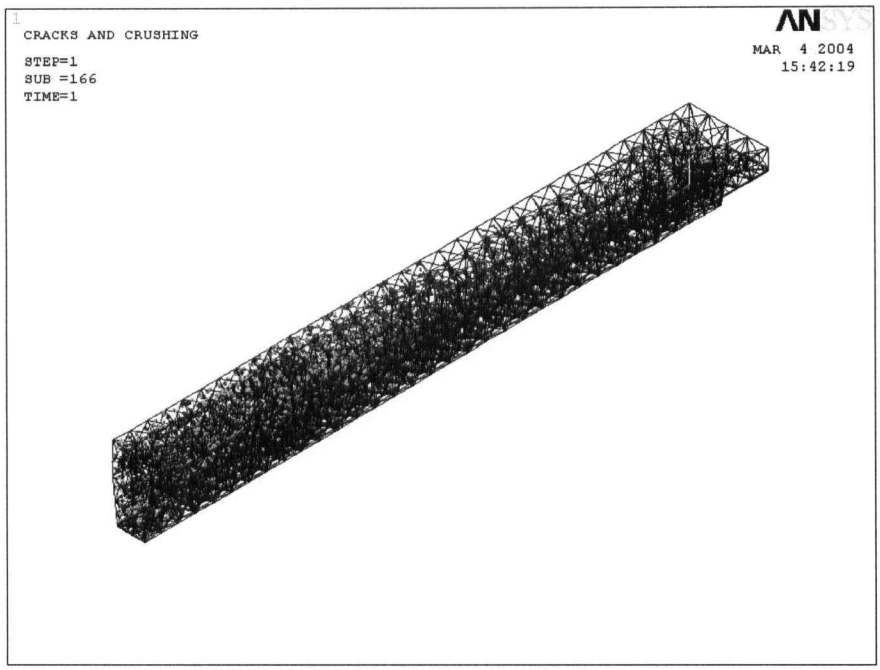

Figure 7.12: Crack pattern for the sprayed GFRP beam at maximum load.

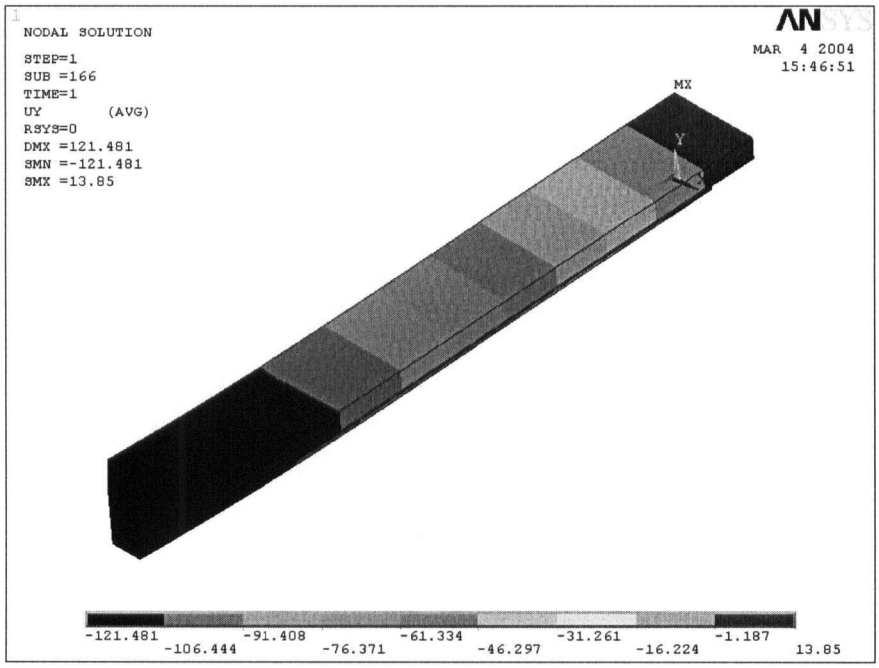

Figure 7.13: Deflection distribution for the sprayed GFRP beam at maximum load.

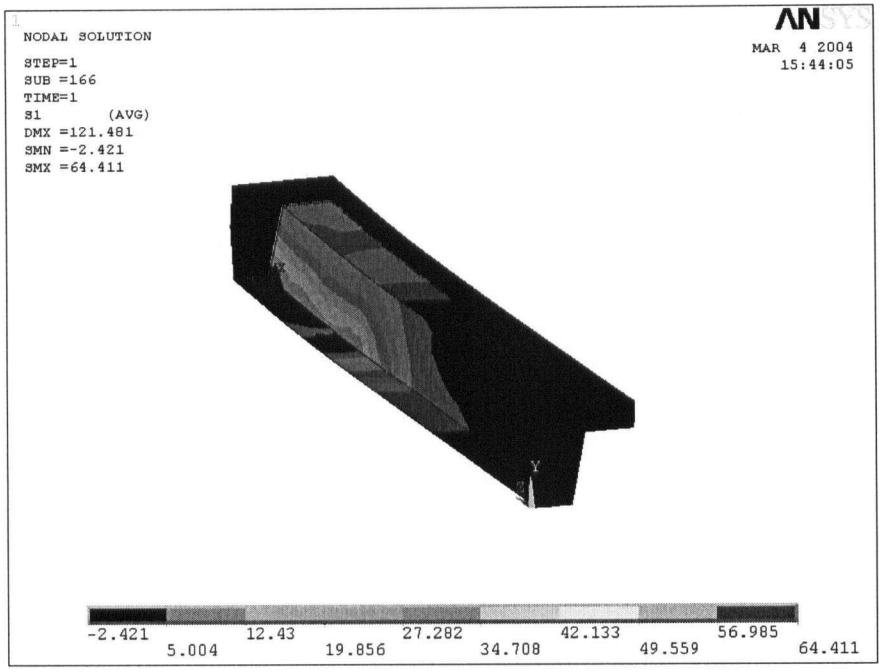

Figure 7.14: Stress distribution for the sprayed GFRP beam at maximum load.

8

CONCLUSION AND RECOMMENDATIONS

The results of an experimental and a comprehensive finite element analysis to investigate the effects of externally bonded sprayed GFRP on structural performance of a reinforced concrete bridge and full scale girders tested in the laboratory were presented. The results from both analyses correlate very well with each other, and indicate that the external bonding of GFRP materials to the bridge girders reduces the average maximum mid-span girder deflection and reinforcing steel stresses.

8.1 – Experimental Results

Experimental testing consisted of two different parts: static and rolling tests. From the static tests it was concluded that the application of sprayed GFRP results in a reduction

of 28% in the maximum strain in reinforcement steel and 22% in maximum girder deflection. Rolling tests demonstrated a similar behavior and showed that the applied GFRP reduced the maximum strain in reinforcement steel by 13% and the maximum girder deflection by 26%. The results for the maximum strain in steel bars had significant change and it was concluded that the strain reading for girder 6 in static load position 6 could be faulty. That was due to significant change in strain for almost the same deflection as it was recorded in load position 5. Nevertheless, both test indicated the superior effectiveness of the sprayed GFRP, and a promising retrofit technique for an uncountable deficient bridges all over the North America.

8.2 – Finite Element Results

The finite element models were created for both before and after the application of sprayed GFRP, and for both cases the results were quite comparable with the experimental results. Moreover, it indicated that the external bonding of sprayed GFRP can enhance the load capacity by 24% and reduces the reinforcing steel stresses by 28%. In the case of full scale lab tests, the model constructed in ANSYS V7.0 using dedicated concrete element, accurately captured the nonlinear flexural response of these beams up to the failure. The dedicated element utilizes a smeared crack model to allow for concrete cracking. It also has the option of modeling the reinforcement in a distributed or discrete manner. It was found that there are not much difference in the results of modeling the reinforcement in distributed or discrete manner, therefore, the smeared reinforcement were chosen for this analysis.

In terms of using finite element models to predict the strength of existing beams, an accurate knowledge of material properties is critical. It was concluded that for a known compressive strength of concrete, which can be measured from extracted cores; existing formulas for the Young's modulus and concrete tensile strength are adequate for use in the FEM models. Concerning the reinforcement, the actual yield strength in tension is likely to be greater than nominal design strength and thus the ultimate load of the beam will be underestimated.

In conclusion the dedicated smeared crack model is an appropriate FEM model for capturing the flexural modes of failure of reinforced concrete beams. In addition it can be an attractive tool for designers when they are asked to accurately predict the deflection of a reinforced concrete beam for a given load and its ultimate strength.

8.3 – Parametric Study

The effect of varying the modulus of elasticity and thickness of the GFRP on the girder deflections and steel reinforcing bar stresses had been investigated and concluded that a 7 times increase in modulus of elasticity can reduce the maximum deflection by 60%, and the maximum reinforcing steel stresses by 58%. Therefore, girders repaired with a higher strength material will exhibit higher ultimate flexural capacity. The effect of the GFRP cross sectional area on reducing both the maximum girder deflection and reinforcing steel stresses have also been studied and although the main function of the applied GFRP was to improve the shear capacity of the girders, it also had some effects on reducing the midspan deflections and rebar stresses, the results show the maximum

girder deflection and maximum reinforcing steel stresses can be reduced by as much as 25% and 30%, respectively.

8.4 - Recommendations on FEM Modeling

1. Symmetry should be used in bridge modeling for computational efficiency. In this project due to complete asymmetric characteristics of the Safe Bridge, it was not possible.
2. For simplification of load configurations, the load from each set of tires can be lumped to the center of each set. The lumped load, at places where it does not coincide with a node in the mesh, should be linearly distributed to the nearest nodes. Therefore, truck positions can be varied more efficiently for more detailed study.
3. Model accuracy can be improved by using more realistic material properties and boundary conditions. For the boundary conditions, the soil-structure interface should be considered for better representation of actual behavior of the structure. The interface can be defined by assigning springs with reasonable stiffness values derived from properties of the on-site soil.

REFERENCES

1- Kachlakev, D., and McCurry, D.D., "Behavior of Full-scale Reinforced Concrete Beams Retrofitted for Shear and flexural with FRP Laminates", Composites: part B 31, (2000), pp. 445-452.

2- Cederquist, S.C., "Repairing America's Deteriorating Bridges", Material Performance, May 1999, pp. 20-25.

3- CAN/CSA-S6-00, "Canadian Highway Bridge Design Code", National Standard of Canada, Dec. 2000, Published by CSA International, Canada.

4- Alexander, J.G., and Cheng, J.R., "Field Application and Studies of Using CFRP Sheets to Strengthen Concrete Bridge Girders", Advanced Composites Materials in Bridges and Structures, Canadian Society of Civil Engineering, Montreal, Quebec, 1996, pp. 465-472.

5- Saadatmanesh, H., "Extending Service Life of Concrete and Masonry Structures with Fiber Composites", Construction and Building Materials, Vol. 11, Nos 5-6 pp. 327-335, 1997.

6- Saadatmanesh, H., and Malek, A.M., "Design Guidelines for Flexural Strengthening of RC Beams with FRP Plates", Journal of Composites for Construction, November 1998.

7- Oehlers, D.J., "Development of Design Rules for Retrofitting by Adhesive Bonding or Bolting either FRP or Steel Plates to RC Beams or Slabs in Bridges and Buildings", Composites: Part A 32 (2001) pp. 1345-1355.

8- Oehlers, D.J., Mohamed Ali, M.S., and Weimin, L.,"Upgrading Continuous Reinforced Concrete Beams by Gluing Steel Plates to Their Tension Faces", Journal of Structural Engineering, March 1998, pp. 224-232.

9- Hussain, M., Sharif, A., Basunbul, I.A., Baluch, M.H., and Al-Sulaimani, G.J., "Flexural Behavior of Prestressed Reinforced Concrete Beams Strengthened Externally by Steel Plates", ACI Structural Journal, January-February 1995, pp. 14-22.

10- Banthia, N., Boyd, A.J., Johnson, M.M., Ross, S.L., and Sexsmith, R.J., "Sprayed Fiber Reinforced Polymers for Infrastructure Restoration", 2nd International Conference on Engineering Materials, San Jose, California, United States, August 16-19, 2001.

11- Banthia, N., Yan, C., and Nandakumar, N., "Sprayed Fiber Reinforced Plastics (FRPs) for Repair of Concrete Structures", Second International Conference on Advanced Composites Materials in Bridges and Structures, Montreal, Canada, August 11-14, 1996, pp. 537-545.

12- Boyd, A.J., "Repair and Retrofit of Damaged Concrete Structures Using Sprayed Fibre Reinforced Plastics", Ph.D Thesis, The University of British Columbia, 2000.

13- Banthia, N., Nandakumar, N., and Boyd, A.J., "Sprayed Fiber Reinforced Polymers: From Laboratory to a Real Bridge", Sixth International Conference on

Short and Medium Span Bridges, Vancouver, BC, Canada, July 31- August 2, 2002, pp. 337-345.

14- Bonacci, J.F., and Maalej, M., "Externally Bonded FRP for Service-Life Extension of RC Infrastructure", Journal of Infrastructure System, March 2000, pp. 41-51.

15- Mohamed Ali, M.S., Oehlers, D.J., and Bradford, M.A., "Interaction Between Flexure and Shear on the Debonding of RC Beams Retrofitted with Compression Face Plates", Advances in Structural Engineering, Vol. 5/4, 2002, pp. 223-230.

16- Mortazavi, A.R., "Sprayed Glass Fiber Reinforced Polymers for Structural Repair and Retrofitting", Direct Study Report, Department of Civil Engineering, University of British Columbia, Vancouver, BC, April 2004.

17- Meier, U., Deuring, M., Meier, H., and Schwegler, G., "Strengthening of Structures with Advanced Composites", Alternative Materials for the Reinforcement and Prestressing of Concrete, Blackie Academic and Professional, Glasgow, UK, 1993, pp. 153-171.

18- Malek, A.M., and Saadatmanesh, H., "Physical and Mechanical Properties of Typical Fibers and Resins. Fiber Composites on Infrastructure, Proceedings of the First International Conference, CSCE, Sherbrooke, Quebec, Canada, 1992, pp. 68-79.

19- Marshall, O.S., Busel, J.P., "Composite Repair/Upgrade of Concrete Structures", Materials for the New Millennium: Proceeding of the Fourth Materials Engineering Conference, Washington, D.C., November 10-14, 1996.

20- Brown R.T., Zureick, A., "Lightweight Composite Truss Section Decking", Marine Structures 14 (2001) pp. 115-132.

21- Nanni, A., "Concrete Repair with Externally Bonded FRP Reinforcement", Concrete International, 17(6), June 1995, pp. 22-26.

22- An, W., Saadatmanesh, H., and Ehsani, M.R., "RC Beams Strengthened with FRP Plates II: Analysis and Parametric Study", ASCE Journal of Structural Engineering, ASCE, Vol. 117, No. 11, 1991, pp. 3434-3455.

23- Malek, A.M., Saadatmanesh, H., and Ehsani, M.R., "Prediction of Failure Load of RC Beams Strengthened with FRP Plate Due to Stress Concentration at the Plate End", ACI Structural Journal, March-April 1998, pp. 142-152.

24- Bonacci, J.F., Maalej, M., "Behavioral Trends of RC Beams Strengthened with Externally Bonded FRP", Journal of Composites for Construction, May 2001, pp. 102-113.

25- Saadatmanesh, H., and Ehsani, M.R., "RC Beams Strengthened with GFRP Plates I: Experimental Study", Journal of Structural Engineering, Vol. 117, No. 11, November 1991, pp. 3417-3433.

26- Sharif, A., Al-Sulaimani, G.J., Basunbul, I.A., Baluch, M.H., and Ghaleb, B.N., "Strengthening if Initially Loaded Reinforced Concrete Beams using FRP Plates", ACI Structural Journal, Vol. 91, No. 2, 1994, pp. 160-168.

27- Arduini, M., and Nanni, A., "Parametric Study of Beams with Externally Bonded FRP Reinforcement", ACI Structural Journal, Vol. 94, No. 5, 1997, pp. 493-501.

28- Sheikh, S.A., "Performance of Concrete Structures Retrofitted with Fibre Reinforced Polymers", Engineering Structures, Vol. 24, 2002, pp. 869-879.

29- Ross, C.A., Jerome, D.M., Tedesco, J.W., and Hughes, M.L., "Strengthening of Reinforced Concrete Beams with Externally Bonded Composite laminates", ACI Structural Journal, Vol. 96, No. 2, 1999, pp. 212-220.

30- Norris, T., Saadatmanesh, H., and Ehsani, M.R., "Shear and Flexural Strengthening of RC Beams with Carbon Fiber Sheets", Journal of Structural Engineering, July 1997, pp. 903-911.

31- Chajes, M.J., Thomson, T.A., Januszka, T.F., and Finch, W.W., "Flexural Strengthening Concrete Beams using Externally Bonded Composite", Construction and Building Materials, Vol. 8, No. 3, 1994, pp. 191-201.

32- Chajes, M.J., Januszka, T.F., Mertz, D.R., Thomson, T.A., and Finch, W.W., "Shear Strengthening of Reinforced Concrete Beams using Externally Applied Composite Fabrics", ACI Structural Journal, Vol. 92, No. 3, May-June 1995, pp. 295-303.

33- Khalifa, A., and Nanni, A., "Improving Shear Capacity of Existing RC T-Section Beams using CFRP Composites", Cement & Concrete Composites Vol. 22, 2000, pp. 165-174.

34- Malek, A.M., and Saadatmanesh, H., "Ultimate Shear Capacity of Reinforced Concrete Beams Strengthened with Web-Bonded Fiber-Reinforced Plastic", ACI Structural Journal, Vol. 95, No. 4, July-August 1998, pp. 391-399.

35- Malek, A.M., and Saadatmanesh, H., "Analytical Study of Reinforced Concrete Beams Strengthened with Web-Bonded Fiber Reinforced Plastic Plates or Fabrics", ACI Structural Journal, Vol. 95, No. 3, May-June 1998, pp. 343-352.

36- Saadatmanesh, H., "Fiber Composites for New and Existing Structures", ACI Structural Journal, Vol. 91, No. 3, May-June 1994, pp. 346-354.

37- Toutanji, H.A., and Gomez, W., "Durability Characteristics of Concrete Beams Externally Bonded with FRP Composite Sheets", Cement and Concrete Composites, Vol.19, 1997, pp. 351-358.

38- Karbhari, V.M., Engineer, M., Eckel II, D.A., "On the Durability of Composite Rehabilitation Schemes for Concrete: Use of a Peel Test", Journal of Materials Science, Vol. 32, 1997, pp. 147-156.

39- Chajes, M.J., Thomson, T.A., Farschman, C.A., "Durability of Concrete Beams Externally Reinforced with Composite Fabrics', Construction and Building Materials, Vol.9, No. 3, 1995, pp. 141-148.

40- Vina, J., Garcia, E.A., Arguelles, A., and Vina, I., "The Effect of Moisture on the Tensile and Interlaminar Shear Strengths of Glass or Carbon Fiber Reinforced PEI", Journal of Materials Science Letters, Vol. 19, 2000, pp. 579-581.

41- Stallings, J.M., Tedesco, J.W., El-Mihilmy, M., and McCauley, M., "Field Performance of FRP Bridge Repairs", Journal of Bridge Engineering, May 2000, pp. 107-113.

42- Tedesco, J.W., Stallings, J.M., El-Mihilmy, M., and McCauley, M.W., "Rehabilitation of a Concrete Bridge using FRP laminates", 4th Material Engineering Conference, Washington, D.C., 1996, pp. 631-637.

43- McCurry, D.D., and Kachlakev, D., "Strengthening of Full-Scale Reinforced Concrete Beams using FRP Laminates and Monitoring with Fiber Optic Strain Gauges", 2nd Conference on Seismic Repair and Rehabilitation of Structures, March 2000, pp. 131-140.

44- Kachlakev, D.I., "Horsetail Creek Bridge: Design Method Calibration and Experimental results of Structural Strengthening with CFRP and GFRP laminates", Advances in Structural engineering, Vol. 5, no. 2, 2002, pp. 87-98.

45- ISIS Canada, Annual Report, 1998/1999, Field Applications, The Canadian Network of Centers of Excellence on Intelligent Sensing for Innovative Structures Website.

46- Banthia, N., Nandakumar, N., and Boyd, A.J., "Sprayed Fiber Reinforced Polymers for Repair and Strengthening", 47th International SAMPE Symposium and Exhibition, Long Beach, CA, United States, May 12-16 2002.

47- Banthia, N., and Boyd, A.J., "Sprayed Fiber Reinforced Plastics for Repairs", Canadian Journal of Civil Engineering, Vol. 27, No. 5, October 2000, pp. 907-915.

48- Boyd, A.J., and Banthia, N., "Shear Strengthening of Reinforced Concrete Beams with Sprayed GFRP", Proceedings, Structural Faults & Repair, 8th International Conference, London, England, July 1999.

49- Zhao, Y., and Roddis, W.M.K., "Fatigue Crack Investigation for the Arkansas River Bridge in Hutchinson, Kansas", Construction and Building Materials, Vol. 14, 2000, pp. 287-295.

50- Meng, J.Y., and Lui, E.M., "Seismic Analysis and Assessment of a Skew Highway Bridge", Engineering Structures, Vol. 22, 2000, pp. 1433-1452.

51- Qiao, P., Davalos, J.F., and Brown, B., "A Systematic Analysis and Design Approach for Single-Span FRP Deck/Stringer Bridges", Composites: Part B, Vol. 31, 2000, pp. 593-609.

52- Halling, M.W., Muhammad, I., and Womack, K.C., "Dynamic Field Testing for Condition Assessment of Bridge Bents", Journal of Structural Engineering, February 2001, pp. 161-167.

53- Hibino, K., and Kojima, T., "FEM Study on the Flexural Crack Behaviors of Concrete by the Use of Crack Element", Transaction of Japan Concrete Institute, JCI, Vol. 21, 2000, pp. 357-364.

54- Arduini, M., Tommaso, A.D., and Nanni, A., "Brittle Failure in FRP Plate and Sheet Bonded Beams", ACI Structural Journal, Vol. 94, No. 4, July-August 1997, pp. 363-370.

55- Fanning, P., "Nonlinear Models of Reinforced and Post-tensioned Concrete Beams", Electronic Journal of Structural Engineering, Vol. 2, 2001, pp. 111-119.

56- William, K.J. and Warnke, E.D. "Constitutive Model for the Triaxial Behaviour of Concrete", Proceedings of the International Association for Bridge and Structural Engineering, 1975, 19, p.174, ISMES, Bergamo, Italy.

57- Barbosa, A.F., and Ribeiro, G.O., "Analysis of Reinforced Concrete Structures using ANSYS Nonlinear Concrete Model", Computational Mechanics, New trends and Applications, Barcelona, Spain 1998.

58- MBrace® Composite Strengthening System. Master Builders, Inc., Cleveland, OH, USA, 1998.

59- Safety & Loss Prevention Bulletin Prepared by Organic Peroxide Producers Safety Division, The Society of the Plastics Industry, Inc., Bulletin No. 19, Revision 2001.

60- DERAKANE® Epoxy Vinyl Ester Resins Technical Product Information. Dow Chemical Company, Midland, MI, USA, 1995.

61- Advantex® Glass Fiber: A New Era in Composites Technology. Owens Corning, Toledo, OH, USA, 1997.

62- Nandakumar, N., "Strengthening of Safe Bridge, Duncan, British Columbia: Use of Hybrid (Polypropylene and Carbon) Fiber Reinforced Mortar and Sprayed Glass Fiber Reinforced Polymer", Department of Civil Engineering, University of British Columbia, 2001.

63- ANSYS, ANSYS User's Manual Revision 5.5, ANSYS, Inc., Cononsburg, Pennsylvania, 1998.

64- Shah, S.P., Swartz, S.E., and Ouyang, C., Fracture Mechanics of Concrete, John Wiley & Sons, Inc., New York, New York, 1995.

65- Bangash, M.Y.H., Concrete and Concrete Structures: Numerical Modeling and Applications, Elsevier Science Publishers Ltd., London, England, 1989.

66- Bathe, K. J., Finite Element Procedures, Prentice-Hall, Inc., Upper Saddle River, New Jersey, 1996.

67- Adams, V. and Askenazi, A., Building Better Products with Finite Element Analysis, OnWord Press, Santa Fe, New Mexico, 1998.

68- Kaw, A. K., Mechanics of Composite Materials, CRC Press LLC, Boca Raton, Florida, 1997.

69- Gibson, R. F., Principles of Composite Material Mechanics, McGraw-Hill, Inc., New York, New York, 1994.

70- Shah, S.P., Swartz, S.E., and Ouyang, C., Fracture Mechanics of Concrete, John Wiley & Sons, Inc., New York.